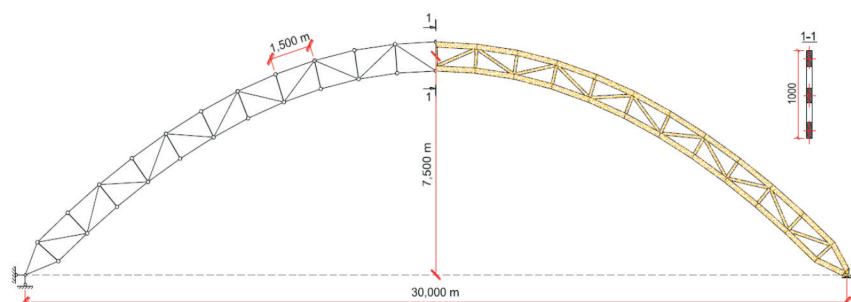
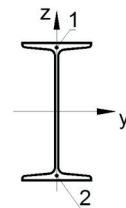
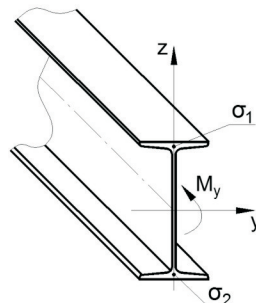
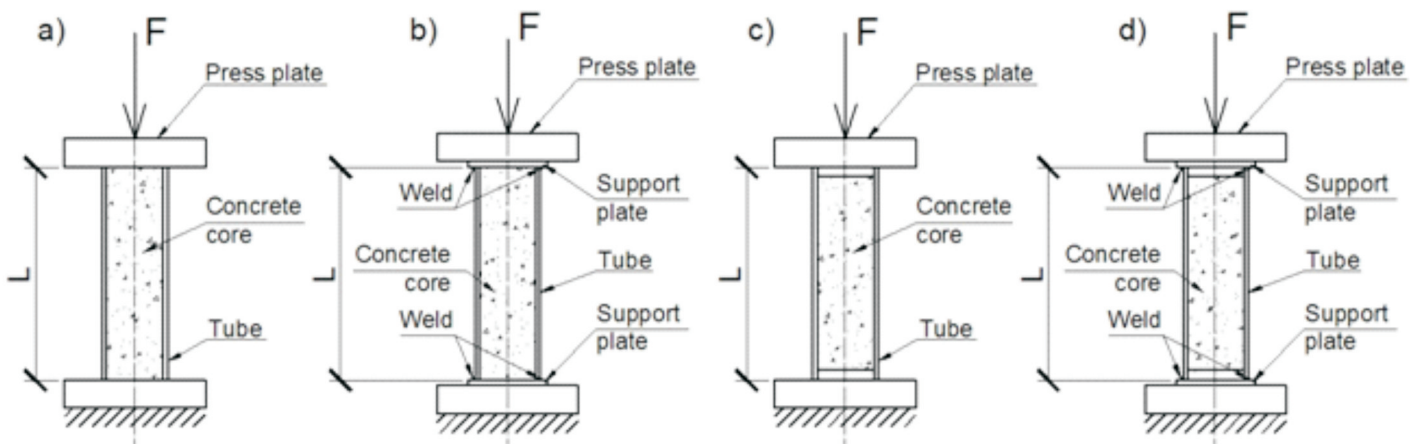
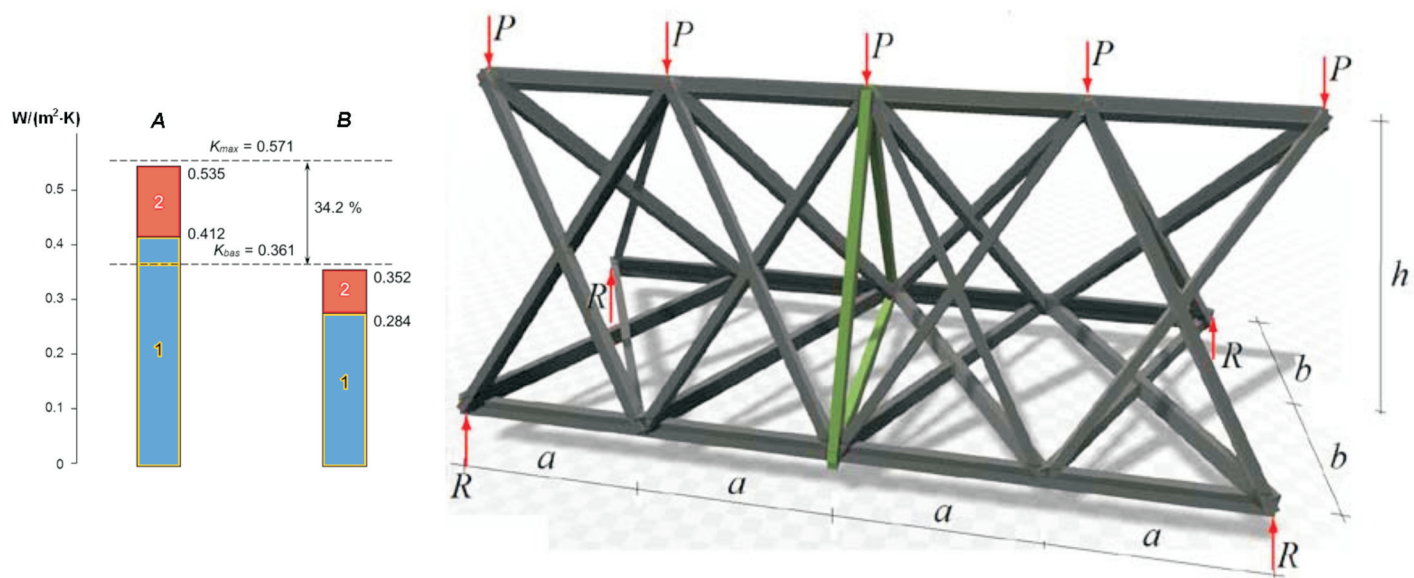




№4(64) 2016

**РАСЧЕТЫ**



**ПОЛИТЕХ**

Санкт-Петербургский  
политехнический университет  
Петра Великого

Инженерно-строительный институт  
Центр дополнительных профессиональных программ  
195251, г. Санкт-Петербург, Политехническая ул., 29,  
тел/факс: 552-94-60, [www.stroikursi.spbstu.ru](http://www.stroikursi.spbstu.ru),  
[stroikursi@mail.ru](mailto:stroikursi@mail.ru)

Приглашает специалистов организаций, вступающих в СРО,  
на курсы повышения квалификации (72 часа)

Код	Наименование программы	Виды работ*
<b>Курсы по строительству</b>		
<b>БС-01-04</b>	«Безопасность и качество выполнения общестроительных работ»	п.1,2, 3, 5, 6, 7, 9, 10, 11, 12, 13, 14
<b>БС-01</b>	«Безопасность и качество выполнения геодезических, подготовительных и земляных работ, устройства оснований и фундаментов»	1,2,3,5
<b>БС-02</b>	«Безопасность и качество возведения бетонных и железобетонных конструкций»	6,7
<b>БС-03</b>	«Безопасность и качество возведения металлических, каменных и деревянных конструкций»	9,10,11
<b>БС-04</b>	«Безопасность и качество выполнения фасадных работ, устройства кровель, защиты строительных конструкций, трубопроводов и оборудования»	12,13,14
<b>БС-05</b>	«Безопасность и качество устройства инженерных сетей и систем»	15,16,17,18,19
<b>БС-06</b>	«Безопасность и качество устройства электрических сетей и линий связи»	20,21
<b>БС-08</b>	«Безопасность и качество выполнения монтажных и пусконаладочных работ»	23,24
<b>БС-12</b>	«Безопасность и качество устройства мостов, эстакад и путепроводов»	29
<b>БС-13</b>	«Безопасность и качество выполнения гидротехнических, водолазных работ»	30
<b>БС-14</b>	«Безопасность и качество устройства промышленных печей и дымовых труб»	31
<b>БС-15</b>	«Осуществление строительного контроля»	32
<b>БС-16</b>	«Организация строительства, реконструкции и капитального ремонта. Выполнение функций технического заказчика и генерального подрядчика»	33
<b>Курсы по проектированию</b>		
<b>БП-01</b>	«Разработка схемы планировочной организации земельного участка, архитектурных решений, мероприятий по обеспечению доступа маломобильных групп населения»	1,2,11
<b>БП-02</b>	«Разработка конструктивных и объемно-планировочных решений зданий и сооружений»	3
<b>БП-03</b>	«Проектирование внутренних сетей инженерно-технического обеспечения»	4
<b>БП-04</b>	«Проектирование наружных сетей инженерно-технического обеспечения»	5
<b>БП-05</b>	«Разработка технологических решений при проектировании зданий и сооружений»	6
<b>БП-06</b>	«Разработка специальных разделов проектной документации»	7
<b>БП-07</b>	«Разработка проектов организации строительства»	8
<b>БП-08</b>	«Проектные решения по охране окружающей среды»	9
<b>БП-09</b>	«Проектные решения по обеспечению пожарной безопасности»	10
<b>БП-10</b>	«Обследование строительных конструкций и грунтов основания зданий и сооружений»	12
<b>БП-11</b>	«Организация проектных работ. Выполнение функций генерального проектировщика»	13
<b>Э-01</b>	«Проведение энергетических обследований с целью повышения энергетической эффективности и энергосбережения»	
<b>Курсы по инженерным изысканиям</b>		
<b>И-01</b>	«Инженерно-геодезические изыскания в строительстве»	1
<b>И-02</b>	«Инженерно-геологические изыскания в строительстве»	2,5
<b>И-03</b>	«Инженерно-гидрометеорологические изыскания в строительстве»	3
<b>И-04</b>	«Инженерно-экологические изыскания в строительстве»	4
<b>И-05</b>	«Организация работ по инженерным изысканиям»	7

\*(согласно приказам Минрегионразвития РФ N 624 от 30 декабря 2009 г.)

По окончании курса слушателю выдается удостоверение о краткосрочном повышении квалификации установленного образца (72 ак. часа)

Для регистрации на курс необходимо выслать заявку на участие, и копию диплома об образовании по телефону/факсу: 8(812) 552-94-60, 535-79-92, , e-mail: [stroikursi@mail.ru](mailto:stroikursi@mail.ru).

[Http://www.engstroy.spbstu.ru](http://www.engstroy.spbstu.ru) – полнотекстовая версия журнала в сети Интернет.  
Бесплатный доступ, обновление с каждым новым выпуском

## Инженерно-строительный журнал

НАУЧНОЕ ИЗДАНИЕ

ISSN 2071-4726

Свидетельство о государственной регистрации: ПИ №ФС77-38070,  
выдано Роскомнадзором

Специализированный научный  
журнал. Выходит с 09.2008.

Включен в Перечень ведущих  
периодических изданий ВАК РФ

Периодичность: 8 раз в год

### Учредитель и издатель:

Санкт-Петербургский  
политехнический университет  
Петра Великого

### Адрес редакции:

195251, СПб, ул. Политехническая,  
д. 29, Гидрокорпус-2, ауд. 227А

### Главный редактор:

Вера Михайловна Якубсон

### Научный редактор:

Николай Иванович Ватин

### Выпускающий редактор:

Екатерина Александровна Линник

### Редакционная коллегия:

д.т.н., проф. В.В. Бабков;  
д.т.н., проф. М.И. Бальзанников;  
к.т.н., проф. А.И. Боровков;  
д.т.н., проф. Н.И. Ватин;  
PhD, professor M. Вельжкович;  
д.т.н., проф. А.Д. Гиргидов;  
д.т.н., проф. Э.К. Завадскас;  
д.ф.-м.н., проф. М.Н. Кирсанов;  
D.Sc., professor M. Кнежевич;  
д.т.н., проф. В.В. Лалин;  
д.т.н., проф. Б.Е. Мельников;  
д.т.н., проф. Ф. Неправиша;  
д.т.н., проф. Р.Б. Орлович;  
Dr. Sc. Ing., professor  
Л. Пакрастиньш;  
Dr.-Ing. Habil., professor  
Х. Пастернак;  
д.т.н., проф. А.В. Перельмутер;  
к.т.н. А.Н. Пономарев;  
д.ф.-м.н., проф. М.Х. Стрелец;  
д.т.н., проф. О.В. Тараканов.

## Содержание

### АНАЛИЗ

- Саинов М.П. Анализ работоспособности каменной плотины с комбинацией противофильтрационных элементов – железобетонного экрана и глиноцементобетонной стены (англ.) 3

- Корниенко С.В., Ватин Н.И., Горшков А.С. Натурные теплофизические испытания жилых зданий из газобетонных блоков (англ.) 10

### КОНСТРУКЦИИ

- Сакните Т., Сердюк Д.О., Горемыкин В.В.,  
Пакрастиньш Л., Ватин Н.И. Проектирование  
огнестойких арочных деревянных покрытий (англ.) 26

- Туснина О.А., Данилов А.И. Жесткость рамных узлов  
сопряжения ригеля с колонной коробчатого  
сечения (англ.) 40

### РАСЧЕТЫ

- Кирсанов М.Н. Анализ прогиба фермы  
пространственного покрытия с крестообразной  
решеткой (англ.) 52

- Канищев Р.А. Анализ местной устойчивости  
трубобетонных конструкций прямоугольного  
сечения (англ.) 59

© ФГАОУ ВО СПбПУ, 2016

На обложке: иллюстрации авторов к статьям номера

Установочный тираж 1000 экз.

Подписано в печать 27.10.16. Формат 60x84/8, усл. печ. л. 8,5. Заказ № 2730.

Отпечатано в типографии СПбПУ. СПб, ул. Политехническая, д. 29

### Контакты:

Тел. +7(812)535-52-47 E-mail: [mce@ice.spbstu.ru](mailto:mce@ice.spbstu.ru)

Web: <http://www.engstroy.spbstu.ru>

[Http://www.engstroy.spbstu.ru](http://www.engstroy.spbstu.ru) – full-text open-access version in Internet. It is updated immediately with each new issue.

## Magazine of Civil Engineering

SCHOLAR JOURNAL

ISSN 2071-4726

Peer-reviewed scientific journal

Start date: 2008/09

8 issues per year

**Publisher:**

Peter the Great St. Petersburg Polytechnic University

**Indexing:**

Scopus, Russian Science Citation Index (WoS), Compendex, DOAJ, EBSCO, Google Academia, Index Copernicus, ProQuest, Ulrich's Serials Analysis System

**Corresponding address:**

227a Hydro Building, 29 Polytechnicheskaya st., Saint-Petersburg, 195251, Russia

**Editor-in-chief:**

Vera M. Yakubson

**Science editor:**

Nikolay I. Vatin

**Executive editor:**

Ekaterina A. Linnik

**Editorial board:**

V.V. Babkov, D.Sc., professor

M.I. Balzannikov, D.Sc., professor

A.I. Borovkov, PhD, professor

M. Veljkovic, PhD, professor

E.K. Zavadskas, D.Sc., professor

M.N. Kirsanov, D.Sc., professor

M. Knezevic, D.Sc., professor

V.V. Lalin, D.Sc., professor

B.E. Melnikov, D.Sc., professor

F. Nepravishta, D.Sc., assoc. professor

R.B. Orlovich, D.Sc., professor

L. Pakrastinsh, Dr.Sc.Ing., professor

H. Pasternak, Dr.-Ing.habil., professor

A.V. Perelmutter, D.Sc., professor

A.N. Ponomarev, PhD, professor

M.Kh. Strelets, D.Sc., professor

O.V. Tarakanov, D.Sc., professor

## Contents

### ANALYSIS

- |   |    |
|---|----|
| Sainov M.P. Analysis of normal operation of a rockfill dam with combination of seepage-control elements: reinforced concrete face and a clay-cement-concrete wall | 3  |
| Korniyenko S.V., Vatin N.I., Gorshkov A.S. Thermophysical field testing of residential buildings made of autoclaved aerated concrete blocks                       | 10 |

### STRUCTURES

- |  |    |
|--|----|
| Saknite T., Serduks D.O., Goremkins V.V., Pakrastins L., Vatin N.I. Fire design of arch-type timber roof | 26 |
| Tusnina O.A., Danilov A.I. The stiffness of rigid joints of beam with hollow section column              | 40 |

### CALCULATIONS

- |  |    |
|--|----|
| Kirsanov M.N. Analysis of the buckling of spatial truss with cross lattice                 | 52 |
| Kanishchev R. A. Analysis of local stability of the rectangular tubes filled with concrete | 59 |

© Peter the Great St. Petersburg Polytechnic University. All rights reserved.

On the cover: authors' illustrations

+7(812) 535-52-47

E-mail: [mce@ice.spbstu.ru](mailto:mce@ice.spbstu.ru)

Web: [Http://www.engstroy.spbstu.ru/eng/index.html](http://www.engstroy.spbstu.ru/eng/index.html)

doi: 10.5862/MCE.64.1

## Analysis of normal operation of a rockfill dam with combination of seepage-control elements: reinforced concrete face and clay-cement-concrete wall

### Анализ работоспособности каменной плотины с комбинацией противофильтрационных элементов – железобетонного экрана и глиноцементобетонной стены

**M.P. Sainov,**  
National Research Moscow State Civil  
Engineering University, Moscow, Russia

**Канд. техн. наук, доцент М.П. Саинов,**  
Национальный исследовательский  
Московский государственный строительный  
университет, Москва, Россия

**Key words:** concrete faced rockfill dam;  
cut-off wall; stress-strain state; numerical  
modeling

**Ключевые слова:** каменная плотина с  
железобетонным экраном; стена в грунте;  
напряжённо-деформированное состояние;  
численное моделирование

**Abstract.** The paper considers results of stress-strain state analysis for a 87 m high rockfill dam that is located in the layer of soil foundation and has a combined seepage-control element. In the lower part of the dam as well as in its foundation there is fixed a grout curtain by using slurry trench cut-off walls, and in the upper part there is fixed a reinforced concrete face. The wall and the face are conjugated via the reinforced concrete gallery. Analyses showed that both seepage-control elements have a favorable stress-strain state: no tensile stresses occur in them. In the considered dam the reinforced concrete face operates in more favorable conditions than in a traditional dam with a reinforced concrete face. This allows recommending this type of the dam for practical application in hydraulic engineering. The alternative is proposed with the design of conjugation of a reinforced concrete face and a seepage-control wall.

**Аннотация.** Рассматриваются результаты расчёта напряжённо-деформирования состояния высокой каменной плотины высотой 87 м, расположенной на слое несkalьного основания и имеющей комбинированный противофильтрационный элемент. В нижней части плотины, а также в её основании методом «стена в грунте» устроена противофильтрационная завеса, а в верхней части – железобетонный экран. Сопряжение стены и экрана осуществляется через железобетонную галерею. Расчёты показали, что оба противофильтрационных элемента имеют благоприятное напряжённо-деформированное состояние – в них не возникает растягивающих напряжений. В рассмотренной плотине железобетонный экран работает в более благоприятных условиях, чем в классической плотине с железобетонным экраном. Это позволяет рекомендовать данный тип плотины для внедрения в практику гидротехнического строительства.

### *Introduction. Task formulation*

The necessity to enhance safety of embankment dams makes search for their new structural solutions, including new structural designs of their seepage-control elements.

Among the not-natural (rock or soil) seepage-control elements of the embankment dam body the reinforced concrete face is considered to be the most promising today. The height of constructed rockfill dams with reinforced concrete faces already exceeded 230 m. However, at some of these dams emergency situations occurred, where cracks appeared in the face [1–8]. One of the causes for crack formation is tensile stresses in the face. Tension may occur due to bending deformation [3], as well as due to longitudinal tensile deformation [9].

Among seepage-control measures in the earth foundation under earthfill dams the most popular were cut-off walls [1–14]. Design studies show [15], that the stress-strain state of such walls may be

Саинов М.П. Анализ работоспособности каменной плотины с комбинацией противофильтрационных элементов – железобетонного экрана и глиноцементобетонной стены // Инженерно-строительный журнал. 2016. №4 (64). С. 3–9.

favorable, if they are made of clay-cement. Under the dam dead weight the foundation soil settles and presses the seepage-control wall, which prevents development of tensile stresses. Recently cut-off walls began to be applied not only in foundations of earthfill dams but as seepage-control elements of the dam body [16, 17].

In case the construction of a rockfill dam is planned on a thick layer of the earth, it is reasonable to consider the dam alternative, where in the dam body the seepage-control element is presented by a reinforced concrete face and in the structure foundation is like a cut-off wall. This is an earthfill dam with a combined seepage-control element.

This article deals with the analysis of workability of such a dam based on the stress-strain state (SSS) analysis.

### Description of the structure under study

There was considered a 87 m high rockfill dam located on a 22.5 m thick layer of the gravel-pebble soil (Fig. 1). The dam body is made of rock mass. The adopted seepage-control element in the earth foundation is a clay-cement wall constructed by the bored pipe wall method. Besides, this wall is a seepage-control element of the upstream cofferdam being part of the dam body. The total depth of the wall is 51 m. In the upper part of the dam the seepage-control element is presented by a 0.5 m thick reinforced concrete face.

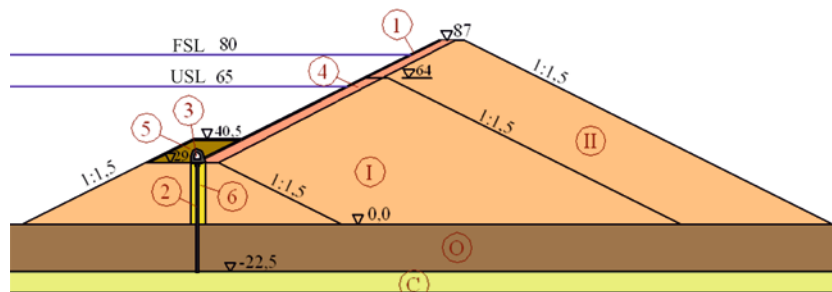


**Figure 1. Design of the earthfill dam under study**

I, II – rockfill dam construction stages, O – earth foundation layer, C – rock foundation, 1 – reinforced concrete face, 2 – cut-off wall, 3 – reinforced concrete gallery, 4 – under-face zone, 5 – filling low-permeable soil, 6 – gravel-sand core in the upstream cofferdam body

There is a gallery arranged at the interface of the reinforced concrete face and the wall. The gallery is located above the top part of the wall, however, the wall does not abut the gallery to provide free settlements of the gallery.

Studies of the dam SSS were conducted by numerical modeling using the finite element method.

Quadrilateral finite elements were used to describe the continuous medium behavior. Contact elements of zero thickness were used to model the contact behavior of earth structures between each other. The numerical model consisted of 721 finite elements (out of which 66 are contact elements), and 746 corner nodes. All the finite elements had a cubic function of displacement approximation. The total number of degrees of freedom in the numerical model was 7222.

Analyses were conducted with the NDS-Ncomputer program developed by Sainov M.P. at the Chair of Hydraulic Engineering of Moscow State Civil Engineering University [18]. This permitted considering non-linearity of soil behavior, as well as non-linearity of interaction of earth structures with each other and with soil mass. The modified soil model proposed by Rasskazov L.N. was used to consider non-linear deformation of soils [19, 20]. Coulomb model was used to assess shear strength of contacts. The face reinforced concrete and the cut-off wall material in the analysis were assumed to be elastic. Deformation modulus of reinforced concrete was assumed equal to 29000 MPa (Poisson's ratio  $\nu = 0.18$ ). Deformation modulus of clay-cement was assumed equal to 100 MPa (Poisson's ratio  $\nu = 0.2$ ). The clay-cement had such a Deformation modulus that its composition should include 120...140 kg of bentonite and 120...160 kg of cement [15].

Analyses were conducted allowing for the staged dam construction. At the first stage the upstream cofferdam and the dam foundation should be constructed. Then a seepage-control wall is constructed in the gravel-sand core of the cofferdam and then a gallery above it. The first-stage CFRD is constructed

under protection of the cofferdam (to  $\nabla$  69 m). Afterwards the reservoir is filled to  $\nabla$  65 m. Then the second-stage dam is constructed and the reservoir is filled to  $\nabla$  80 m.

Technological features of constructing seepage-control structures were also taken into account. The arrangement of the cut-off wall was modeled by replacing one material (gravel-sand soil) in the structure model with another (clay-cement). However, it was taken into account that the wall clay-cement takes up the dead weight in the non-hardened state. Its Poisson's ratio is taken equal to 0.45, and the deformation modulus is 20 MPa. Clay-cement took up other loads after gaining strength. A reinforced concrete face was constructed fully for the whole height of the dam stage after the completion of its filling.

Totally 52 steps of the analysis were considered and each step was characterized by modeling parts of the structure or occurring a new load.

### Analysis results

Figures 2–8 show the results of the earthfill dam SSS analysis with a cut-off wall and a reinforced concrete face for two moments of time. The first one is before the second-stage reservoir filling, the second after the completion of construction and the reservoir filling to  $\nabla$  80 m. In the figures the red curves correspond to the first moment of time, the green ones – to the second.

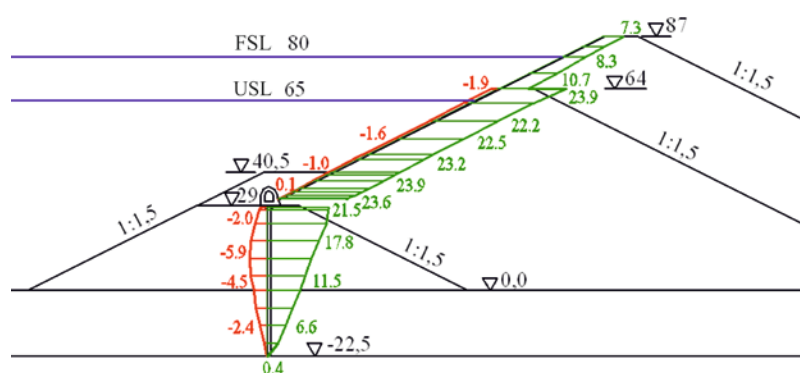
The analyses showed that main displacements and settlements occurred in the reinforced concrete face and the wall after the reservoir filling. The character of settlement distribution of the reinforced concrete face and that of the wall is different. Nearly the uniform distribution pattern during construction stages is peculiar for the reinforced concrete face. For example, horizontal displacements of the second-stage dam face are in the range of 22.2  $\div$  23.9 cm (Fig. 2), and settlements – 12.2...15.6 cm (Fig. 3).

Figure 4 shows the face displacements in the direction to normal. The shape of the curve (Fig. 4) evidences that the face bending deformations are not large. Bending occurs only in the zone of abutment to the concrete gallery and that of the first-stage dam crest. In the first case the bend occurs toward the downstream side, in the second – towards the upstream side.

Figure 5 shows the face longitudinal displacements, i.e. the displacements are directed along the slope. After the reservoir filling these displacements are directed from the face foot to the dam crest. They reach 15 cm. The occurrence of such displacements is caused by the fact that the face horizontal displacements have a larger value than their settlements. As in the lower part of the face the longitudinal displacements are somewhat larger than in the upper part, the face is subject to a pressing longitudinal force.

The wall displacement distribution pattern is determined by locking its lower end by the rock foundation. The wall foot displacements and settlements are actually equal to 0. Maximum wall displacements and settlements are observed in their top part. At the moment of the end of reservoir filling the top maximum displacement amounted to 21.5 cm (Fig. 2). The shape of the displacement curve is close to linear, which evidences about low development of bending deformations.

Maximum displacements of the wall top amounted to 41.2 cm (Fig. 3). A large value of settlements is explained by the fact that they are caused by the wall dead weight when clay-cement is in a semi-liquid state. Settlements of the top under the impact of other loads accounted for only 15.5 cm, i.e. nearly similar to the concrete gallery settlements (16 cm).



**Figure 2. Horizontal displacements (cm) of dam seepage-control elements**  
**Red color indicates displacements before the reservoir filling.**  
**Green color indicates displacements at the reservoir filling to  $\nabla$  80 m**

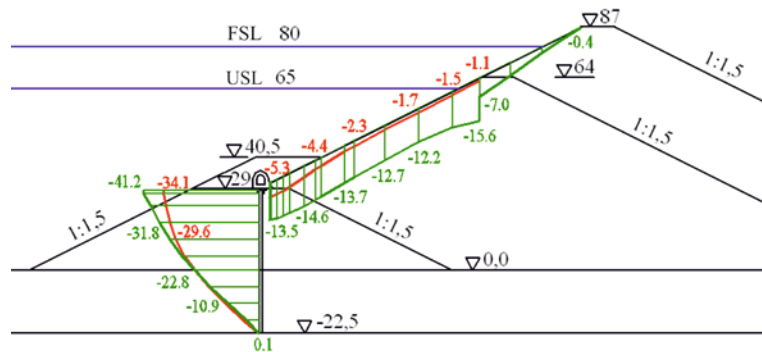


**Figure 3. Settlements (cm) of dam seepage-control elements**

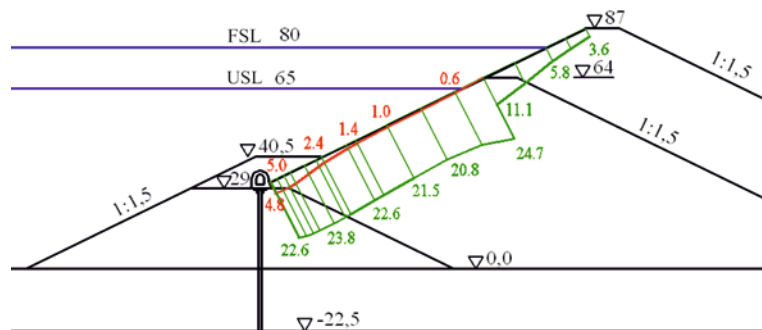


**Figure 4. Reinforced concrete face displacements (cm) in the direction perpendicular to the slope**

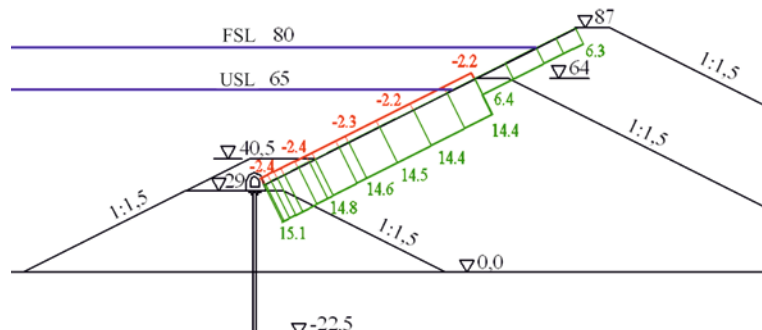


**Figure 5. Reinforced concrete face displacements (cm) in the direction along the slope**

It is interesting that displacements in the zone of the reinforced concrete face interface with the gallery: displacements in the perimeter joint. At the reservoir filling the perimeter joint opens for 0.4 mm. The value of shear displacements in the joint is considerably larger – 2.9 mm. Such deformations are not dangerous for the joint tightness: they may be perceived by water stops.

Figures 6–7 shows the distribution of stresses in the reinforced concrete face. Stresses in the direction across the slope are formed by water hydrostatic pressure; they are not large. Stresses in the direction along the slope are determined by a character of deformation distribution of the face and rock fill under it. Before the reservoir filling the zones of tensile longitudinal stresses are formed due to bending in the face. At the upstream face they reach 2.08 MPa (Fig. 6), at the downstream face they are 2.98 MPa (Fig. 7). These stresses may be taken up by reinforcement.

After the reservoir filling the compressive longitudinal deformations compensate tensile stresses in the face, therefore the face SSS becomes more favorable. The upstream face is compressed by longitudinal stresses actually for the whole length (Fig. 6). Compressive stresses reach 7.14 MPa. Not large tensile longitudinal stresses are connected with face local bending deformations. On the downstream face there are only compressive longitudinal stresses (Fig. 7); they do not exceed 4.3 MPa. However, in the zone where the face abuts the concrete gallery there formed the zone of compressive stress concentration equaling up to 12.8 MPa.

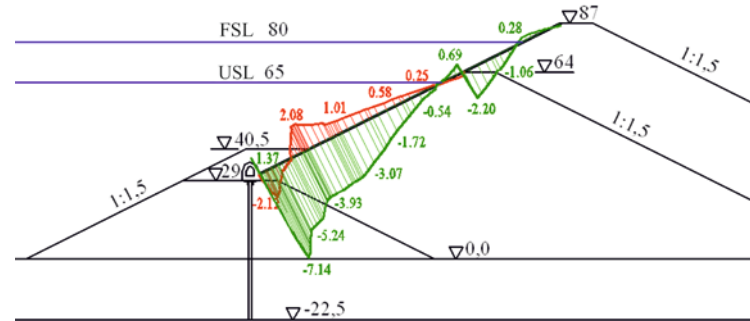


**Figure 6. Stresses (MPa) on the upstream face of the reinforced concrete face in the direction along the face**

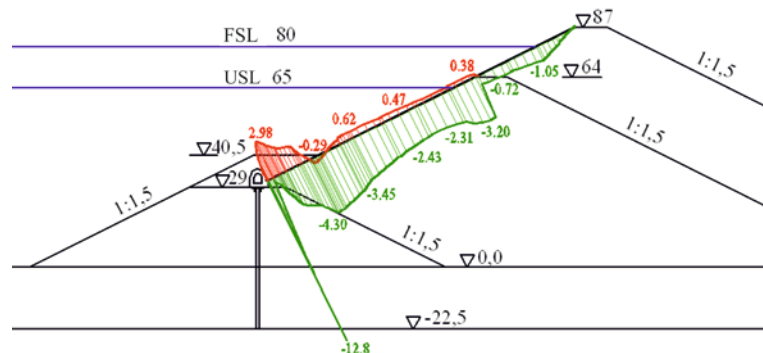


**Figure 7. Stresses (MPa) on the downstream face of the reinforced concrete face in the direction along the face**

The seepage-control wall has favorable SSS: it is compressed from all sides. The maximum level of compression is observed in a vertical direction by stresses  $\sigma_y$  (Fig. 8). This is explained by the fact that the soil surrounding the wall settles under the weight of the earthfill dam and also compresses the wall. Stresses  $\sigma_y$  are distributed heightwise uniformly. Compression deformations prevail over bending deformations, therefore, stresses vary slightly within the thickness of the wall. The maximum value of compressive stresses  $\sigma_y$  in the wall amounts to 1.1 MPa. It is less than the clay-cement uniaxial compression strength, and it is equal to 1.27 MPa at  $E = 100$  MPa [15, 21].

Opening the wall contact with the rock foundation occurs for the length of 20 cm, which comprises only 1/6 of the wall thickness.

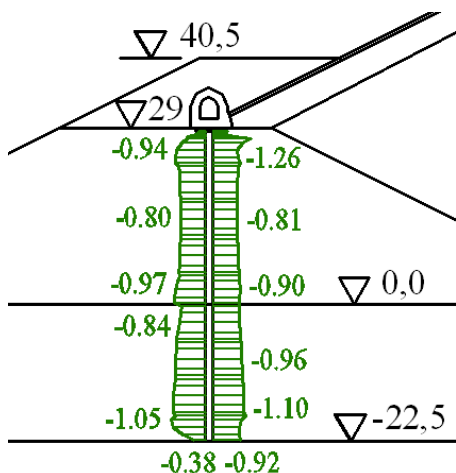


**Figure 8. Stresses  $\sigma_y$  (MPa) on the faces of the seepage-control wall**

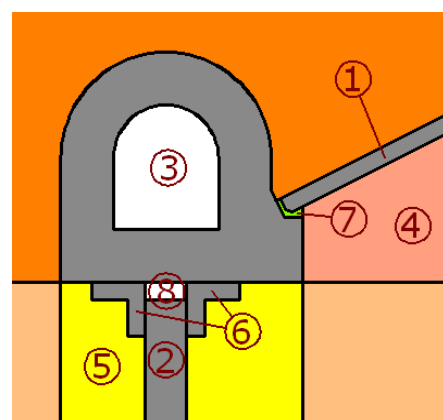


**Figure 9. Scheme of conjugation for seepage-control elements 1 – reinforced concrete face, 2 – wall, 3 – gallery, 4 – under-face zone, 5 – sand core, 6 – foreshaft, 7 – filling the perimeter joint, 8 – air cavity**

Thus, in the considered dam design both seepage-control elements are in a favorable stress state: they are compressed, but the compression level is not large. Compressive strengths may be disturbed only in the interface zone of the reinforced concrete face and the gallery, where stresses are concentrated up to 12.8 MPa. There is a danger of cleavage of the thin face corner, which can lead to the seal failure of the perimeter joint.

To prevent the concentration of compressive stresses in the reinforced concrete face, the interface of the reinforced concrete face with the concrete gallery may be provided in the form of soft hinged connection (Fig. 9).

### Conclusion

1. On the whole, the design of the high earthfill dam with two combined seepage-control elements (a reinforced concrete face and a clay-cement cut-off wall) is favorable and safe. In dam displacements under the impact of hydrostatic pressure the seepage-control elements have free displacements not subjected to strong bending deformations. The connecting gallery plays the role of a hinge. On the one hand, it preserves connection of seepage-control elements; on the other hand, it compensates possible bending deformations.

In the considered structural design both seepage-control elements are in a favorable stress state: they are compressed actually in all the sections. The connection points of the seepage-control elements with the connecting gallery work reliably: displacements in the joints are not large; their tightness may be usually provided by the used seals.

2. The only disadvantage of the considered design is the concentration of compressive stresses on the downstream surface of the reinforced concrete face in the interface zone with the gallery. To cope with this disadvantage, it is proposed to make a soft connection between the face and the gallery filling the perimeter joint with a soft polymer material.

### References

1. ICOLD. «Concrete Face Rockfill dam: Concepts for design and construction». International Commission on Large Dams. Bulletin 141. 2010. 401 p.
2. Cooke J.B., Sherard J.L. In Proceedings of the 2nd Symposium on Concrete Face Rockfill Dams: Design, Construction, and Performance. Detroit, Mich. October 1985. American Society of Civil Engineers (ASCE). New York. Pp. 1–658.
3. Markes F.P., Pinto N. de S. Kharakteristiki kamenno-nabrosnykh plotin s betonnym ekranom, poluchennyye opytnym putem [Features concrete faced rockfill dam, obtained by experience]. Mezhdunarodnyy daydzhest po gidroenergetike i plotinam. 2007. Pp. 69–74. (rus)
4. Manoel S., Freitas Jr. Concepts on CFRDs Leakage Control – Cases and Current Experiences. Inter. Society for Soil Mechanics and Geotechnical Engineering, 2009, Vol.3. Issue 9. Pp. 11–18.
5. Song W, Sun Y, Li L, Wang Y. Reason analysis and treatment for the 1st phase slab cracking of Shuibuya CFRD. *Journal of Hydroelectric Engineering*. 2008. No. 3(27). Pp. 33–37.
6. Yifeng Chen, Ran Hu, Wenbo Lu, Dianqing Li, Chuangbing Zhou. Modeling coupled processes of non-steady seepage flow and non-linear deformation for a concrete-faced rockfill dam. *Computers and Structures*. 2011. Vol. 89. Pp. 1333–1351.
7. Mokhtar Pour, E., Freitas Jr., M.S. Rehabilitation for high concrete faced rockfill dam (CFRD): Availability and vulnerability Dam Maintenance and Rehabilitation II. *Proceedings of the 2nd International Congress on Dam Maintenance and Rehabilitation*. Zaragoza, Spain. 2011. Pp. 881–887.
8. De Pinto N.L.S. Very high CFRDs: Behaviour and design features. *International Journal on Hydropower and Dams*. 2008. No. 15(4). Pp. 43–49.
9. Sainov M.P. Vliyanie deformiruyemosti kamennoy nasypy na napryazheno-deformirovannoye sostoyaniye zhelezobetonного экрана плотины // Вестник МГСУ.

Sainov M.P. Analysis of normal operation of a rockfill dam with combination of seepage-control elements: reinforced concrete face and a clay-cement-concrete wall. *Magazine of Civil Engineering*. 2016. No. 4. Pp. 3–9. doi: 10.5862/MCE.64.1

### Литература

1. ICOLD. «Concrete Face Rockfill dam: Concepts for design and construction». International Commission on Large Dams. Bulletin 141. 2010. 401 p.
2. Cooke J.B., Sherard J.L. In Proceedings of the 2nd Symposium on Concrete Face Rockfill Dams: Design, Construction, and Performance. Detroit, Mich. October 1985. American Society of Civil Engineers (ASCE). New York. Pp. 1–658.
3. П. Маркес Фильо, Н. де С. Пинто Характеристики каменно-набросных плотин с бетонным экраном, полученные опытным путем // Международный дайджест по гидроэнергетике и плотинам. 2007. С. 69–74.
4. Manoel S., Freitas Jr. Concepts on CFRDs Leakage Control – Cases and Current Experiences // Inter. Society for Soil Mechanics and Geotechnical Engineering. 2009. Vol.3. Issue 9. Pp. 11–18.
5. Song W, Sun Y, Li L, Wang Y. Reason analysis and treatment for the 1st phase slab cracking of Shuibuya CFRD. *Journal of Hydroelectric Engineering*. 2008. No. 3(27). Pp. 33–37.
6. Yifeng Chen, Ran Hu, Wenbo Lu, Dianqing Li, Chuangbing Zhou. Modeling coupled processes of non-steady seepage flow and non-linear deformation for a concrete-faced rockfill dam // *Computers and Structures*. 2011. Vol. 89. Pp. 1333–1351.
7. Mokhtar Pour, E., Freitas Jr., M.S. Rehabilitation for high concrete faced rockfill dam (CFRD): Availability and vulnerability Dam Maintenance and Rehabilitation II // *Proceedings of the 2nd International Congress on Dam Maintenance and Rehabilitation*. 2011. Pp. 881–887.
8. De Pinto N.L.S. Very high CFRDs: Behaviour and design features // *International Journal on Hydropower and Dams*. 2008. No. 15 (4). Pp. 43–49.
9. Сайнов М.П. Влияние деформируемости каменной насыпи на напряженно-деформированное состояние железобетонного экрана плотины // Вестник МГСУ.

- zhelezobetonnogo ekrana plotiny [Impact of Rockfill Deformation on Stress-Strain State on Dam Reinforced Concrete Face]. *Vestnik MGSU*. 2015. No. 3. Pp.69–78. (rus)
10. Mirghasemi A.A., Pakzad M., Shadravan B. The world's largest cutoff wall at Karkheh dam. *Hydropower & Dams*. Issue 2. 2005. Pp.2–6.
  11. Ehrhardt T., Scheid Y., El Tayeb A. Entwurf und ausfuhrung der steinschuttdamme und der schlitzwand des Merowe-Projektes. *WasserWirtschaft*. 2011. No. 101 (1–2). Pp. 36–42.
  12. Balian S. Cut-off wall construction. International. *Water Power and Dam Construction*. 2007. No. 59 (2). Pp. 42–44.
  13. Noll H., Langhagen K., Popp M., Lang T. Ertuchtigung des Sylvenstein-Staudamms – Planung und Ausfuhrung der Dichtwand. *WasserWirtschaft*. 2015. No. 103(5). Pp. 76–79.
  14. Baranov A.Ye. Iz opyta proyektirovaniya i stroitelstva Yumaguzinskogo gidrouzla na r.Belyy [The Experience of Designing and Building Yumagusinskiy Hydroelectric Complex on the River Belya]. *Vestnik MGSU*. 2006. No. 2. Pp.112–122. (rus)
  15. Sainov M.P. Prostranstvennaya rabota protivofiltratsionnoy steny [3D performance of a seepage control wall in dam and foundation]. *Magazine of Civil Engineering*. 2015. No. 5(57). Pp.20–33. (rus)
  16. Radchenko V.G., Lopatina M.G., Nikolaychuk Ye.V., Radchenko S.V. Optyt vozvedeniya protivofiltratsionnykh ustroystv iz gruntotsementnykh smesey [Experience in construction of impervious devices from soil-cement mixtures]. *Gidrotekhnicheskoye stroitelstvo*. 2012. No. 12. Pp.46–54. (rus)
  17. Malyshev L.I., Shishov I.N., Kudrin K.P., Bardukov V.G. Tekhnicheskiye resheniya i rezulaty pervochedernykh rabot po sooruzheniyu protivofiltratsionnoy steny v grunte v yadre i v osnovanii plotiny Kureyskoy GES [Technical Solutions and Working Results in the Process of Building Filtration-proof Wall in the Soil of the Core and Foundation of Kureyskaya Water Power Plant]. *Gidrotekhnicheskoye stroitelstvo*. 2001. No. 3. Pp. 31–36. (rus)
  18. Sainov M.P. Vychislitel'naya programma po raschetu napryazhенно-deformirovannogo sostoyaniya gruntovykh plotin: optyt sozdaniya, metodiki i algoritmy [Computer program for the calculation of the stress-strain state of soil dams: the experience of creation, techniques and algorithms]. *International Journal for Computational Civil and Structural Engineering*. 2013. No. 9(4). Pp. 208–225. (rus)
  19. Goldin A.L., Rasskazov L.N. *Proyektirovaniye gruntovykh plotin* [Design of earthfill dams]. Moscow. ASV. 2001. 375 p. (rus)
  20. Sainov M.P. *Parametry deformiruyemosti krupnoblomochnykh gruntov v tele gruntovykh plotin* [Deformation Parameters of Macrofragment Soils in Soil Dams]. Sistem requirements: AdobeAcrobatReader. URL: [http://www.nso-journal.ru/public/journals/1/issues/2014/02/2\\_Sainov.pdf](http://www.nso-journal.ru/public/journals/1/issues/2014/02/2_Sainov.pdf) (date of application: 14.03.2016). (rus)
  21. Rasskazov L.N., Radzinsky A.V., Sainov M.P. Prochnost i deformiruyemost glinozemtobetona v slozhnom napryazhennom sostoyanii [Deformation Parameters of Macrofragment Soils in Soil Dams]. *Gidrotekhnicheskoye stroitelstvo*. 2014. No. 8. Pp. 29–33. (rus)
  2015. № 3. С. 69–78.
  10. Mirghasemi A.A., Pakzad M., Shadravan B. The world's largest cutoff wall at Karkheh dam // *Hydropower & Dams*. Issue 2. 2005. Pp. 2–6.
  11. Ehrhardt T., Scheid Y., El Tayeb A. Entwurf und ausfuhrung der steinschuttdamme und der schlitzwand des Merowe-Projektes // *WasserWirtschaft*. 2011. No. 101 (1–2). Pp. 36–42.
  12. Balian S. Cut-off wall construction // *International Water Power and Dam Construction*. 2007. No. 59(2). Pp. 42–44.
  13. Noll H., Langhagen K., Popp M., Lang T. Ertuchtigung des Sylvenstein-Staudamms - Planung und Ausfuhrung der Dichtwand // *WasserWirtschaft*. 2015. No. 103(5). Pp. 76–79.
  14. Баранов А.Е. Из опыта проектирования и строительства Юмагузинского гидроузла на р.Белой // Вестник МГСУ. 2006. №2. С. 112–122.
  15. Саинов М.П. Пространственная работа противофильтрационной стены // Инженерно-строительный журнал. 2015. №5(57). С. 20–33.
  16. Радченко В.Г., Лопатина М.Г., Николайчук Е.В., Радченко С.В. Опыт возведения противофильтрационных устройств из грунтоцементных смесей. // Гидротехническое строительство. 2012. №12. С. 46–54.
  17. Малышев Л.И., Шишов И.Н., Кудрин К.П., Бардюков В.Г. Технические решения и результаты первоочередных работ по сооружению противофильтрационной стены в грунте в ядре и в основании плотины Курейской ГЭС // Гидротехническое строительство. 2001. №3. С. 31–36.
  18. Саинов М.П. Вычислительная программа по расчёту напряжённо-деформированного состояния грунтовых плотин: опыт создания, методики и алгоритмы // *International Journal for Computational Civil and Structural Engineering*. 2013. No. 9(4). Pp. 208–225.
  19. Гольдин А.Л., Рассказов Л.Н. Проектирование грунтовых плотин. Изд. 2-е, перераб. и доп. М.: ACB. 2001. 375 с.
  20. Саинов М.П. Параметры деформируемости крупнообломочных грунтов в теле грунтовых плотин [Электронный ресурс]. Систем. требования: Adobe Acrobat Reader. URL: [http://www.nso-journal.ru/public/journals/1/issues/2014/02/2\\_Sainov.pdf](http://www.nso-journal.ru/public/journals/1/issues/2014/02/2_Sainov.pdf) (дата обращения: 14.03.2016).
  21. Рассказов Л.Н., Радзинский А.В., Саинов М.П. Прочность и деформируемость глиноцементобетона в сложном напряженном состоянии // Гидротехническое строительство. 2014. № 8. С. 29–33.

Mikhail Sainov,  
+7(926)6078931; mp\_sainov@mail.ru

Михаил Петрович Саинов,  
+7(926)6078931; эл. почта: mp\_sainov@mail.ru

© Саинов М.П., 2016

doi: 10.5862/MCE.64.2

## Thermophysical field testing of residential buildings made of autoclaved aerated concrete blocks

### Натурные теплофизические испытания жилых зданий из газобетонных блоков

**S.V. Korniyenko,**

*Volgograd State University of Architecture and Civil Engineering, Volgograd, Russia*

**N.I. Vatin,**

**A.S. Gorshkov,**

*Peter the Great St. Petersburg Polytechnic University, St. Petersburg, Russia*

**Канд. техн. наук, доцент С.В. Корниенко,**

*Волгоградский государственный архитектурно-строительный университет, Волгоград, Россия*

**д-р техн. наук, директор Инженерно-**

**строительного института Н.И. Ватин,**

**канд. техн. наук, доцент кафедры**

**"Строительство уникальных зданий и сооружений" А.С. Горшков,**

*Санкт-Петербургский политехнический*

*университет Петра Великого, Санкт-*

*Петербург, Россия*

**Key words:** buildings; construction; energy efficiency; civil engineering; autoclaved aerated concrete; thermophysical field testing; heat monitoring; thermogram

**Ключевые слова:** здания; конструкция; энергетическая эффективность; строительство зданий и сооружений; автоклавный газобетон; натурные теплофизические испытания; тепловизионный контроль; термограмма

**Аннотация.** Объектом исследования является группа однотипных многоквартирных жилых зданий, расположенных на территории Волгоградской области (Россия, 48°с.ш.). Оценка соответствия уровня тепловой защиты зданий требованиям СП 50.13330.2012 выполнена на основе натурных теплофизических испытаний с применением экологически безопасных методов неразрушающего контроля. По результатам натурных теплофизических испытаний жилых зданий из газобетонных блоков установлено следующее. Проектирование двухслойных наружных стен в виде кладки автоклавных газобетонных блоков с наружной облицовкой кирпичной кладкой несет теплотехнические риски, связанные с увеличением неравноэффективности теплозащиты оболочки зданий, обусловленным существенным влиянием на теплозащиту зданий краевых зон. Проектный уровень теплоизоляции указанных конструкций не соответствует базовому уровню теплозащиты для большинства регионов Российской Федерации. Двухслойные наружные стены без дополнительной теплоизоляции практически не имеют резерва по тепловой защите и энергосбережению. Снижение фактического уровня теплоизоляции ограждающих конструкций по сравнению с проектным обусловлено как несанкционированными отступлениями от проекта, допущенными подрядчиком в ходе строительства, так и некачественным выполнением строительно-монтажных работ. С целью снижения теплотехнических рисков при проектировании рассматриваемых зданий следует, прежде всего, совершенствовать конструктивное решение краевых зон оболочки. Другим мероприятием для повышения уровня теплозащиты зданий является применение дополнительной теплоизоляции по всей плоскости стены.

**Abstract.** The object of investigation is one-type neighbouring blocks of flats located in Volgograd region (Russia, N 48°). Thermophysical field testing using eco-friendly nondestructive test methods was carried out to estimate whether the level of heat protection in buildings meets requirements of the Russian construction norms SP 50.13330.2012. According to the results of thermophysical field tests of residential buildings made of autoclaved aerated concrete blocks, the following was found out. Design of double-layer exterior walls in the form of AAC blocks with front brick masonry bears thermotechnical risks due to an increase in non-uniform heat protection of buildings' covers caused by a significant impact on heat protection of buildings' edge zones. The designed level of heat insulation does not conform to the basic level of heat protection for the majority of regions in the Russian Federation. Two-layer exterior walls without supplementary insulation practically do not have heat protection and energy saving reserves. The reduction of the actual insulation in envelopes, compared to the designed one, can be

explained by both unapproved deviations from the design project made by a subcontractor during construction and low-quality construction and assembly work. It is strongly suggested to improve the structural solution of edge zones in envelopes to reduce thermotechnical risks when designing buildings. Supplementary insulation along the surfaces of the walls can be considered as another activity to increase heat protection.

### *Introduction*

Nowadays, autoclaved aerated concrete is widely used in residential construction throughout the Russian Federation. According to statistic data available in reference books, the share of autoclaved aerated concrete blocks used on the Russian construction market can be compared with insulating fire bricks [1]. Autoclaved aerated concrete is primarily applied as a structural and insulating material. The widespread use of autoclaved aerated concrete elements is due to high consumer properties of AAC blocks [2–6]:

- raw materials availability;
- low fire hazard and high fire-resistance;
- high-fidelity products;
- masonry manufacturability and high work performance;
- low-cost product.

Strength properties and service performance of autoclaved aerated concrete are thoroughly studied [7–21]. Research findings for mechanical properties of autoclaved aerated concrete are given in the articles [7–10]. Methods to improve thermotechnical properties of AAC-products are described in the articles [10–15]. Humidity conditions of AAC exterior walls and the impact on insulating properties of envelope constructions have been studied in the articles [16–18]. Thermotechnical defects of exterior walls made of autoclaved aerated concrete are assessed in the articles [19, 20]. Mathematical models and methods to estimate heat performance of envelopes with thermotechnical inhomogeneous sections (edge zones) are considered in the articles [21–24]. Results of measuring moisture production caused by various sources are described in the article [25].

However, there are not enough findings about thermophysical field testing of buildings made of autoclaved aerated concrete in the references considered. Thermophysical field testing of buildings requires costly equipment, has high labour intensity and implies a relevant qualification of workers. There is an urgent need for thermophysical field testing to be conducted in residential buildings made of autoclaved aerated concrete due to unavailability of experimental data on temperature distribution inside and outside thermally insulated building enclosures, resistance to heat transfer of envelopes, structure of heat loss through envelopes in the cold season.

An object to be tested is one-type neighbouring blocks of flats located in Volgograd region (Russia, N 48°). Average monthly outside air temperature in January is equal to  $-6.9^{\circ}\text{C}$ , in July is  $23.9^{\circ}\text{C}$ . The humid area is 3 (dry). Each three-story double-section building under consideration has a basement and an attic (Figure 1). Buildings were constructed in 2011. There were stabilized humidity conditions while conducting thermotechnical tests.



**Figure 1. General view of neighbouring buildings**

The standard type of building construction B1.020.1–7 (“ARKOS–1”) designed in the republic of Belarus was taken as a design solution for constructing the buildings mentioned herein. Geometric characteristics of buildings are given in Table 1.

**Table 1. Geometric characteristics of buildings**

Performance feature	Subscript, measurement unit	Value
Total area of envelopes including:		
exterior walls	$A_{sum}$ , $\text{m}^2$	2729
windows, balcony doors	$A_w$ , $\text{m}^2$	1077
attic slab	$A_F$ , $\text{m}^2$	256
slabs over basement	$A_c$ , $\text{m}^2$	698
	$A_b$ , $\text{m}^2$	698
Heated volume	$V_h$ , $\text{m}^3$	6073
Building compactness	$k_e$ , 1/m	0.449
Coefficient of glazing for facades	$k_F$	0.192

The major structural feature of the project is that functions of load-bearing structures and envelopes are separated.

The load-bearing base of the system “ARKOS–1” is a braced-frame precast framework with flat slab plates formed by hollow-core units. The hollow-core units in each slab are joined with solid-cast reinforced girders hidden inside the slabs and supported by precast columns. In order to reduce the heat loss in the cold season, the girders have perforation holes filled with polystyrene-foam heat-insulating inserts and arranged along external contours. Heat-insulating covering of buildings consists of different types of envelopes. Walls are constructed in the form of masonry made of autoclaved aerated concrete blocks with internal plaster and external facing of brick masonry (Figure 1). The walls are floor-by-floor supported by slab plates. Brick masonry is connected to autoclaved aerated concrete blocks using flexible ties. Double-pane windows and balcony doors are made of PVC profiles. Attic slabs and slabs over the basement are thermally insulated.

Buildings are operated under conditions of the moderately continental climate of Russia. The estimated value of heating degree days HDD 20/8 = 3925 K days/year.

There is a centralized heat supply. The source of the centralized heat supply is a boiler-house which has parameters of a heat carrier for heating 95–70 °C. All buildings are naturally ventilated. Air intake is secured through the regulated window casement in living rooms and kitchens; air recovery is carried out through the exhaust ventilation in kitchens and sanitary facilities. In order to reduce energy costs in buildings, individual heat supply stations are placed in basements. Engineering systems of buildings are equipped with metering devices for heat energy, cold and hot water, electric power and gas.

While conducting thermotechnical testing, the service life of buildings amounts to 5 years.

Adding a group of buildings into the object under research makes it possible to increase validity of the research data and apply results for a wider group of buildings with a similar architectural and structural design.

## Methods

The following characteristics to estimate heat protection levels in buildings are taken in Russian construction regulations: specific resistance to heat transfer of envelopes, specific heat-protection characteristic of a building, and internal surface temperature of envelopes.

Specific resistance to heat transfer of envelopes is a physical value which features – an area-averaged heat-flow density through a fragment of the heat-protective building covering under steady-state conditions of heat transfer, which is equal to the ratio of the difference between temperatures of opposing sides of the fragment to the area-averaged heat-flow density through the fragment.

A specific heat-protection characteristic of the building is a physical value which is equal to the heat loss of a volume unit per time unit provided there is temperature drop of 1 K through the heat-protective building cover.

Thermophysical field testing using eco-friendly nondestructive test methods was carried out to estimate whether the level of heat protection in buildings meets requirements of the Russian construction norms SP 50.13330.2012. The following NDT methods were used:

- heat monitoring to estimate quality of heat insulation in buildings;
- determination of an actual level of heat protection in buildings;
- estimating a level of heat protection in buildings.

### *Heat monitoring to estimate quality of heat insulation in buildings*

Heat monitoring to asses heat insulation quality in buildings under consideration was carried out with the aim to find out temperature anomalies and defects of heat-protective buildings' covers under natural conditions.

The method of heat monitoring to asses heat insulation quality in buildings is based on distance measuring of temperature fields on envelope surfaces using an IR imager. The method is used to visualize temperature anomalies and find out defects in the form of areas with higher than usual heat loss due to heat insulation, and identify sections on internal surfaces of envelopes while in service which temperature may go down below dew point as well.

Heat monitoring of the object was carried out in the cold season starting from 14.01.2015 till 10.02.2015 with technical assistance provided by "Promstroyexpertiza" OOO (Ltd) according to GOST P 54852–2011. All the buildings were heated while heat monitoring. The regime of heat transfer through envelopes was close to stationary. Heat monitoring was held in the daytime while there was no wind, atmospheric precipitation, fog and smokiness. While monitoring external surfaces of buildings' covers were not exposed to direct and reflected solar radiation. Thermovision measurements were taken using an IR imager branded as FLIR SC660 (fab. No. 404003616) with meteorological parameters which meet standard requirements.

While heat monitoring the following activities were carried out:

- inspection of the object under control using IR imager to identify general characteristics of the object and find out sections, which are subject to further thermal mapping;
- overall thermal mapping of external surfaces of envelopes to find out temperature anomalies;
- detailed thermal mapping of identified sections on internal surfaces of envelopes to specify temperature anomalies.

186 calibrated thermal images, including 154 ones on external surfaces, were obtained while heat monitoring, which is enough to get statistically valid results.

### *Determination of an actual level of heat protection in buildings*

Thermophysical measurements under natural conditions were carried out to determine an actual level of heat protection in buildings.

The major heat protection of an envelope is an ability to resist to passing heat flow, which is quantified in Russia as resistance to heat transfer  $R_o$ ,  $\text{m}^2 \cdot \text{K/W}$ , and in Europe – heat transfer coefficient  $U_o$  ( $U_o = 1/R_o$ ).

Estimating the specific resistance to heat transfer of building components according to requirements of the Russian construction norms it is necessary to consider all edge zones. Therefore in this case measurements need to be performed on numerous envelope fragments, as it is made in the article.

The method to determine resistance to heat transfer under natural conditions is based on measuring outside and inside air temperature, temperature of envelope surfaces, and passing heat flow density as well (under conditions close to stationary heat transfer), with respect to which an unknown value can be calculated.

Resistance to heat transfer of envelopes' fragments was specified in the cold season according to the Russian standard GOST P 54853–2011 with the parameters given herein. The gist of the method is that meters for temperature and heat flow density are placed on the surfaces and in the area of adjacent air environment of an envelope under test, which fix values of these characteristics during specified time. Resistance to heat transfer of an envelope can be determined as the ratio of the difference between averaged outside and inside air temperatures while testing to an averaged heat flow density passing through an envelope. Measurements are taken using multi-channel meters to measure heat flow density and temperatures of the brand ITP–MG 4.03–10 "Potok" (fab. No. 1177) with meteorological parameters

which correspond to the Russian standards. Measurements in the buildings mentioned were carried out in living areas where there was an access for experts at reference points. Reference points were located on certain sections of envelopes found out while heat monitoring including edge zones. Measurements were taken during two weeks with a registration interval of 5 minutes.

Resistance to heat transfer at a point of heat-protective covers of the buildings was determined by an averaging method according to the Russian standard GOST P 54853–2011 under the formula:

$$R_0 = \frac{\sum_{j=1}^n (t_j^{int} - t_j^{ext})}{\sum_{j=1}^n q_j}, \quad (1)$$

where  $n$  – number of measurements;  $t_j^{int}$ ,  $t_j^{ext}$  – inside and outside air temperatures correspondingly in case of  $j$ -measurement;  $q_j$  – heat flow density in case of  $j$ -measurement.

As it is stated in the regulations of GOST P 54853–2011, when computing the results after each measurement taken the data obtained asymptotically come close to an actual value of thermotechnical characteristics. An asymptotic value is close to an actual one provided the following requirements are met:

- a) temperature, heat capacity and humidity of the fragment under research while measuring;
- b) a heat meter is not directly exposed to solar radiation;
- c) heat transfer of the fragment under test is constant.

Accuracy when measuring thermotechnical characteristics depends on the following factors:

- a) calibration accuracy of a heat meter and temperature sensors (about 5 %);
- b) accuracy of the data recording system (in case of an automated data recording system is close to zero);
- c) random deviations caused by slight differences in heat contact between sensors and surface (about 5 % of an average value);
- d) deviations when using heat meters caused by modifications of isotherms due to availability of a heat meter (2...3 %);
- e) deviations caused by fluctuations of temperatures and heat flow in time (about  $\pm 10$  % of the value measured);
- f) other sources of deviations (if the data are not available – about 5 %).

The values of deviations for this type of measurement devices and regime parameters when conducting tests are given in the brackets.

If the requirements stated above are met then the total deviation can be defined as the one between quadratic and arithmetic sums, i.e. between

$$\Delta_1 = \sqrt{5^2 + 0^2 + 5^2 + 3^2 + 10^2 + 5^2} = 13.6 \% \quad \text{and } \Delta_2 = 5 + 0 + 5 + 3 + 10 + 5 = 28 \%$$

Actually, the double-layer exterior walls in the form of AAC blocks with front brick masonry are air-permeable. Penetration of the indoor damp air into the wall is dangerous in terms of moisture transfer with air and decrease in heat-protection properties. Humidity of the internal air in rooms of the residential operated buildings was within admissible values. During thermophysical testing the moisture in the exterior walls was stabilized. The actual parameters of moisture conditions in rooms conform to required parameters according to the Russian standard (GOST 30494-2011). Inside the face of AAC blocks was plastered; the front brick masonry was flushing. Therefore it is expected that the process of filtering damp air through the exterior wall can be neglected.

### *Estimating level of heat protection in buildings*

Estimation of level of heat protection in buildings can be carried out in a more accurate way provided reduced resistance to heat transfer of envelopes is taken according to computing results of two- and three-dimensional temperature fields [22].

The specified resistance to heat transfer of building component at stationary heat transfer in the most general view is to be defined under the formula:

$$R_o^{red} = \frac{(t_{int} - t_{ext})A}{\int q dA}_{\Omega}, \quad (2)$$

where  $t_{int}$  – estimated inside air temperature in the building;  $t_{ext}$  – estimated outside air temperature in the cold season of the year;  $A$  – area of the envelope along the inner contour;  $\Omega$  – fragment of the envelope;  $q$  – heat flow density in a point of envelope.

Exact calculation of  $R_o^{red}$  on the formula (2) is possible only for the elementary designs. At engineering assessment the specified resistance to heat transfer of envelopes is to be defined under the formula [23]:

$$R_o^{red} = \frac{(t_{int} - t_{ext})A}{Q_{bas} + \sum_{i=1}^m Q_i^{ad}}, \quad (3)$$

where  $Q_{bas}$  is a main heat flow through the envelope under design conditions;  $m$  is a number of edge zones of the envelope;  $Q_i^{ad}$  is a supplementary heat flow through  $i$ -edge zone defined under the temperature field.

Estimating a heat regime of envelopes was carried out with mathematic modeling of the process using programming and computing software "Energy efficiency and heat protection of buildings (ENTEZA)" [22]. Programming and computing software "ENTEZA" makes it possible to estimate the impact of edge zones on heat protection properties of envelopes and outline ways to improve elements of buildings' covers according to computing the temperature fields.

## Results and Discussion

Thermograms, obtained via thermovision, make it possible to explicitly identify temperature anomalies and define defects in edge zones of buildings' envelopes (Figures 2–5).

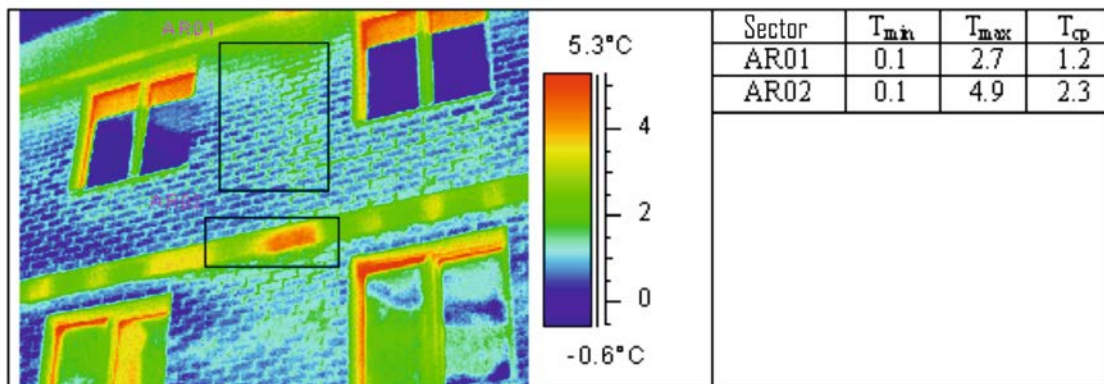


Figure 2. Thermogram of the part of the building's facade

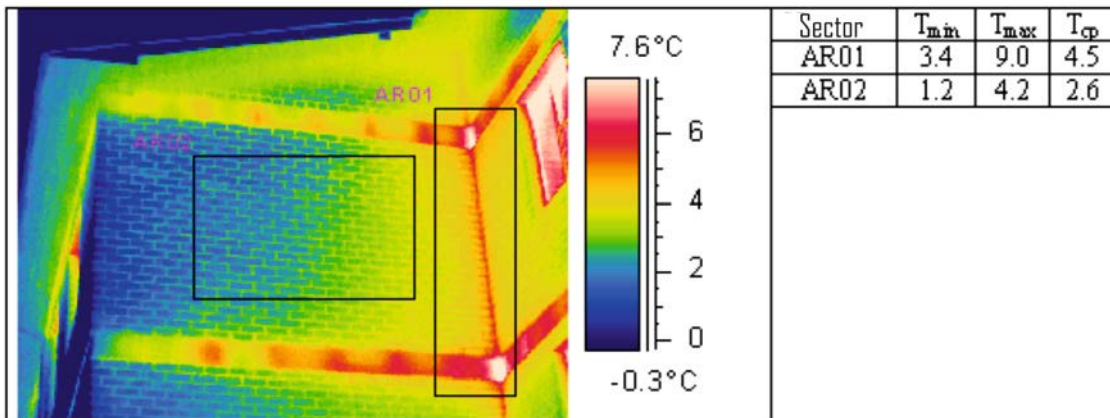


Figure 3. Thermogram of the exterior and reentrant angles

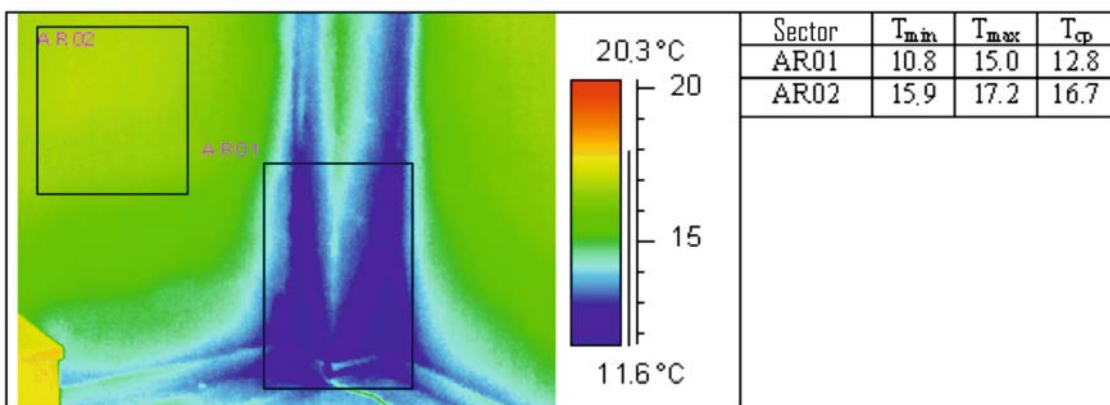


Figure 4. Thermogram of the coupling joint between the walls and the column in the floor area

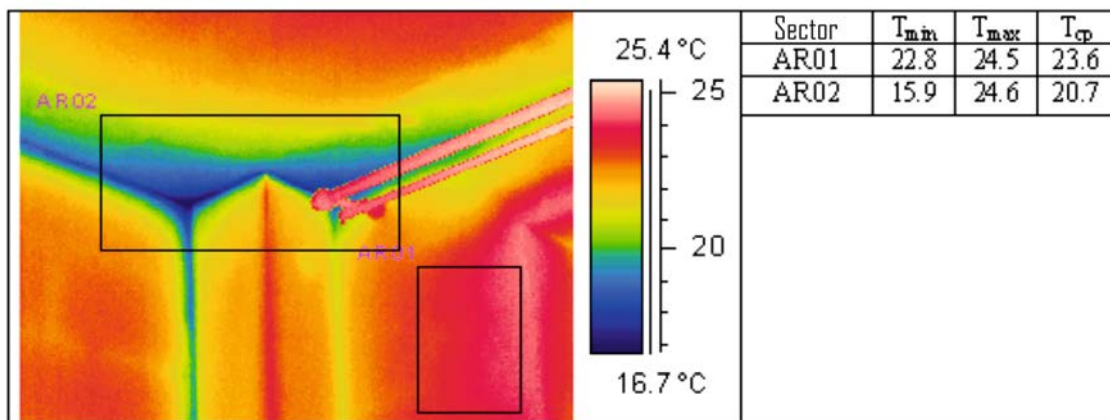


Figure 5. Thermogram of the coupling joint between the walls and the column in the ceiling area

Such an analysis of the thermotechnical defects was made by Kornienko S.V. in his work [20].

Temperature anomalies and defects in the edge zones of envelopes can cause a decrease in temperature on internal surfaces of envelopes (radiant temperature), deterioration of microclimate parameters in the rooms, decline in thermotechnical uniformity of exterior walls, growth of heat loss through covers in the cold season.

Thermovision monitoring results can be featured as valuable information required to correctly estimate the level of heat protection in buildings. They make it possible to choose right edge zones of envelopes to conduct thermotechnical computing.

Measurement results of resistance to heat transfer at different points of heat-protection covers in buildings are shown in Figures 6 and 7.

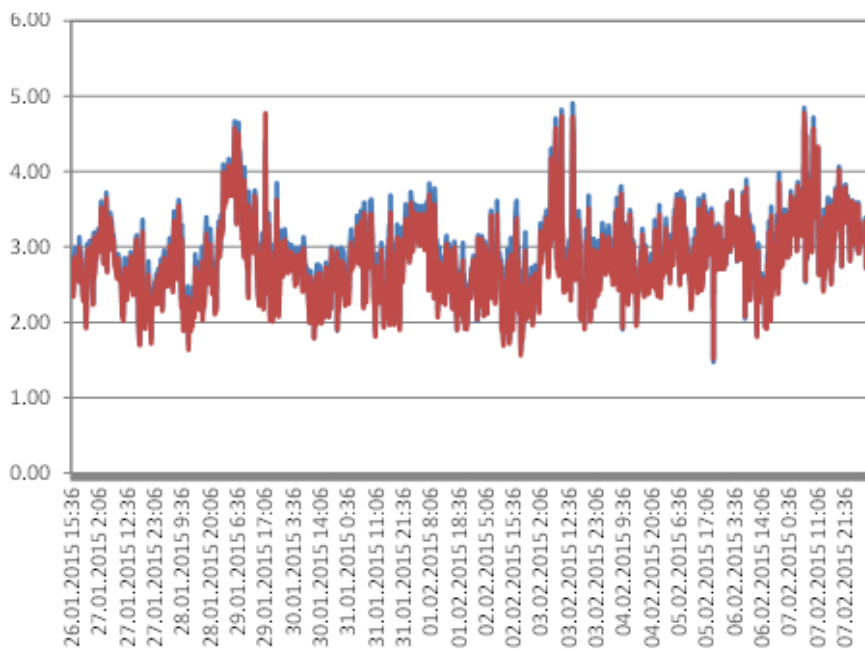


**Figure 6. Measurement results of resistance to heat transfer at the point of exterior wall (building 1, flat 2)**

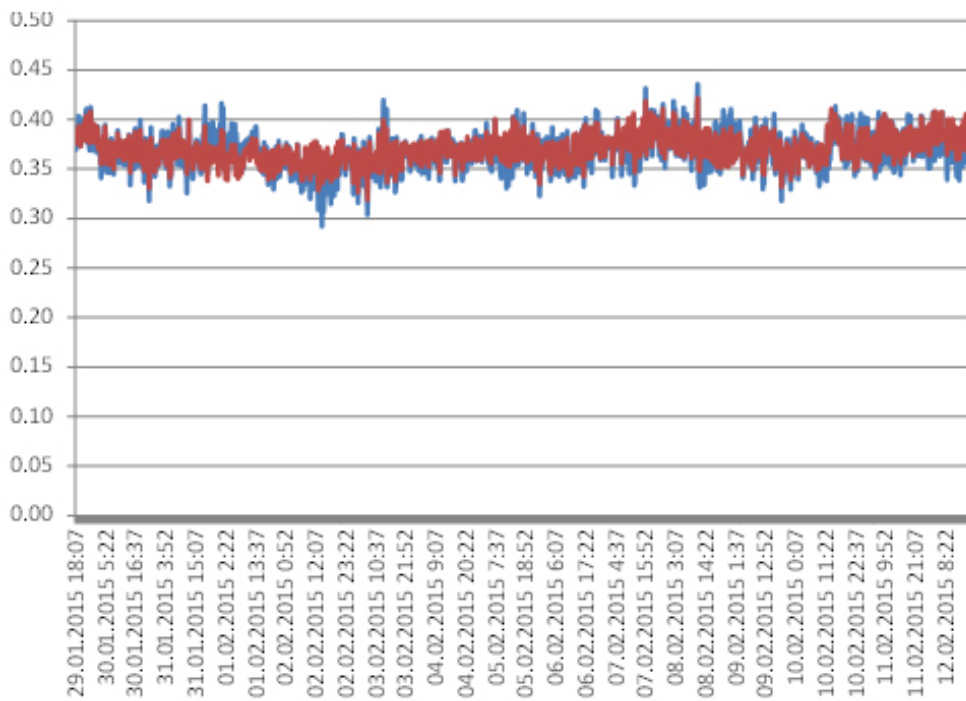


**Figure 7. Measurement results of resistance to heat transfer in the central part of the double-glazed window (building 1, flat 4)**

Measurement results of resistance to heat transfer of envelopes in the group of buildings monitored are given in Table 2.

**Table 2. Actual values of resistance to heat transfer of envelopes**

Building number	Flat number	Actual resistance to heat transfer, m <sup>2</sup> .K/W			
		exterior wall	double-glazed window	attic slab	slab over basement
1	1	1.85±0.29	0.40±0.02	—	2.64±0.40
	2	2.89±0.40	0.64±0.19	—	3.34±0.62
	3	2.12±0.38	—	—	1.87±0.55
	4	2.01±0.53	0.40±0.02	2.17±0.55	—
2	5	0.95±0.11	0.37±0.01	—	—
	6	1.06±0.13	0.31±0.06	—	—
	7	2.30±0.27	0.34±0.02	0.76±0.15	—
	8	2.00±0.35	—	1.45±0.22	—
3	9	1.59±0.24	—	0.63±0.07	—

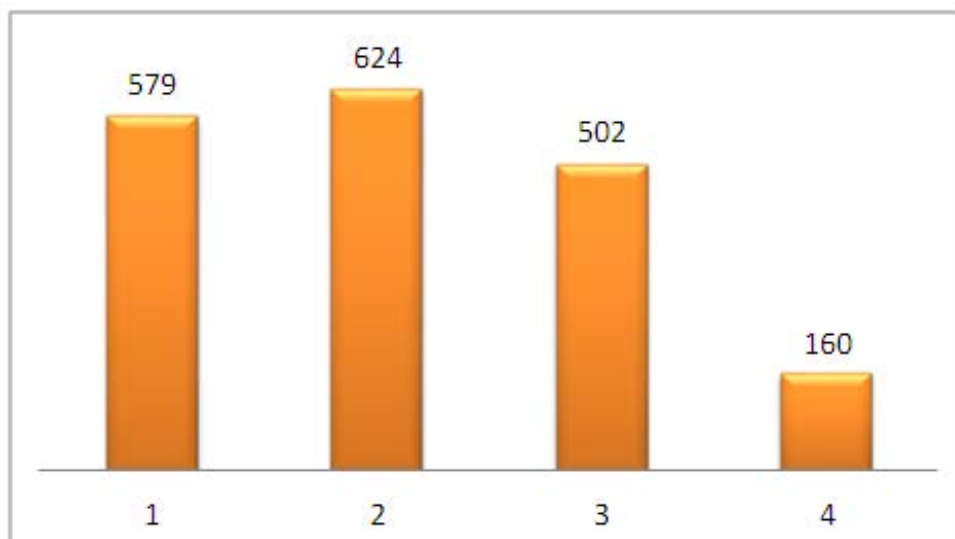
An element-by-element estimation of heat protection in buildings was made on the basis of the measurements (Table 3).

**Table 3. Element-by-element estimation of heat protection in buildings according to measurement results**

Envelopes	Resistance to heat transfer, m <sup>2</sup> .K/W	
	Minimum allowed	actual (measured)
exterior walls	1.75	0.95...2.89
windows	0.42	0.31...0.64
attic slab	2.94	0.63...2.17
slab over basement	2.94	1.87...3.34

As it is shown in Table 3, values of resistance to heat transfer measured at different points of envelopes fluctuate in a wide range, and it indicates high non-uniform heat protection performance of covers. Thermoprotective properties in the edge zones of envelopes dramatically decrease. Minimum allowed element-by-element requirements (as provided by Russian construction norms SP 50.13330.2012, p. 5.1, a) which are not ensured.

Specific heat loss through the building cover (Figure 8) was computed with measured values of resistance to heat transfer of envelopes (Table 2) and geometric characteristics of the building (Table 1).

**Figure 8. Structure of heat loss through the building cover, W/K: 1 – exterior walls; 2 – windows, balcony doors; 3 – attic slabs; 4 – slab over basement**

As it is shown in Figure 8, the bigger part of heat loss (64 %) is monitored through the building's facades, and it can be explained by a crucial impact of edge zones in exterior walls, and by low heat protective properties of windows as well. A significant part of heat losses goes through the attic slab (27 %), and can be specified due to a comparatively low level of heat insulation of this structure.

The estimated value of an actual specific heat-protective feature of the building is equal to  $0.307 \text{ W}/(\text{m}^3\cdot\text{K})$ , which is higher than the rated value of  $0.257 \text{ W}/(\text{m}^3\cdot\text{K})$ . Consequently, a multiple requirement (according to the Russian construction norm SP 50.13330.2012, p. 5.1, b) was not met.

Thre inspection of envelopes under sanitary and hygienic requirement (SP 50.13330.2012, p. 5.1, c) revealed that the structures do not meet this requirement. In many cases the temperature on the internal surface of envelopes in the edge zones is lower than a dew point of inside air in the cold season, and it results in humidity condensation and mold formation [20]. Coupling joints between columns and the inter-floor slab and between window and wall opening are the most vulnerable ones (Figures 9, 10).



**Figure 9. Humidity condensation and mold formation on the internal surface of the coupling joint between the column and the inter-floor slab**



**Figure 10. Humidity condensation and mold formation on the internal surface of the coupling joint between window and the wall opening**

Consequently, according to the field measurements, the following was specified: an actual level of heat protection in the buildings does not meet the requirements provided by the Russian construction norm SP 50.13330.2012.

The authors of the article estimated the level of heat protection using design data to find out the reasons for the emergence of temperature anomalies and thermotechnical defects in the covers of buildings.

As a case a detailed estimation of the thermal regime of exterior walls was conducted.

The fact that there are multiple edge zones, identified due to thermovision monitoring (Figures 2–5), is the major feature of exterior walls made of autoclaved aerated concrete. Neglecting edge zones when designing envelopes may cause significant deviations in the case of defining thermotechnical features.

Mathematical modeling of the thermal regime of the structure in the cold season was carried out under the following boundary conditions:

- estimated inside air temperature in the building  $t_{int} = 20 \text{ C}$  (Russian standard GOST 30494–2011);
- estimated outside air temperature  $t_{ext} = -22 \text{ C}$  (Russian construction norm SP 50.13330.2012);
- estimated heat transfer coefficient at the internal surface of the envelope  $\alpha_{si} = 8.7 \text{ W}/(\text{m}^2 \cdot \text{K})$  (Russian construction norm SP 50.13330.2012);
- estimated heat transfer coefficient at the external surface of the envelope  $\alpha_{se} = 23 \text{ W}/(\text{m}^2 \cdot \text{K})$  (Russian construction norm SP 50.13330.2012).

The following types of edge zones were considered while carrying out estimations:

- coupling joint between exterior walls and inter-floor slabs;
- coupling joint between windows and wall openings;
- exterior angle in the case of exterior walls;
- reentering angle in the case of exterior walls;
- coupling joint between columns and walls;
- coupling joint between exterior walls and slabs over basements;
- coupling joint between exterior walls and attic slabs.

Due to a negligible impact that flexible ties may produce relatively to the temperature field of the exterior walls according to the results of thermovision monitoring, flexible ties were not considered in the estimation.

The structural diagram of the wall under design is given in Figure 11.

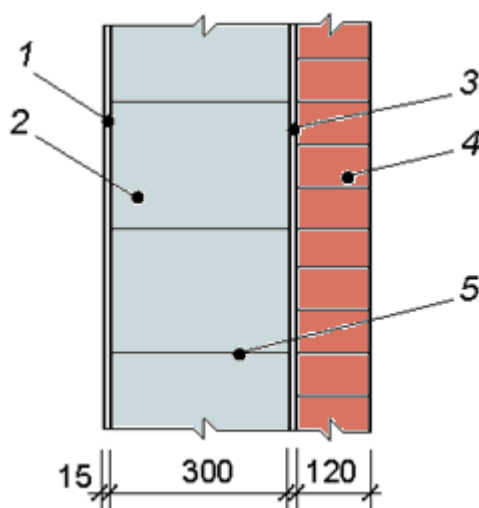


**Figure 11. Cross-section of the wall: 1 – plaster; 2 – aerated concrete blocks; 3 – manufacturing clearance; 4 – front brick masonry; 5 – glue line**

Thermotechnical characteristics of construction materials given in Table 4 were used in the estimation.

**Table 4. Estimated thermotechnical characteristics of materials (SP 50.13330.2012)**

Layer number	Material of a layer	Material density $\rho_0$ , kg/m <sup>3</sup>	Thermal conductivity $\lambda$ , W/(m·K)
1	Compound mortar-based plaster	1700	0.7
2	AAC block masonry using adhesive	450	0.16
3	Closed air cavity	—	0.067 (equivalent) with thickness of air cavity of 0.01 m
4	Front brick masonry	1400	0.52

Calculation results of the thermal regime f or wall structures are given in Table 5.

**Table 5. Estimation results of the thermal regime of exterior walls**

Indicator	Subscript, measurement unit	Value
Major specific heat flow	$Q_{bas}$ , W/K	442
Supplementary specific heat flow through edge zones including:		
coupling joints between exterior walls and inter-floor slabs	$Q_{ad}$ , W/K	132
coupling joints between windows and wall openings	$Q_1^{ad}$ , W/K	48.1
exterior angles	$Q_2^{ad}$ , W/K	35.6
reentrant angles	$Q_3^{ad}$ , W/K	4.08
coupling joints between columns and walls	$Q_4^{ad}$ , W/K	-3.95
coupling joints between exterior walls and slabs over basements	$Q_5^{ad}$ , W/K	2.51
coupling joints between exterior walls and attic slabs	$Q_6^{ad}$ , W/K	21
Total heat flow	$Q_{sum}$ , W/K	574

The structure of the specific heat loss through exterior walls (Figure 12) was defined using the data taken from Table 5.

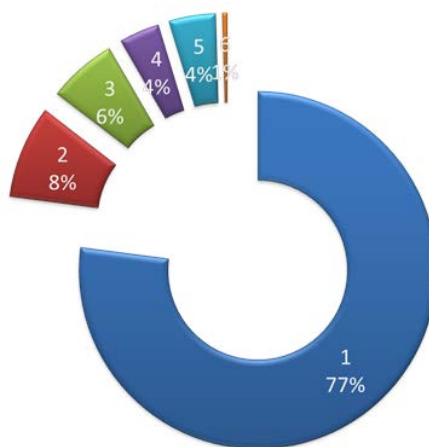


**Figure 12. Structure of the specific heat loss through exterior walls: 1 – major heat loss; 2 – supplementary heat loss through coupling joints between exterior walls and inter-floor slabs; 3 – supplementary heat loss through coupling joints between windows and wall openings; 4 – supplementary heat loss through coupling joints between exterior walls and slabs over the basement; 5 – supplementary heat loss through coupling joints between exterior walls and attic slabs; 6 – other**

The analysis of the obtained results shows that 23 % of the heat loss emerges through edge zones. The bigger part of the heat loss was found through coupling joints between the exterior walls and the inter-floor slabs (8 %) due to perforated holes in slabs. Along with the heat loss through coupling joints between windows and wall openings (6 %) they amount to a bigger part of the supplementary heat loss (14 %). Lower heat loss through coupling joints between the exterior walls and the slab over the basement (4 %), and the attic slab (4 %) can be explained by a shorter length of these joints.

The estimated reduced resistance to heat transfer in exterior walls  $R_o^{red} = 1.88 \text{ m}^2\cdot\text{K/W}$ , which is close to a minimum allowed value ( $R_o^{min} = 1.75 \text{ m}^2\cdot\text{K/W}$ ). Approximation of  $R_o^{red}$  to  $R_o^{min}$  causes thermotechnical risks when designing envelopes. The value of thermotechnical uniformity of the exterior walls is low enough ( $r = 0.774$ ) and can be explained by a significant impact of edge zones.

Results of heat protection for buildings' covers are given below.

The designed level of heat protection of envelopes meets element-by-element requirements SP 50.13330.2012 (Table 6).

**Table 6. Element-by-element estimation of heat protection for buildings' covers with design data**

Envelope	Rated resistance to heat transfer, $\text{m}^2\cdot\text{K/W}$		Estimated resistance to heat transfer, $\text{m}^2\cdot\text{K/W}$
	Minimum allowed level of heat protection	Basic level of heat protection	
Exterior walls	1.75	2.77	1.88
Windows	0.42	0.44	0.50
Slab attic	2.94	3.67	3.84
Slab over basement	2.94	3.67	3.08

The estimated specific heat protective characteristic of buildings obtained using the design data is equal to  $0.228 \text{ W}/(\text{m}^3\cdot\text{K})$ , which is less than the rated value of  $0.257 \text{ W}/(\text{m}^3\cdot\text{K})$ , hereby the design solution of buildings meets multiple requirements for heat protection according to the Russian norm SP 50.13330.2012.

The temperature on the internal surfaces of envelopes at the points with heat-conducting inclusions is higher than a dew point of the inside air in the case of the estimated outside air temperature, hereby the design solution of envelopes meets the sanitary and hygienic requirement of the Russian construction norm SP 50.13330.2012.

Thus, it was specified that an actual level of heat protection in buildings is lower than a designed one according to field thermophysical tests of residential buildings made of AAC blocks and checking thermotechnical calculation. It can be explained by both multiple unapproved deviations from the design project made by a subcontractor during construction, low-quality performance and assembly works. The building design project itself bears certain thermotechnical risks due to neglecting the impact of edge zones produced on thermal protective properties of envelopes.

To ensure the designed level of heat protection in an object, it is required to eliminate non-compliance of actual works performed with the design requirements. The study suggests that there should be a strong focus on how to improve construction solutions for edge zones of envelopes [20]. Applying supplementary exterior insulation along the whole surface of the wall according to the preliminary estimates can level off the temperature field (Figure 13). Meanwhile both the supplementary heat loss in edge zones and major heat loss of the walls reduce (Figure 14).

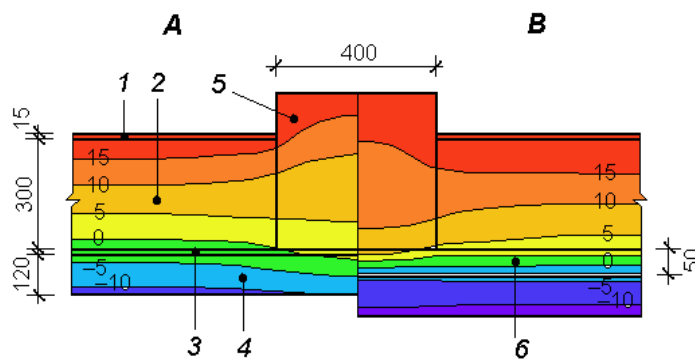


**Figure 13. Temperature field of coupling joint between the exterior wall and the column (A – without the application of supplementary insulation, B – with the application of supplementary insulation):** 1 – plaster; 2 – aerated concrete blocks; 3 – manufacturing clearance; 4 – front brick masonry; 5 – column; 6 – supplementary insulation

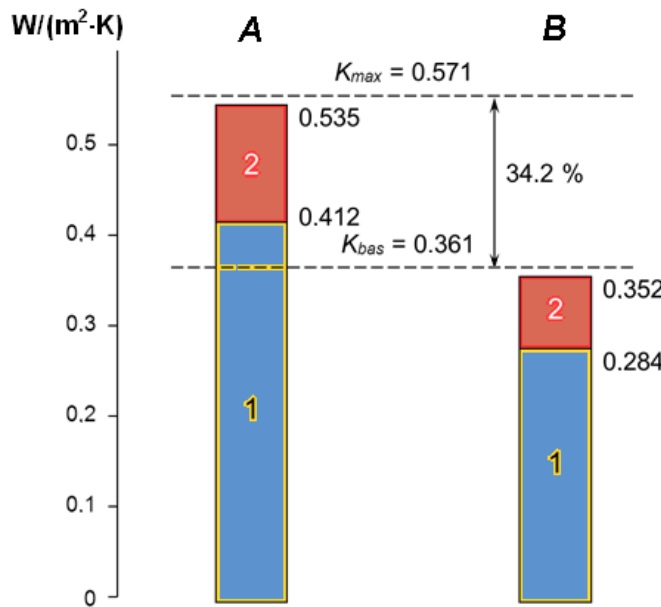


**Figure 14. Thermal transmission coefficient of the exterior walls (A – without the application of supplementary insulation, B – with the application of supplementary insulation): 1 – without considering edge zones; 2 – considering only edge zones**

It is recommended to replace one chamber-glass units with more energy efficient translucent envelopes. It is also necessary to improve the level of heat protection in the area of basement and attic slab. The activities mentioned above are to improve heat protective properties in buildings and able to be implemented only under a design project of buildings redevelopment.

### Conclusion

According to the results of field thermophysical tests of residential buildings made of autoclaved aerated concrete blocks, the following was found out:

1. Design of double-layer exterior walls in the form of AAC blocks with front brick masonry bears thermotechnical risks due to an increase in non-uniform heat protection of buildings' covers caused by a significant impact on heat protection of buildings' edge zones. Meanwhile there is a significant growth of the impact on two- and three-dimension elements of the internal surface structure, and there is a decline in the thermotechnical uniformity of envelopes. Estimation of three-dimension temperature fields and development of new construction solutions is required to consider the impact of edge zones.

2. The designed level of heat insulation does not correspond to the basic level of heat protection for the majority of regions in the Russian Federation. Two-layer exterior walls without supplementary insulation practically do not have heat protection and energy saving reserves.

3. The reduction of an actual level of insulation in envelopes, compared to the designed one, can be explained by both unapproved deviations from the design project made by a subcontractor during construction, low-quality performance and assembly works.

4. It is strongly suggested to improve a structural solution of edge zones of envelopes to reduce thermotechnical risks when designing buildings. Supplementary insulation along the whole surfaces of the walls can be considered as another activity to increase the level of heat protection. As preliminary estimates show, while leveling off temperature fields, not only supplementary heat loss in edge zones but a major heat loss of walls can be reduced as well.

The materials for the article were reported and approved at X International Congress «Energy efficiency. XXI century. Engineering methods to reduce energy consumption in buildings», workshop «Construction thermophysics and energy efficient design of envelopes».

### Acknowledgement

This article is to be published within the project work: Erasmus+ 561890-EPP-1-2015-1-IT\_EPPKA2-CBHE-JP.

## References

- Vishnevskiy A.A., Grinfeld G.I., Smirnova A.S. Proizvodstvo avtoklavnogo gazobetona v Rossii [Production of autoclaved aerated concrete in Russia]. *Stroitelnyye materialy*. 2015. No. 6. Pp. 52–54. (rus)
- Suhasini R. Autoclaving cement concrete: A review. *International Journal of Applied Engineering Research*. 2014. No. 9(11). Pp. 1603–1617.
- Vatin N.I., Gorshkov A.S., Kornienko S.V., Pestryakov I.I. Potребительские свойства стеноых изделий из автоклавного газобетона [The consumer properties of wall products from AAC]. *Construction of Unique Buildings and Structures*. 2016. No. 1. Pp. 78–101. (rus)
- Nemova D.V., Spiridonova T.I., Kurazhova V.G. Neizvestnyye svoystva izvestnogo materiala [Unknown properties of the well-known material]. *Construction of Unique Buildings and Structures*. 2012. No. 1. Pp. 36–46. (rus)
- Van Boggelen W., Völker K. New opportunities for autoclaved aerated concrete [Neue Chancen für Porenbeton]. *Betonwerk und Fertigteil-Technik/Concrete Precasting Plant and Technology*. 2004. No. 70(3). Pp. 60–64.
- Narayanan N., Ramamurthy K. Structure and properties of aerated concrete: A review. *Cement and Concrete Composites*. 2000. No. 22 (5). Pp. 321–329.
- Sakharov G.P. Razvitiye proizvodstva i povysheniye konstruktivnykh svoystv avtoklavnogo yacheistogo betona i izdeliy na yego osnove [Development of production and increase of constructive properties of autoclave cellular concrete and products on his basis]. *Concrete Technologies Magazine*. 2012. No. 11–12 (76–77). Pp. 56–58. (rus)
- Tanner J.E., Varela J.L., Klingner R.E., Brightman M.J., Cancino U. Seismic testing of autoclaved aerated concrete shearwalls: A comprehensive review. *ACI Structural Journal*. 2005. No. 102 (3). Pp. 374–382.
- Gorshkov A.S. Usloviya obespecheniya ustoychivosti dlya poetazhno-opertykh sten iz gazobetonykh blokov [Conditions of ensuring stability for a floor-by-floor walls from aerated concrete blocks]. *Concrete Technologies Magazine*. 2014. No. 4(93). Pp. 49–55. (rus)
- Gorshkov A.S., Vatin N.I. Svoystva stenoых конструкций из ячеистобетонных изделий автоклавного твердения на полиуретановом kleyu [Properties of the wall structures made of autoclaved cellular concrete products on the polyurethane foam adhesive]. *Magazine of Civil Engineering*. 2013. No. 5 (40). Pp. 5–19. (rus)
- Gorshkov A.S., Grinfeld G.I., Mishin V.Ye., Nikiforov Ye.S., Vatin N.I. Povysheniye teplotekhnicheskoy odnorodnosti sten iz yacheisto-betonnykh izdeliy za scet ispolzovaniya v kladke poliuretanovogo kleya [Improvement of thermotechnical uniformity of walls made of cellular concrete products through the use of polyurethane glue in masonry]. *Stroitelnyye materialy*. 2014. No. 5. Pp. 57–64. (rus)
- Kočí V., Maděra J., Černý R. Exterior thermal insulation systems for AAC building envelopes: Computational analysis aimed at increasing service life. *Energy and Buildings*. 2012. No. 47. Pp. 84–90.
- Leontyev S.V., Golubev V.A., Saraykina K.A., Shamanov V.A. Opyt polucheniya avtoklavnogo teploizolyatsionnogo gazobetona [Experience of autoclaved aerated heat-insulating concrete production]. *Vestnik Yuzhno-Ural'skogo gosudarstvennogo universiteta. Seriya: Stroitelstvo i arkhitektura*. 2014. No. 14 (1). Pp. 46–49. (rus)
- Jin H.Q., Yao X.L., Fan L.W., Xu X., Yu Z.T. Experimental determination and fractal modeling of the effective thermal conductivity of autoclaved aerated concrete: Effects of moisture content. *International Journal of Heat and Mass Transfer*. 2016. No. 92. Pp. 589–602.

## Литература

- Вишневский А.А., Гринфельд Г.И., Смирнова А.С. Производство автоклавного газобетона в России // Строительные материалы. 2015. № 6. С. 52–54.
- Suhasini R. Autoclaving cement concrete: A review // International Journal of Applied Engineering Research. 2014. № 9 (11). Pp. 1603–1617.
- Ватин Н.И., Горшков А.С., Корниенко С.В., Пестряков И.И. Потребительские свойства стеновых изделий из автоклавного газобетона // Строительство уникальных зданий и сооружений. 2016. № 1. С. 78–101.
- Немова Д.В., Спиридонова Т.И., Куражова В.Г. Неизвестные свойства известного материала // Строительство уникальных зданий и сооружений. 2012. № 1. С. 36–46.
- Van Boggelen W., Völker K. New opportunities for autoclaved aerated concrete [Neue Chancen für Porenbeton] // Betonwerk und Fertigteil-Technik/Concrete Precasting Plant and Technology. 2004. № 70 (3). Pp. 60–64.
- Narayanan N., Ramamurthy K. Structure and properties of aerated concrete: A review // Cement and Concrete Composites. 2000. № 22 (5). Pp. 321–329.
- Сахаров Г.П. Развитие производства и повышение конструктивных свойств автоклавного ячеистого бетона и изделий на его основе // Технологии бетонов. 2012. № 11–12 (76–77). С. 56–58.
- Tanner J.E., Varela J.L., Klingner R.E., Brightman M.J., Cancino U. Seismic testing of autoclaved aerated concrete shearwalls: A comprehensive review // ACI Structural Journal. 2005. № 102 (3). Pp. 374–382.
- Горшков А.С. Условия обеспечения устойчивости для поэтажно-опертых стен из газобетонных блоков // Технологии бетонов. 2014. № 4 (93). С. 49–55.
- Горшков А.С., Ватин Н.И. Свойства стеновых конструкций из ячеистобетонных изделий автоклавного твердения на полиуретановом клею // Инженерно-строительный журнал. 2013. № 5 (40). С. 5–19.
- Горшков А.С., Гринфельд Г.И., Мишин В.Е., Никифоров Е.С., Ватин Н.И. Повышение теплотехнической однородности стен из ячеисто-бетонных изделий за счет использования в кладке полиуретанового клея // Строительные материалы. 2014. № 5. С. 57–64.
- Kočí V., Maděra J., Černý R. Exterior thermal insulation systems for AAC building envelopes: Computational analysis aimed at increasing service life // Energy and Buildings. 2012. № 47. Pp. 84–90.
- Леонтьев С.В., Голубев В.А., Сарайкина К.А., Шаманов В.А. Опыт получения автоклавного теплоизоляционного газобетона // Вестник Южно-Уральского государственного университета. Серия: Строительство и архитектура. 2014. Т. 14. № 1. С. 46–49.
- Jin H.Q., Yao X.L., Fan L.W., Xu X., Yu Z.T. Experimental determination and fractal modeling of the effective thermal conductivity of autoclaved aerated concrete: Effects of moisture content // International Journal of Heat and Mass Transfer. 2016. № 92. Pp. 589–602.
- Campanale M., Moro L. Autoclaved aerated concrete: Experimental evaluation of its thermal properties at high temperatures // High Temperatures-High Pressures. 2015. № 44 (5). Pp. 369–382.
- Пастушков П.П., Гринфельд Г.И., Павленко Н.В., Беспалов А.Е., Коркина Е.В. Расчетное определение эксплуатационной влажности автоклавного газобетона в различных климатических зонах строительства // Вестник МГСУ. 2015. № 2. С. 60–69.
- Rubene S., Vilnitis M., Noviks J. Frequency Analysis and Measurements of Moisture Content of AAC Masonry Constructions by EIS // Procedia Engineering. 2015. № 123. Pp. 471–478.

15. Campanale M., Moro L. Autoclaved aerated concrete: Experimental evaluation of its thermal properties at high temperatures. *High Temperatures-High Pressures*. 2015. No. 44 (5). Pp. 369–382.
16. Pastushkov P.P., Grinfeld G.I., Pavlenko N.V., Bespalov A.Ye., Korkina Ye.V. Raschetnoye opredeleniye ekspluatatsionnoy vlazhnosti avtoklavnogo gazobetona v razlichnykh klimaticheskikh zonakh stroitelstva [Settlement determination of operating moisture of autoclaved aerated concrete in different climatic zones]. *Proceedings of Moscow State University of Civil Engineering*. 2015. No. 2. Pp. 60–69. (rus)
17. Rubene S., Vilnitis M., Noviks J. Frequency Analysis and Measurements of Moisture Content of AAC Masonry Constructions by EIS. *Procedia Engineering*. 2015. No. 123. Pp. 471–478.
18. Yao X.L., Yi S.Y., Fan L.W., Xu X., Yu Z.T., Ge J. Effective thermal conductivity of moist aerated concrete with different porosities. *Zhejiang Daxue Xuebao (Gongxue Ban)* [Journal of Zhejiang University (Engineering Science)]. 2015. No. 49 (6). Pp. 1101–1107.
19. Koudelka T., Kruis J., Madéra J. Coupled shrinkage and damage analysis of autoclaved aerated concrete. *Applied Mathematics and Computation*. 2015. No. 267. Pp. 427–435.
20. Korniyenko S.V. Kompleksnaya otsenka energoeffektivnosti i teplovoy zashchity zdaniy [Complex assessment of energy efficiency and thermal performance for buildings]. *Construction of Unique Buildings and Structures*. 2014. No. 11 (26). Pp. 33–48. (rus)
21. Gorshkov A.S., Rymkevich P.P., Vatin N.I. Modelirovaniye protsessov nestatsionarnogo perenosa tepla v stenovyx konstruktsiyakh iz gazobetonnykh blokov [Simulation of non-stationary heat transfer processes in autoclaved aerated concrete-walls]. *Magazine of Civil Engineering*. 2014. No. 8 (52). Pp. 38–48. (rus)
22. Korniyenko S.V. Mnogofaktornaya otsenka teplovogo rezhima v elementakh obolochki zdaniya [Multifactorial assessment of thermal behavior in building envelope elements]. *Magazine of Civil Engineering*. 2014. No. 8 (52). Pp. 25–37. (rus)
23. Korniyenko S.V. Povysheniye energoeffektivnosti zdaniy za schet snizheniya teplopoter cherez krayevyye zony ograzhdayushchikh konstruktsiy [The increase of power efficiency of building at the expense of reduction of heat losses through edge zones of enclosure]. *Academia. Arkhitektura i stroitelstvo*. 2010. No. 3. Pp. 348–351. (rus)
24. Korniyenko S. Evaluation of thermal performance of residential building envelope. *Procedia Engineering*. 2015. No. 117. Pp. 191–196.
25. Zemitis J., Borodinecs A., Frolova M. Measurements of moisture production caused by various sources. *Energy and Buildings*. 2016. No. 127. Pp. 884–891.

Sergey Korniyenko,  
+79884912459; svkorn2009@yandex.ru

Nikolai Vatin,  
+79219643762; vatin@mail.ru

Alexander Gorshkov,  
+7(921)3884315; alsgor@yandex.ru

Сергей Валерьевич Корниенко,  
+79884912459; эл. почта:  
svkorn2009@yandex.ru

Николай Иванович Ватин,  
+79219643762; эл. почта: vatin@mail.ru

Александр Сергеевич Горшков,  
+7(921)3884315; эл. почта: alsgor@yandex.ru

© Korniyenko S.V., Vatin N.I., Gorshkov A.S., 2016

doi: 10.5862/MCE.64.3

## Fire design of arch-type timber roof

### Проектирование огнестойких арочных деревянных покрытий

**T. Sakanite,**  
**D. Serduks,**  
**V. Goremkins,**  
**L. Pakrastins,**  
*Riga Technical University, Riga, Latvia*

**N.I. Vatin,**  
*Peter the Great St. Petersburg Polytechnic  
University, St. Petersburg, Russia*

**Студент Т. Сакните,**  
**д-р техн. наук, профессор Д.О. Сердюк,**  
**д-р техн. наук, ведущий научный сотрудник**  
**В.В. Горемыкин,**  
**д-р техн. наук, руководитель кафедры**  
**Л. Пакрастиньш,**  
*Рижский технический университет, Рига,  
Латвия*  
**д-р техн. наук, директор Инженерно-  
строительного института Н.И. Ватин,**  
*Санкт-Петербургский политехнический  
университет Петра Великого, Санкт-  
Петербург, Россия*

**Key words:** punched steel plates; response surface method; fire resistance

**Ключевые слова:** перфорированные стальные пластины; метод поверхности отклика; огнестойкость

**Abstract.** Lattice timber structures, which are made of elements connected by punched steel plates, are widely used for residential and industrial buildings. The main types of the structures are trusses, frames, and arches, which enables covering spans up to 30 m and more. The behavior of structures on fire plays an important role in the design process of the structures. The cylindrical roof with a 30 m span and the main load-bearing structures of lattice arches with elements connected by punched metal plates was considered as an object of investigation. The rational geometrical parameters of a lattice timber arch with punched steel plated joints were evaluated. Fire resistance and a possibility to increase it for an arch-type timber roof was also considered. It was obtained that using a protective layer is a preferable method of a fire resistance increase for the lattice timber arch due to arch joints; the material consumption was also increased by 1.65 times. It was shown that the rational values of the height of the arch, depth of the arch cross-section, and distance between the nodes on the top chord are equal to 7.85, 1.10, and 0.95 m respectively.

**Аннотация.** Решетчатые деревянные конструкции с узлами, выполненными с применением зубчатых стальных пластин, широко используются в промышленном и гражданском строительстве. Фермы, рамы и арки являются основными типами данных конструкций позволяющих перекрывать пролеты до 30 м и более. Оценка огнестойкости конструкций имеет большое значение при проектировании. Цилиндрическое покрытие пролетом 30 м с главными несущими элементами в виде решетчатых деревянных арок с узлами, выполненными с применением зубчатых стальных пластин, рассмотрено в качестве объекта исследования. Рациональные с точки зрения расхода конструктивных материалов геометрические параметры цилиндрического покрытия определены при помощи численного эксперимента. При этом произведена оценка огнестойкости основных конструктивных элементов, а так же возможности ее повышения. Показано, что наиболее эффективным способом повышения огнестойкости решетчатых деревянных арок является использование защитных покрытий. Расход конструктивных материалов при этом возрастает в 1.65 раз. Показано, что рациональные с точки зрения расхода материалов величины высоты арки, высоты сечения арки и длины панели верхнего пояса равны 7.85, 1.10 и 0.95 м, соответственно.

### Introduction

Lattice timber structures can be divided into the groups depending on the types of fasteners which are used for joints. Nails, split rings, tooth steel plates, and punched steel plates are the main types of fasteners, which are used for joints of the lattice timber structures. The lattice timber structures, which are made of elements connected by punched steel plates (Fig. 1), are widely used for residential and

industrial buildings in Latvia and abroad. The main types of the structures are trusses, frames, and arches, which enables covering the spans up to 30 m and more [1, 2].



**Figure 1. Lattice frame with elements connected by punched steel plates**

The lattice timber arches, which are made of elements connected by punched steel plates (Fig. 2), cause an increased interest due to relatively low consumption of materials in comparison with similar lattice timber structures due to rational distribution of internal forces.

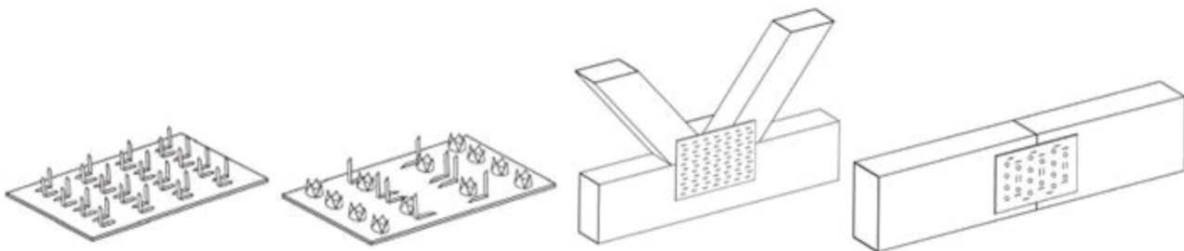


**Figure 2. Joints of the lattice timber structures, which are made of elements connected by punched steel plates**

Moreover, the decreased dead weight of one unit simplifies the assembling process. However, the lattice timber structures possess a number of disadvantages: increased number of assembling units, decreased fire resistance, and decreased span. All these disadvantages are derivative from the limited dimensions of the member's cross-sections. Therefore, the width of the chords and elements of the lattice is limited to 60 mm. It can be increased up to 70 mm in outstanding cases. The choice of rational geometrical parameters enables decreasing consumption of structural materials and increasing effectiveness of the structure.

The behaviour of structures on fire plays an important role in the design process of structures [3]. Since the 1990s, many research projects have been focused on the fire behavior of timber structures worldwide, in particular, light timber frame constructions [4, 5].

The cylindrical roof with the main load-bearing structures of lattice arches with the elements connected by punched metal plates was considered as an object of investigation. The step of the lattice arches is equal to 1.5 m (Fig. 3).

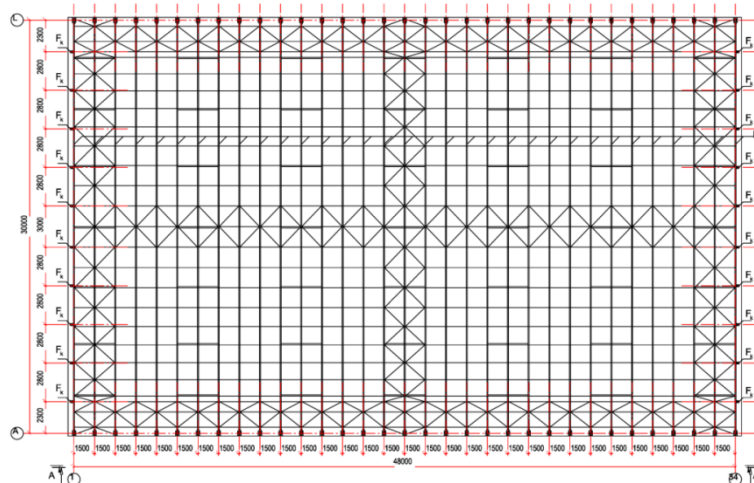


**Figure 3. Scheme of the considered cylindrical roof: Nj – load-bearing lattice arches; Fk – columns of the framework**

The lattice arch has rational geometrical parameters in terms of materials consumption, which were evaluated in the course of the previous investigation [6]. The height of the arch, depth of the arch cross-section, and distance between the nodes on the top chord were equal to 7.5, 1.0, and 1.5 m respectively (Fig. 4).

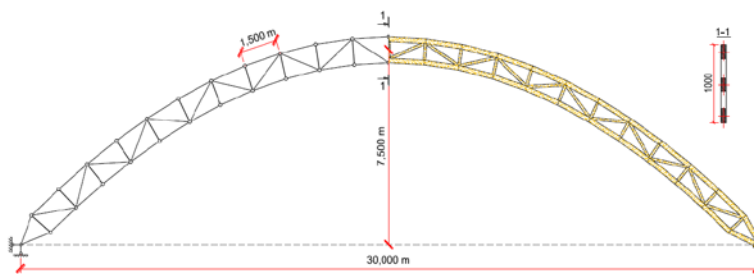


**Figure 4. Lattice arches with the nodes made of punched metal plates**

All members of the arch are made of C24 strength class solid timber. The cross-section depth and width of the top and bottom chords of the arch are equal to 180 and 70 mm respectively. All elements of the lattice have equal dimensions of the cross-section: depth and width are equal to 100 and 70 mm respectively. The lattice arch elements are joined with the punched steel plates Kartro. The thickness and teeth length of the Kartro punched steel plates are equal to 1.2 and 12 mm respectively. The top and bottom chords of lattice arches are joined with freely supported solid timber purlins, which were placed with the step equal to 1.5 m. The purlins with cross-section dimensions equal to 120 x 70 mm and 100 x 70 mm join the top and bottom chords of arches respectively. The strength class of solid timber is C24. Profiled steel sheets are the main load-bearing elements of the roofing [6].

The considered roof is analysed for Latvian climatic conditions [7]. The current place is the city of Riga. The characteristic values of permanent snow and wind loads were equal to 0.37, 1.25, and 0.56 kN/m<sup>2</sup> respectively.

The aim of this study is to evaluate rational geometrical parameters of the above mentioned lattice timber arch with the punched steel plated joints. The lattice timber arch is the main load-bearing structure of the considered arch-type timber roof. Fire resistance and the possibility to increase it for the arch-type timber roof should also be considered.

## Methods and results

### Choice of a design method

The object of investigation, considered in this study, is a timber framework of cylindrical roof. It means that mechanical resistance, or criteria R, will be considered as determinant parameters, which reflect fire resistance of object of investigation [8, 9]. Design procedures for mechanical resistance explained in EN 1995-1-2 include:

- reduced cross-section method;

- reduced properties method;
- parametric design method.

Choice of the method for fire resistance analyse was carried out on the base of results comparison, which were obtained by the reduced cross-section method, reduced properties method and by the published experimental results [10, 11]. The two mentioned methods were chosen due to its simplicity, which is significant advantage in the case of big volume of calculations. The experimental results were obtained for the glued laminated timber beams with dimensions of cross-section 190X266 mm [8]. Value of the mean timber density changes within the limits from 300 to 464 kg/m<sup>3</sup>. The beams were exposed to fire action from three sides. The charring rates and depths were fixed after 30, 45 and 60 minutes.

The experimental results indicate that charring rates and depths differed for the sides and bottom surfaces. So, for the side surfaces charring depth changes from 19.70 to 22.50 mm, from 26.40 to 28.90 mm and from 42.10 to 45.90 mm for the times of fire exposure equal to 30, 45 and 60 min, correspondingly. Charring depth changes from 20.00 to 26.90 mm, from 27.70 to 31.90 mm and from 46.00 to 49.00 mm for the times of fire exposure equal to 30, 45 and 60 min, correspondingly, for the bottom surfaces. The charring rates changes within the limits from 0.587 to 0.757 mm/min and from 0.614 to 0.897 mm/min for the side and bottom surfaces of the beams, correspondingly. The mean value of design notional charring rate that was obtained by the experiment was equal to 0.71 mm/min, what is much closed to the value 0.7 mm/min, which is given in EN 1995-1-2. Notional charring depth was determined by the following equation [10]:

$$d_{char,n} = \beta_n \cdot t, \quad (1)$$

where  $\beta_n$  – design notional charring rate;  $t$  – time of fire exposure.

Effective charring depth is determined by the equation:

$$d_{ef} = d_{char,n} + k_0 \cdot d_0, \quad (2)$$

where  $d_{char,n}$  – notional charring depth;  $k_0$  – coefficient;  $d_0$  – depth of layer with assumed zero strength and stiffness.

The value of coefficient  $k_0$  was taken equal to 1.0 for non-protected surfaces for the time of fire exposure bigger than 20 minutes. Depth of the layer with assumed zero strength and stiffness  $d_0$  was taken equal to 7 mm [10].

Area of residual cross-section of the element, which is subjected to fire from three sides, in accordance with the reduced cross-section method, must be determined by the formula:

$$A_{ef} = (h - d_{ef}) \cdot (b - 2 \cdot d_{ef}), \quad (3)$$

where  $d_{ef}$  – effective charring depth;  $h$  and  $b$  are depth and width of cross-section before fire exposure, correspondingly.

Area of residual cross-section of the element in accordance with the reduced stress and stiffness method must be determined by the formula:

$$A_{ef} = (h - d_{char,n}) \cdot (b - 2 \cdot d_{char,n}) \quad (4)$$

Area of residual cross-section of the element, which was obtained by the experimental results, must be determined by the equation:

$$A_{ef,exp} = (h - d_{char,exp,bot}) \cdot (b - 2 \cdot d_{char,exp,side}), \quad (5)$$

where  $d_{char,exp}$  is the charring depth, which was determined by the experiment.

The values of effective charring depths and areas of the residual cross-sections, which were determined by the experiment and with the reduced cross-section and reduced strength and stiffness methods, are given in Table 1.

**Table 1.** The values of effective charring depths and areas of residual cross-sections [8].

Fire exposure time, $t$ (min)	Timber density, $\rho$ (kg/m <sup>3</sup> )	Calculated charring depth, $d_{\text{char},n}$ (mm)	Experimentally obtained charring depth, $d_{\text{char},\text{exp}}$ (mm)		Remaining cross-section area calculated with the reduced cross-section method, $A_{\text{ef},1}$ (mm <sup>2</sup> )	Remaining cross-section area calculated with the reduced properties method, $A_{\text{ef},2}$ (mm <sup>2</sup> )	Experimentally obtained remaining cross-section area, $A_{\text{ef},\text{exp}}$ (mm <sup>2</sup> )
			Beam side face	Beam bottom face			
30	399	21.00	22.50	26.90	31892.00	36260.00	34669.50
	445		21.30	22.60			35877.16
	420		19.70	20.00			37047.60
45	411	31.50	26.40	31.90	25707.50	29781.50	32218.52
	444		28.90	29.00			31331.40
	437		27.40	27.70			32218.16
60	412	42.00	43.40	46.00	19964.00	23744.00	22704.00
	464		42.10	46.80			23191.36
	408		45.40	49.00			21526.40

The differences in percentage between the values of the residual cross-section, determined by the experiment and with the reduced cross-section and reduced strength and stiffness methods, are given in Figure 4.

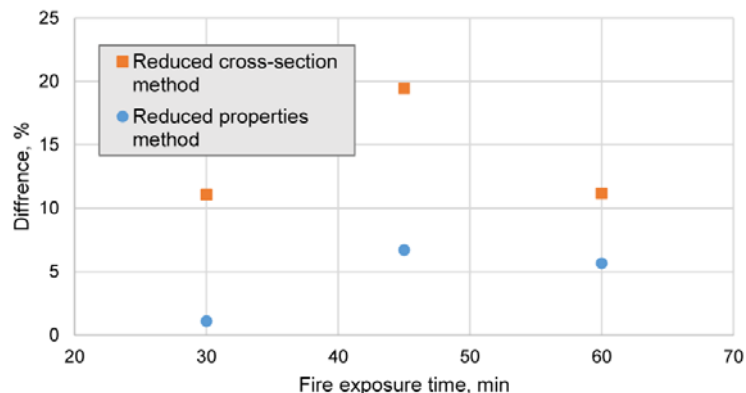


**Figure 5.** The differences in percentage between the values of the residual cross-section, determined by the experiment and with the reduced cross-section and reduced strength and stiffness methods

The comparison of results, obtained analytically and by the experiment, indicates that the values of the residual cross-sections, which were obtained with the reduced stress-stiffness method, differ from the experimentally obtained values by 0.76-4.82 % [11]. Therefore, for the fire resistance analysis of the arch-type timber roof, the reduced stress-stiffness method will be used.

Simplified rules of designing connections, which are explained in section 6 of EN 1995-1-2, will be used for the joint analysis during the fire exposure.

### Design of fire-resistant arch-type timber roof

#### Design of fire-resistant purlins

Let us start the design of the fire-resistant arch-type timber roof from the purlins. The purlins are placed in the planes of top and bottom chords of the considered lattice timber arch. The purlins are subject to dead weight, snow, and wind loads. Loading the purlins differed depending on their position in

the roof. Therefore, determination of the most heavy loaded purlins is the first stage of the analysis. Positions of the heaviest-loaded purlins are indicated in Figure 6 with red circles [6].

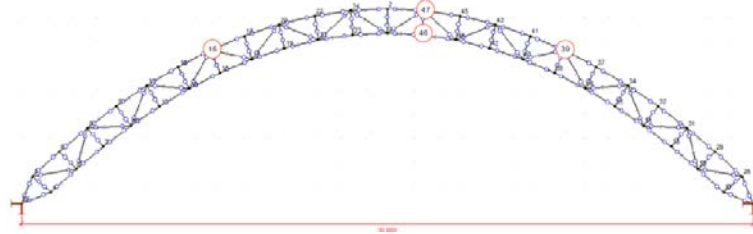


**Figure 6. Nodes numbering of lattice timber arch and position of the heaviest loaded purlins**

The heaviest loaded purlins are joined with the top chord of the lattice timber arch in nodes 16, 47, 39 and in node 46 with the bottom chord. Angles of the cross-sections inclinations are equal to 22 for the purlins joined with the lattice timber arch in nodes 16 and 39 and 5 for the purlins joined with the lattice timber arch in nodes 46 and 47, correspondingly. The total load acting at the purlin in case of fire was determined by the equation [12]:

$$G_{d,sum,fi} = (g_{k,1} + g_{k,2}) \cdot \gamma_{G,A} + q_{k,1} \cdot \psi_1, \quad (6)$$

where  $g_{k,1}$  – characteristic value of purlins dead weight;  $g_{k,2}$  – characteristic value of dead weight of the roofing;  $q_{k,1}$  – characteristic value of snow load;  $\gamma_{G,A}$  – load safety factor;  $\psi_1$  – combination factor for variable load.

The values of load safety factor and combination factor for variable load were taken equal to 1.0 and 0.2, correspondingly [12]. Geometrical parameters of purlins cross-sections in case of fire action were determined by the reduced strength and stiffness method (see Table 2). The purlins were considered as subjected to fire action from four sides.

**Table 2. Geometrical parameters of purlins in case of fire action**

	Top chord purlines		Bottom chord purlines	
t (min)	$h_{fi}$ (mm)	$b_{fi}$ (mm)	$h_{fi}$ (mm)	$b_{fi}$ (mm)
5	112.00	62.00	92.00	62.00
8	107.20	57.20	87.20	57.20
10	104.00	54.00	84.00	54.00
13	99.20	49.20	79.20	49.20
15	96.00	46.00	76.00	46.00

The values of geometrical parameters of the purlins cross-sections were determined for the time of fire exposure equal to 5, 8, 10, 13 and 15 minutes [8]. The purlins were analysed at the fire action taking in to account strength and stability conditions. The strength of the purlins as the member subjected to compressing with the bending was checked by the equations (7) and (8) [13].

$$\left( \sigma_{c,0,d,fi} / f_{c,0,d,fi} \right)^2 + \sigma_{m,y,d,fi} / f_{m,y,d,fi} + k_m \cdot \sigma_{m,z,d,fi} / f_{m,z,d,fi} \leq 1, \quad (7)$$

$$\left( \sigma_{c,0,d,fi} / f_{c,0,d,fi} \right)^2 + k_m \cdot \sigma_{m,y,d,fi} / f_{m,y,d,fi} + \sigma_{m,z,d,fi} / f_{m,z,d,fi} \leq 1, \quad (8)$$

where:  $\sigma_{c,0,d,fi}$  – design compressive stress along the grain in case of fire action,  $\sigma_{m,y,d,fi}$  – design bending stress about the principal y-axis in case of fire action,  $\sigma_{m,z,d,fi}$  – design bending stress about the principal z-axis in case of fire action,  $f_{m,y,d,fi}$  – design bending strength about the principal y-axis in case of fire action,  $f_{m,z,d,fi}$  – design bending strength about the principal z-axis in case of fire action,  $k_m$  – factor, considering redistribution of bending stress in cross-section.

The stability of the purlins as the member subjected to compressing with the bending, was checked by the equations (9) and (10) [13].

$$\sigma_{c,0,d,fi} / k_{c,y,fi} f_{c,0,d,fi} + \sigma_{m,y,d,fi} / f_{m,y,d,fi} + k_m \cdot \sigma_{m,z,d,fi} / f_{m,z,d,fi} \leq 1, \quad (9)$$

$$\sigma_{c,0,d,fi} / k_{c,z,fi} f_{c,0,d,fi} + k_m \cdot \sigma_{m,y,d,fi} / f_{m,y,d,fi} + \sigma_{m,z,d,fi} / f_{m,z,d,fi} \leq 1, \quad (10)$$

where  $k_{c,y,fi}$  is an instability factor along the principal y-axis under fire impact,  $k_{c,z,fi}$  is an instability factor along the principal z-axis under fire impact; other designations are the same as for equations (7) and (8).

The dependence of fire-resistance on the time of fire exposure for the four heaviest-loaded purlins obtained by the strength condition is shown in Figure 7.

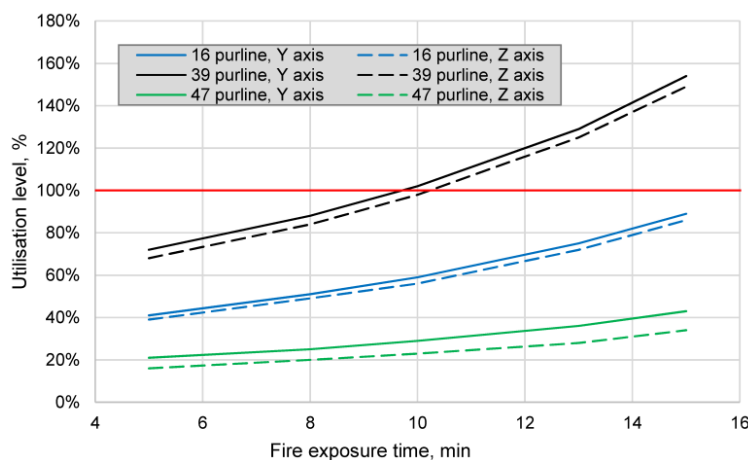


**Figure 7. The utilisation level of purlins by strength criteria depending on fire exposure time**

The dependence of fire-resistance on the time of fire exposure for the four heaviest-loaded purlins obtained by the stability condition is shown in Figure 8.

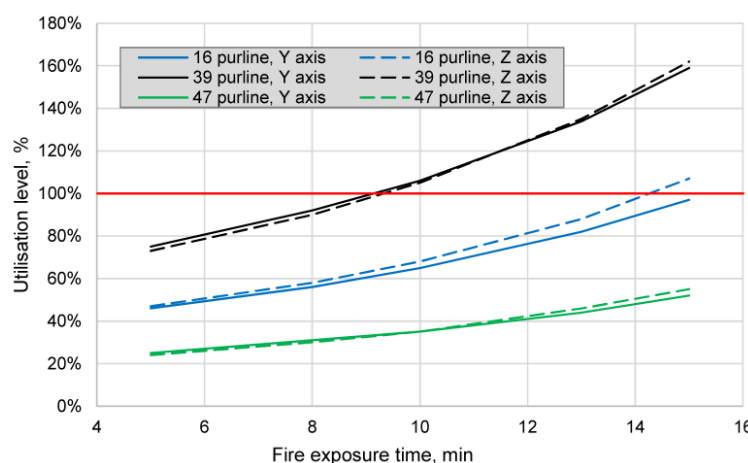


**Figure 8. The utilisation level of purlins by strength criteria depending on fire exposure time**

It was shown that the strength and stability conditions were not satisfied in 9.8 and 9.4 minutes of fire exposure respectively. The area of the residual cross-section of the purlins placed in the plane of the top chord of the lattice timber arch was equal to 82.7 and 52.6 % of its initial value in 5 and 15 min of fire exposure respectively. It means that fire resistance of purlins is equal to R9.4, which is less than the minimum required value R15 [8, 9].

#### Design of fire-resistant lattice arch members

Analyzing fire-resistance of the lattice timber arch was carried out using the program AXIS VM 11 during the impact of the most unpleasant loads combination. The scheme of fire impact at the top chord of the lattice timber arch is shown in Figure 9.

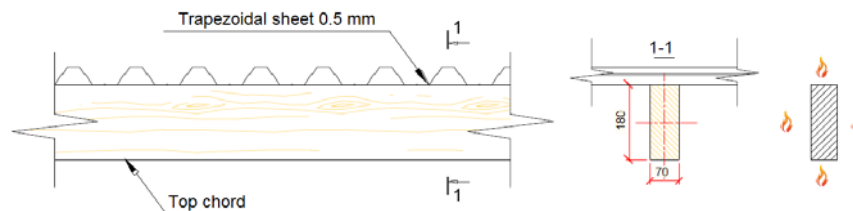


**Figure 9. Scheme of fire impact at the top chord of the lattice timber arch**

The element is exposed to fire from all four sides, as the profiled steel sheets of the roofing were not taken into account as a protective layer. Geometrical parameters of chords cross-sections in the case of fire exposure were determined with the reduced strength and stiffness method (see Table 3) [10].

**Table 3. Geometrical parameters of purlins in the case of fire exposure**

Top chord purlines		
t (min)	h <sub>fi</sub> (mm)	b <sub>fi</sub> (mm)
5	172.00	62.00
8	167.20	57.20
10	164.00	54.00
13	159.20	49.20
15	156.00	46.00

The decrease in dimensions of the member cross-sections due to fire exposure has a significant influence on the load-bearing capacity of the timber lattice arch. The area of the residual cross-section of the chords element in 15 min of fire exposure is equal to 57 % of the initial area of the cross-section. The area of the residual cross-section for the elements of the lattice is equal to 49.9 % of its initial value in 15 minutes of fire exposure.

The values of geometrical parameters of the chords and cross-sections of lattice elements were determined for the time of fire exposure equal to 5, 8, 10, 13, and 15 minutes [8]. The elements were analysed under fire impact allowing for the strength and stability conditions [13]. The elements of the chords are subject to compression with bending. The elements of the lattice are loaded axially. The dependence of the sum of stress-to-strength relations on the time of fire exposure for the elements of the lattice timber arch obtained by the strength condition is shown in Figure 10.

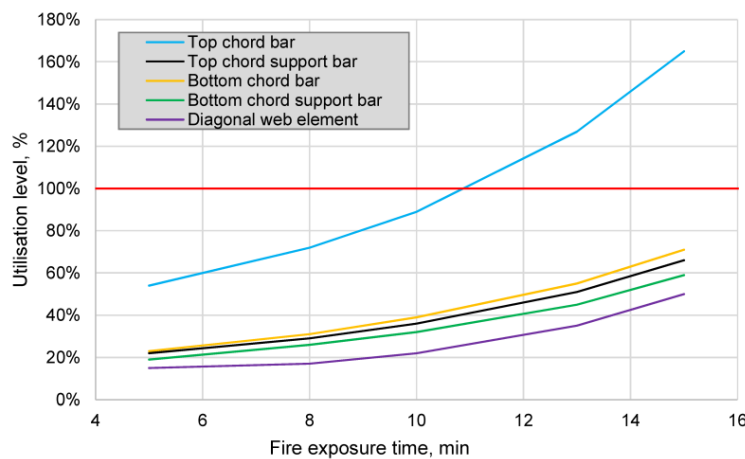


**Figure 10. The utilisation level of arch elements by strength criteria depending on the fire exposure time**

The dependence of the sum of stress-to-strength relations from the time of fire exposure for the elements of the lattice timber arch obtained by the stability condition relative to y-axis is shown in Figure 11.

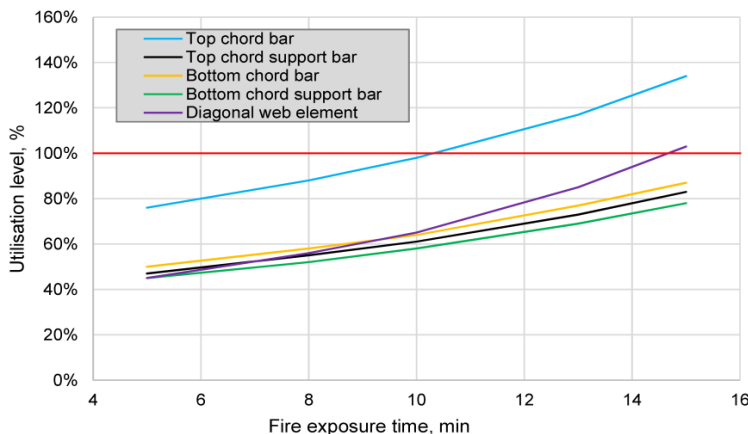


**Figure 11. The utilisation level of arch elements by stability criteria relative to Y axis depending on fire exposure time**

The dependence of the sum of stress-to-strength relations from the time of fire exposure for the elements of the lattice timber arch obtained by the stability condition relative to z-axis is shown in Figure 12.

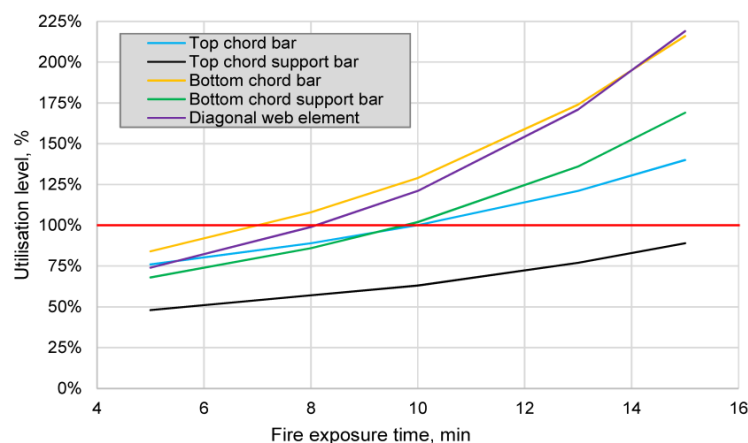


**Figure 12. The utilisation level of arch elements by stability criteria relative to Z axis depending on fire exposure time**

The dependence indicates that the strength condition for the top chord of the timber lattice arch is not satisfied just in 11.1 minutes of fire exposure. The buckling of the top chord occurs in 10.5 minutes of fire exposure relative to y-axis. The buckling of the bottom chord occurs in 7.2 minutes of fire exposure relative to z-axis. It means that fire resistance of the lattice timber arch is equal to R7.2, which is more than twice less, than the minimum required value R15 [8].

#### Design of fire-resistant lattice arch joints

Punched steel plates KARTRO with zinc coating with thickness 1.2 mm and length of teeth in 12 mm were considered as a type of fasteners for the joints of the lattice timber arch. Steel of punched plates just after 7.5-8.5 minutes of standard fire exposure come in to a plastic stage. Fire resistance of unprotected joint must be determined by the equation [10]:

$$t_{d,fi} = -1/k \cdot \ln \left( \eta_{fi} \gamma_{M,fi} / \gamma_M k_{fi} \right), \quad (11)$$

where  $k$  – is a constant parameter, which depends on the type of joint,  $\eta_{fi}$  is a reduction factor;  $\gamma_{M,fi}$  is a partial factor for timber under fire impact,  $\gamma_M$  is a partial factor for material properties.

Fire resistance of the lattice timber arch joints was evaluated as 8.61 minutes. So, it can be concluded that fire resistance of the whole roof can be evaluated as R7.2, which is more than twice less than the minimum required value R15 [8]. Fire resistance increase to the minimum required level R15 will be considered in the next chapter of the paper.

## Discussion

### Fire resistance increase of timber roof's load-bearing members

Fire resistance of purlins can be increased by the increasing of depths of its cross-sections [14]. It was shown that the minimum required level of fire resistance R 15 can be obtained if the depth of purlins cross-sections will be increased to 180 mm. So, considered dimensions of the purlins cross-sections are 180 x 70 mm.

The width of member cross-sections must be increased to provide the necessary fire resistance R15 for the lattice timber arch. But this possibility is limited due to the small typical dimensions of members: 45, 60, and 70 mm. The greater width of cross-section can be provided if several arches will be placed together one next to the other (see Fig. 13).

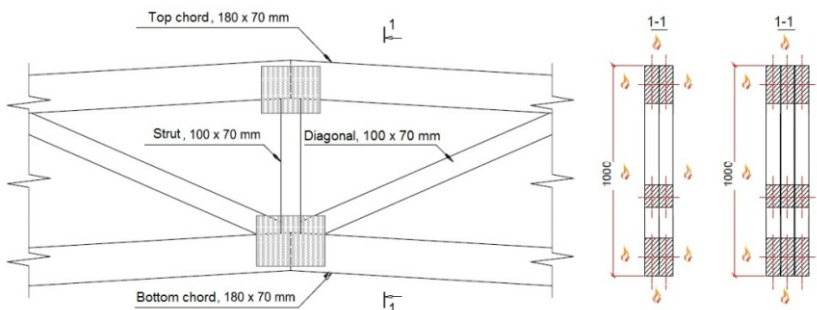


**Figure 13. Increase of the width of lattice arch by placing one arch next to the other**

The cases when two and three lattice timber arches are placed together, were considered in this study. The clearances between the arches were equal to 2.4 mm because the nodes were created with the punched steel plates with the thickness equal to 1.2 mm. So, all the arches were considered under fire impact from the four sides. It was shown that the necessary fire resistance R15 can only be provided for three arches placed together. Fire resistance of two arches placed together is only limited by R14.5.

Protective covering is another way to provide the necessary level of fire resistance for the lattice timber arch (see Fig. 14). It was shown that the necessary fire resistance R15 can be provided if the arch is covered with plywood sheets with the thickness of 12 mm [10, 15]. The density of the considered plywood is equal to 715 kg/m<sup>3</sup>.

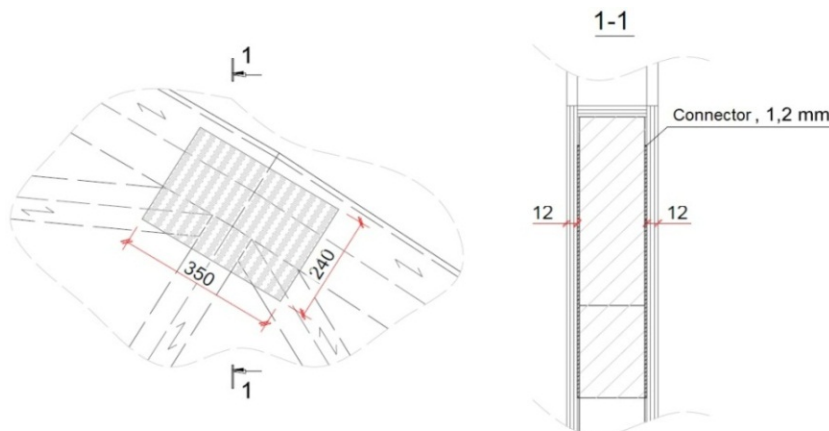


**Figure 14. Protective covering of lattice arch by the plywood sheets with thickness in 12 mm.**

Thickness of the plywood sheets in 12 mm was determined basing on the condition:

$$a_{fi} = \beta_n \cdot k_{flux} \cdot (t_{req} - t_{d,fi}), \quad (12)$$

where  $a_{fi}$  is minimum required thickness of the protective layer,  $\beta_n$  is a charring rate for plywood,  $k_{flux}$  is a constant factor,  $t_{req}$  is a required characteristic value of fire resistance,  $t_{d,fi}$  is fire resistance of an unprotected joint.

Сакните Т., Сердюк Д.О., Горемыкин В.В., Пакрастиныш Л., Ватин Н.И. Проектирование огнестойких арочных деревянных покрытий // Инженерно-строительный журнал. 2016. № 4(64). С. 26–39.

The values of a charring rate for plywood, the constant factor, the required characteristic value of fire resistance, and fire resistance of an unprotected joint were equal to 1.02 mm/min, 1.5, 15 min, and 7.5 min respectively. The minimum required thickness of the protective layer, which had been obtained by equation (12), was equal to 11.48 mm. So, the thickness of the protective layer was taken as 12 mm.

The comparison of the effectiveness of elements cross-sections increase and the protective layer usage for the fire resistance increase is given in Figure 15.

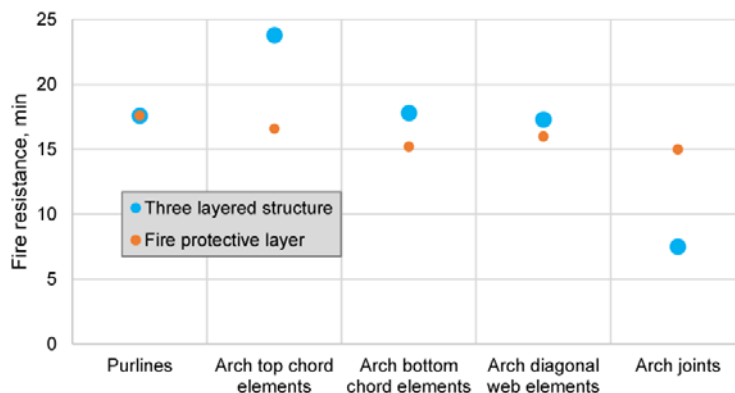


**Figure 15. Comparison of the effectiveness of element cross-section increase and the protective layer usage for the fire resistance increase**

The increase in element cross-sections cause the growth of the lattice timber arches materials consumption from 1.307 to 3.921 m<sup>3</sup> when three arches are placed together one next to the other. The protective layer usage causes the growth of the lattice timber arches materials consumption from 1.307 to 2.163 m<sup>3</sup>. But the elements cross-section increase did not allow protecting the nodes of the edge arches, as it is shown in Figure 15. Therefore, based on the comparison of both methods, the usage of protective layer is considered as a preferable method of fire resistance increase for the lattice timber arch [16].

#### *Evaluation of rational parameters of the arch-type timber roof*

The response surface method was used to evaluate rational values of the main geometrical parameters of the arch-type timber roof [17, 18]. The height of the arch (*f*), depth of the arch cross-section (*h*), and distance between the nodes on the top chord (*a*) are considered as the main geometrical parameters (Fig. 16.).

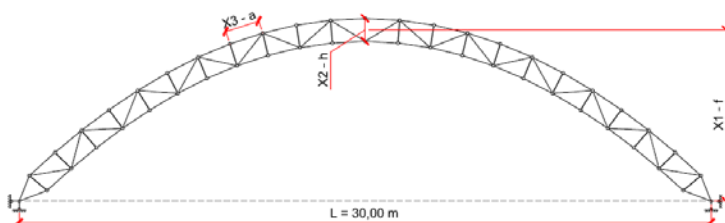


**Figure 16. The main geometrical parameters of arch-type timber roof: (f) height of the arch; (h) depth of the arch cross-section; (a) distance between the nodes on the top chord.**

Materials consumption of purlins and lattice timber arch so as maximum axial force acting in the top chord of the arch were considered as the parameters of optimization [19]. The dependences of the main geometrical parameters of the arch-type timber roof on the material consumption were determined as the second order polynomial equations in case of fire action and without taking in to consideration the fire action.

$$Y' = b_0 + b_1 f + b_2 h + b_3 a + b_{12} fh + b_{13} fa + b_{23} ha + b_{123} fX_2 a + b_{11} f^2 + b_{22} h^2 + b_{33} a^2, \quad (13)$$

where *Y'* is materials consumption (m<sup>3</sup>); *f* is height of the arch (m); *h* is depth of the arch cross-section (m); *a* is a distance between the nodes on the top chord (m).

The values of the height of the arch, depth of the arch cross-section, and the distance between the nodes on the top chord change within the limits from 5.5 to 7.5 m, from 0.5 to 1 m, and from 1 to 1.5 m respectively. Coefficients of the second order polynomial equations are given in the table.

**Table 4. Coefficients of the second order polynomial equations**

	In the context of material consumption		In the context of axial forces in the arch top chord	
	Fire is not taken into account	Fire is taken into account	Fire is not taken into account	Fire is taken into account
$b_0$	9.46184	10.9741	547.358	551.152
$b_1$	-1.50739	-1.37964	-22.7047	-23.5849
$b_2$	-5.69789	-6.27883	-411.36	-407.507
$b_3$	-1.44156	-3.74211	-123.181	-124.552
$b_{12}$	0.304	0.397667	-0.262333	-0.711667
$b_{13}$	0.07	0.231333	1.528	1.30067
$b_{23}$	-1.956	-3.01333	-5.87333	-5.21467
$b_{123}$	0.0	0.0	0.0	0.0
$b_{11}$	0.0872222	0.0575	0.9335	1.03778
$b_{22}$	3.52622	4.776	190.216	190.946
$b_{33}$	1.13156	1.992	46.5093	47.4604

Values of coefficients of the second order polynomial equations were determined with the EdaOpt computational program [20]. The obtained polynomial equations enable describing the obtained results with the precision up to 13.18 and 14.62 % under fire impact and without taking the fire impact into consideration.

The dependence of the height of the arch ( $f$ ) and depth of the arch cross-section ( $h$ ) on the materials consumption under fire impact and without taking the fire impact into consideration is given in Figure 17.

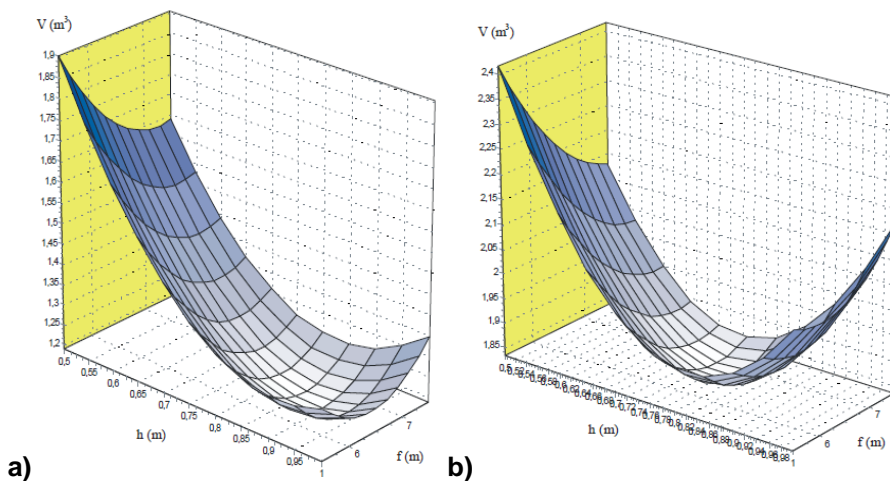


**Figure 17. The dependences of height of the arch ( $f$ ) and depth of the arch cross-section ( $h$ ) on the materials consumption in case of fire action a) and without taking in to consideration the fire action b).**

The rational from the point of view of materials consumption values of height of the arch, depth of the arch cross-section and distance between the nodes on the top chord were determined by the system of equations [16]:

$$\begin{cases} \frac{\partial G}{\partial f} = b_1 + b_{12}h + b_{13}a + b_{123}ha + 2b_{11}f = 0 \\ \frac{\partial G}{\partial h} = b_2 + b_{12}f + b_{23}a + b_{123}fa + 2b_{22}h = 0 \\ \frac{\partial G}{\partial a} = b_3 + b_{13}f + b_{23}h + b_{123}fh + 2b_{33}a = 0 \end{cases} \quad (14)$$

The rational values of the height of the arch, depth of the arch cross-section, and the distance between the nodes on the top chord were given in Table 5.

**Table 5. Rational values of geometrical parameters of the arch-type timber roof**

Variable factors		In the context of material consumption	In the context of axial forces in the arch top chord
<b>Fire is not taken into account</b>			
$X_1 - f$	Arch axe camber (m)	6.70	11.30*
$X_2 - h$	Arch cross-section height (m)	0.80	1.10*
$X_3 - a$	Arch top chord segment length (m)	1.15	1.2
<b>Fire is taken into account</b>			
$X_1 - f$	Arch axe camber (m)	7.85*	10.95*
$X_2 - h$	Arch cross-section height (m)	0.6	1.10*
$X_3 - a$	Arch top chord segment length (m)	0.95*	1.2

\* – the values are out of the initially considered limits

It can be concluded that the finally adopted rational values of the height of the arch ( $f$ ), depth of the arch cross-section ( $h$ ), and distance between the nodes on the top chord ( $a$ ) are equal to 7.85, 1.10 and 0.95 m respectively.

## Conclusions

The paper considers the possibility of a fire resistance increase to R15 for the arch-type timber roof by using the protective layer and increase in the elements cross-sections dimensions. Using the protective layer is considered as a preferable method of the fire resistance increase for the lattice timber arch because it is joined with the growth of materials consumption by 1.65 times. The increase in the elements cross-sections dimensions causes the growth of materials consumption by 3 times.

Rational values of the height of the arch, depth of the arch cross-section, and distance between the nodes on the top chord were evaluated for the arch-type timber roof with the response surface method. Fire resistance of the roof was taken into account. The span of the considered arch-type timber roof was equal to 30 m. The values of the height of the arch, depth of the arch cross-section, and distance between the nodes on the top chord change within the limits from 5.5 to 7.5 m, from 0.5 to 1 m, and from 1 to 1.5 m respectively. It was shown that the rational values of the height of the arch, depth of the arch cross-section, and distance between the nodes on the top chord are equal to 7.85, 1.10, and 0.95 m respectively. The corresponding minimum material consumptions were equal to 1.856 and 1.273 m<sup>3</sup> in case of fire impact and without taking it into consideration.

## Acknowledgement

The research leading to these results has received its funding from the Latvia state research program under the grant agreement "Innovative Materials and Smart Technologies for Environmental Safety, IMATEH". Project Nr.3, PVS ID1854, Task Nr.3.

## References

1. Ozola L. *Konektoru kopņu projektaešana*. Elgava: LLU, 1999. 62 p.
2. Serduks D., Goremkins V., Šliseris J. *Metodiskie norādījumi priekšmetā BBK 560 „Koka un plastmasu konstrukcijas” (speciālais kurss)*. Riga: RTU, 2012. 46 p.
3. Goremkins V., Šejnoha J., Wald F., Bednar J. Analytical model of composite floors with steel fibre reinforced concrete slab subjected to fire. *Journal of Civil Engineering and Management*. November 2015. Pp. 1–9.
4. Frangi A., Fontana M., Hugi E., Jübsti R. Experimental analysis of cross-laminated timber panels in fire. *Fire Safety*

Saknīte T., Serduks D., Goremkins V., Pakrastins L., Vatin N.I. Fire design of arch-type timber roof. *Magazine of Civil Engineering*. 2016. No. 4. Pp. 26–39. doi: 10.5862/MCE.64.3

## Литература

1. Ozola L. *Konektoru kopņu projektaešana*. Elgava: LLU, 1999. 62 p.
2. Serduks D., Goremkins V., Šliseris J. *Metodiskie norādījumi priekšmetā BBK 560 „Koka un plastmasu konstrukcijas” (speciālais kurss)*. Riga: RTU, 2012. 46 p.
3. Goremkins V., Šejnoha J., Wald F., Bednar J. Analytical model of composite floors with steel fibre reinforced concrete slab subjected to fire // *Journal of Civil Engineering and Management*. November 2015. Pp. 1–9.
4. Frangi A., Fontana M., Hugi E., Jübsti R. Experimental analysis of cross-laminated timber panels in fire // *Fire*

- Journal.* 2009. No. 44(8). Pp. 1078–1087.
5. Frangi A., Knobloch M., Fontana M. Fire design of timber slabs made of hollow core elements. *Engineering Structures.* 2009. No. 31(1). Pp. 150–157.
  6. Saknīte T. *Lokveida koka kopnes racionāla risinājuma pamatojums.* Riga: RTU, 2014. 187 p.
  7. LBN 201-15. *Būvju ugunsdrošība.* Riga. 2015. 33 p.
  8. LBN 003-01. *Būvklimatoloģija.* Riga, 2001. 50 p.
  9. Gravit M., Vaitickii A., Imasheva M., Nigmatulina D., Shpakova A. Classification of Fire Technical Characteristic of Roofing Materials in European and Russian Regulation Documents. *MATEC Web of Conferences.* 2016.
  10. EN 1995-1-2. Eurocode 5: *Design of timber structures.* Part 1-2: General - Structural fire design. Brussels: European Committee for Standardisation, 2004. 69 p.
  11. Yang T.H. The charring depth and charring rate of glued laminated timber after a standard fire exposure test. *Building and Environment.* 2009. No. 44 (2), Pp. 231–236.
  12. EN 1990. Eurocode 0: *Basis of structural design.* Brussels: European Committee for Standardisation, 2002. 69 p.
  13. EN 1995-1-1. Eurocode 5: *Design of timber structures.* Part 1-1: General - Common Rules and Rules for Buildings. Brussels: European Committee for Standardisation, 2004. 123 p.
  14. Serduks D., Goremkins V. *Ugunsdrošu koka konstrukciju projektaešana saskaņā ar LVS EN 1995–1–2. Metodiskie norādījumi.* Riga: RTU, 2014. 46 p.
  15. Krivtsov A., Gravit M., Zimin S., Nedryshkin O., Pershakov V. Calculation of Fire Resistance for Structures with Fire Retardant Coating. *MATEC Web of Conferences.* 2016.
  16. Saknīte T. *Lokveida koka pārseguma ugunsizturības analīze.* Riga: RTU, 2015. 100 p.
  17. Hirkovskis A., Serduks D., Goremkins V., Pakrastins L., Vatin N.I. Behaviour analysis of load-bearing aluminium members. *Magazine of Civil Engineering.* 2015. No. 5. Pp. 86–96.
  18. Villar J.R., Vidal P., Fernández M.S., Guaita M. Genetic algorithm optimisation of heavy timber trusses with dowel joints according to Eurocode 5. *Biosystems Engineering.* 2016. No. 144. Pp. 115–132.
  19. Goremkins V., Rocens K., Serduks D., Pakrastins L., Vatin N. Cable truss topology optimization for prestressed long-span structure. *Advances in Civil Engineering and Building Materials IV.* 2014. Pp. 363–368.
  20. Auzukalns J. *Manual of software EdaOpt.* Riga: RTU. 2007.
  5. Frangi A., Knobloch M., Fontana M. Fire design of timber slabs made of hollow core elements // Engineering Structures. 2009. № 31(1). Pp. 150–157.
  6. Saknīte T. Lokveida koka kopnes racionāla risinājuma pamatojums. Riga: RTU, 2014. 187 p.
  7. LBN 201-15. Būvju ugunsdrošība. Riga. 2015. 33 p.
  8. LBN 003-01. Būvklimatoloģija. Riga, 2001. 50 p.
  9. Gravit M., Vaitickii A., Imasheva M., Nigmatulina D., Shpakova A. Classification of Fire Technical Characteristic of Roofing Materials in European and Russian Regulation Documents // MATEC Web of Conferences. 2016.
  10. EN 1995-1-2. Eurocode 5: Design of timber structures. Part 1-2: General - Structural fire design. Brussels: European Committee for Standardisation, 2004. 69 p.
  11. Yang T.H. The charring depth and charring rate of glued laminated timber after a standard fire exposure test // Building and Environment. 2009. № 44 (2), Pp. 231–236.
  12. EN 1990. Eurocode 0: Basis of structural design. Brussels: European Committee for Standardisation, 2002. 69 p.
  13. EN 1995-1-1. Eurocode 5: Design of timber structures. Part 1-1: General - Common Rules and Rules for Buildings. Brussels: European Committee for Standardisation, 2004. 123 p.
  14. Serduks D., Goremkins V. Ugunsdrošu koka konstrukciju projektaešana saskaņā ar LVS EN 1995–1–2. Metodiskie norādījumi. Riga: RTU, 2014. 46 p.
  15. Krivtsov A., Gravit M., Zimin S., Nedryshkin O., Pershakov V. Calculation of Fire Resistance for Structures with Fire Retardant Coating // MATEC Web of Conferences. 2016
  16. Saknīte T. Lokveida koka pārseguma ugunsizturības analīze. Riga: RTU, 2015. 100 p.
  17. Hirkovskis A., Serduks D., Goremkins V., Pakrastins L., Vatin N.I. Behaviour analysis of load-bearing aluminium members // Magazine of Civil Engineering. 2015. № 5. Pp. 86–96.
  18. Villar J.R., Vidal P., Fernández M.S., Guaita M. Genetic algorithm optimisation of heavy timber trusses with dowel joints according to Eurocode 5 // Biosystems Engineering. 2016. № 144. Pp. 115–132
  19. Goremkins V., Rocens K., Serduks D., Pakrastins L., Vatin N. Cable truss topology optimization for prestressed long-span structure. Advances in Civil Engineering and Building Materials IV. 2014. Pp. 363–368.
  20. Auzukalns J. Manual of software EdaOpt. Riga: RTU. 2007.

*Tatjana Saknīte,*  
+37167089145; [tatjana.saknīte@rtu.lv](mailto:tatjana.saknīte@rtu.lv)

*Dmitrijs Serduks,*  
+37126353082; [Dmitrijs.Serduks@rtu.lv](mailto:Dmitrijs.Serduks@rtu.lv)

*Vadims Goremkins,*  
+37129231772; [goremkins@gmail.com](mailto:goremkins@gmail.com)

*Leonids Pakrastins,*  
+37129452138; [leonids.pakrastins@rtu.lv](mailto:leonids.pakrastins@rtu.lv)

*Nikolai Vatin,*  
+79219643762; [vatin@mail.ru](mailto:vatin@mail.ru)

*Татьяна Сакните,*  
+37167089145; эл. почта: [tatjana.saknīte@rtu.lv](mailto:tatjana.saknīte@rtu.lv)

*Дмитрий Олегович Сердюк,*  
+37126353082; эл. почта:  
[Dmitrijs.Serduks@rtu.lv](mailto:Dmitrijs.Serduks@rtu.lv)

*Вадим Валерьевич Горемыкин,*  
+37129231772; эл. почта: [goremkins@gmail.com](mailto:goremkins@gmail.com)

*Леонид Пакрастиньш,*  
+37129452138; эл. почта:  
[leonids.pakrastins@rtu.lv](mailto:leonids.pakrastins@rtu.lv)

*Николай Иванович Ватин,*  
+79219643762; эл. почта: [vatin@mail.ru](mailto:vatin@mail.ru)

© Saknīte T., Serduks D., Goremkins V., Pakrastins L., Vatin N.I., 2016

doi: 10.5862/MCE.64.4

## The stiffness of rigid joints of beam with hollow section column

### Жесткость рамных узлов сопряжения ригеля с колонной коробчатого сечения

O.A. Tusnina,  
A.I. Danilov,

National Research Moscow State University of Civil  
Engineering, Moscow, Russia

Канд. техн. наук, старший  
преподаватель О.А. Туснина,  
канд. техн. наук, доцент А.И. Данилов,  
Национальный исследовательский  
Московский государственный  
строительный университет, Москва,  
Россия

**Key words:** rigid joint; steel frameworks; hollow  
section; frame

**Ключевые слова:** жесткий узел; стальной  
каркас; коробчатое сечение; рамный каркас

**Abstract.** At present steel framework based buildings are prevalent in civil engineering. Application of hollow section columns have proven to be efficient in low-rise buildings. In some cases frame joints of beam to column connections are needed in this kind of building structures. This paper considers rigid joints of I-beam to hollow section column connections allowing for an elastic pliability. The results of pliability estimation of these joints are represented for various construction solutions. Dependences are obtained for the relation of the support moment in a beam to its corresponding value in absolutely stiff connection on the rigidity of the joint. The dependence diagrams of rigidity of the joint on the parameters of its elements are obtained.

**Аннотация.** В настоящее время широкое распространение в строительстве получают здания на основе стальных каркасов. В малоэтажных зданиях целесообразно применять колонны коробчатого сечения. В таких зданиях часто оказывается необходимым обеспечить работу каркаса по рамной или рамно-связевой схемам. В связи с этим возникает необходимость выполнения жестких узлов соединения ригеля с колонной. В данной статье рассматриваются жесткие узлы соединения ригеля двутаврового сечения с колонной из замкнутого квадратного профиля с учетом их податливости. Выполнена оценка жесткости соединения ригеля с колонной при различном конструктивном решении узла их сопряжения. Получены зависимости отношения опорного момента ригеля к его величине при абсолютно жестком закреплении опорного сечения ригеля от жесткости соединения. Построены графики зависимости жесткости соединения от некоторых параметров соединительных элементов, используемых в сопряжении.

#### Introduction

Buildings based on steel frameworks are widespread in civil engineering. Steel frameworks have some advantages in comparison to concrete buildings:

- lower loads on foundation are caused by low dead load of the support framework;
- high speed of mounting ;
- ability to mount structures in winter without any additional measures;
- environmental friendliness.

At present the output of low-rise buildings increases. Low-rise buildings are used as apartment buildings, cabins, dormitories etc.

Today the buildings based on light thin-walled structures are widespread. Many articles are devoted to the issue of designing such structures [1–3]

Thin-walled cold-formed profiles used in light steel thin-walled constructions (LSTC) have such geometry parameters (low thickness less than 4 mm) that allow the loss of its local stability. The effect of local stability loss must be taken into account when calculating LSTC structures [4–7].

The paper [8] represents the results of the experimental research that shows the necessity to consider geometric nonlinearity in calculation of thin-walled structures.

Tusnina O.A., Danilov A.I. The stiffness of rigid joints of beam with hollow section column. *Magazine of Civil Engineering*. 2016. No. 4. Pp. 40–51. doi: 10.5862/MCE.64.4

The paper [9] studies deformability of joints depending on the constructive solution experimentally and by finite element analysis. It determines the factors which affect the loss of local stability in joints.

Because of all the mentioned complications in calculating and design structures made from cold-formed thin-walled profiles (LSTC) the use of hot-rolled profiles is more preferable.

Steel frameworks built from hot-rolled and bent welded profiles are more efficient than frameworks built with the use of light thin-walled structures [10].

To provide the freedom of planning it is necessary to design the framework without braces so it is necessary to make rigid joints of beam to column connection.

The well-known construction solutions of rigid joints between I-beam and column of I-section and analysis guidelines are represented in papers [11–14].

Hollow sections as columns and I-beams are expedient to be applied in steel frameworks of low-rise buildings with quite small loads. Such a solution allows decreasing the consumption of material and simplifying mounting.

Some constructive solutions of the connection of beam with hollow section column are represented in the paper [15]. Such construction solutions provide higher stiffness of the joint and allow it to be applied in earthquake-prone regions.

The results of the researched work of rigid joint of beam to hollow section column connection are represented in the papers [16–18]. Also a constructive solution increasing the joint bearing capacity has been developed.

However, it is difficult to apply these constructive solutions in mass buildings because of a large scope of work.

According to the European norms for the analysis of joint stress-strain state 2D and 3D component methods are used.

The spread of the component method on the columns of hollow sections is represented in the article [19].

The papers [20–22] are dedicated to the development of 3D component method.

In the paper [23] the work of the joint of connection I-beam to hollow section column with the use of T-shaped elements is researched. T-shaped elements increase the thickness of the column in the points of effort transfer on the column from beam flanges. But a conclusion is made that such a structure of joint does not provide sufficient stiffness of the joint.

The problems of design and analysis of joints of I-beam connection with the column are also formulated in the articles [24–31].

The rigid joints of I-beam to hollow section column connections allowing for elastic pliability are considered in this paper.

## Methods

At first the beam made of I22 on GOST 8239-89 with absolutely rigid supports loaded by uniformly distributed load was considered (Figure 1).

Finite element analysis was made with the use of program MSC.NASTRAN. The beam was modeled with the use of elastic quadrilateral PLATE elements. The finite elements were located on the middle surface of the profile.

To achieve satisfactory convergence, the finite element mesh with 10 finite elements on the height of I-beam was assigned. The size of the plate finite element was adopted based on the results of the test analyses carried out for a similar problem [32].

The span of the beam was 6 m. Half of the beam was modeled with appropriate constraints on the cross section on the axis of symmetry. The constraints of axial displacement (translation along global axis X) and those of rotation around Y-axis were set on the nodes of flanges and web of the beam in the cross section in the middle of the beam span.

The uniformly distributed load on beam  $q=10 \text{ kN/m}$ . The distributed load was brought to the concentrated loads which were applied in the nodes of the flange to the web connection line.

Static linear analysis was carried out. Geometrical and physical nonlinearity was not taken into account.

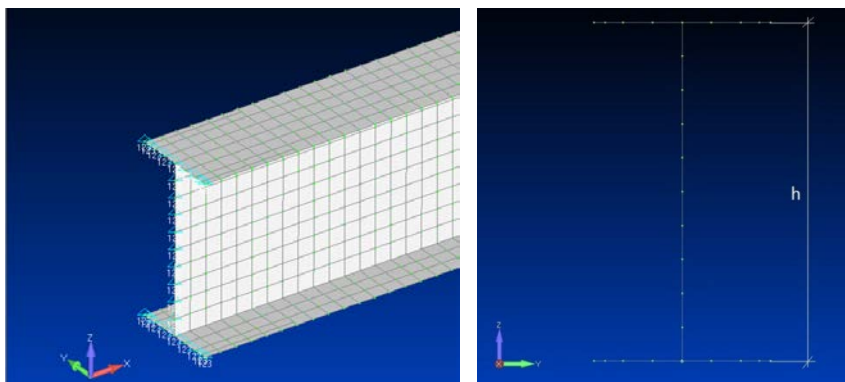


**Figure 1. Finite-element model of I-beam**

The diagram of bending moments in a beam with absolutely rigid supports is represented in Figure 2.

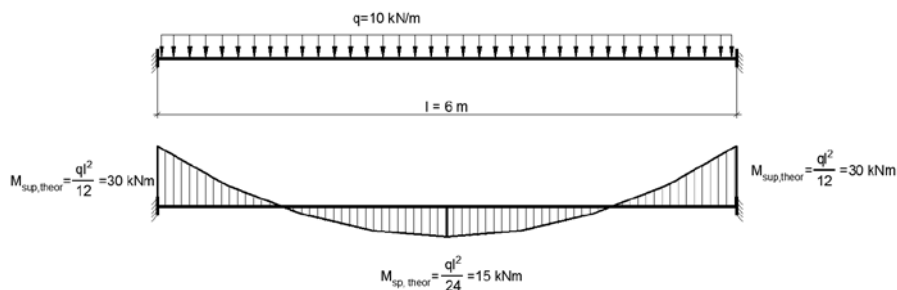


**Figure 2. The diagram of bending moments in a beam with absolutely rigid supports**

But it is impossible to make the beam-column joint absolutely rigid and fix the support cross-section of the beam from rotation. Flexibility of the joint will be determined by deformations occurring in connective elements, columns, beam. So the support cross-section of the beam will be rotated by some angle  $\varphi$ .

Flexibility of the joint influences the effort distribution between the beam and the column, especially in bending moment distribution along the beam.

Stiffness of the joint C is determined as a ratio of the bending moment acting on the support to the rotation angle of the support cross-section of the beam:

$$C = \frac{M}{\varphi}, \quad (1)$$

where  $M$  – the bending moment acting on the support;

$\varphi$  – rotation angle of the support cross-section of the beam.

The finite element analysis was conducted to estimate the influence of the connection stiffness on the bending moment acting on the support. The numerical analysis of bending moment distribution in the beam considered above was made with the different stiffness of support joint C.

Flexibility of the joint was modeled by the use of spring elements in the nodes of the beam flange in the support cross-section (Figure 3). Elements spring with different axial stiffness  $K$  prevents free movement of beam flanges and, thereby, prevents free rotation of its support cross-section.

Axial stiffness of elements  $K$ , related to the stiffness of connection C is as follows:

$$K = \frac{2C}{h^2}, \quad (2)$$

where  $h$  – height of the beam (in this case – distance between nodes on the middle surfaces of the flanges, Figure 1).

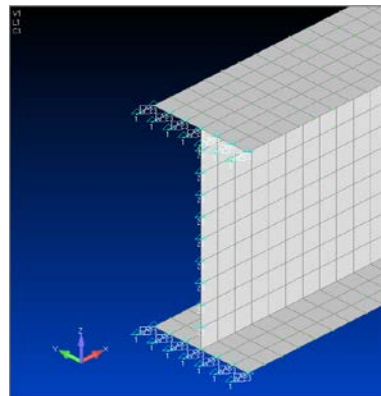


**Figure 3. Flexible fixation of the beam on the support**

Normal stresses in the cross-sections of the beam in the considered loading conditions were determined by bending moment  $M_y$ . Normal stresses in the middle surface of the beam cross-section in the 1 and 2 points in the middle of the beam span were determined in the result of numerical analysis. The value of the bending moment acting in the middle of the span can be determined by solving the equation (3):

$$\sigma_1 = \sigma_2 = \frac{M_{sp}}{W}, \quad (3)$$

where  $\sigma_1$  и  $\sigma_2$  – normal stresses acting in points 1 and 2 in the middle of the beam span (Figure 4).

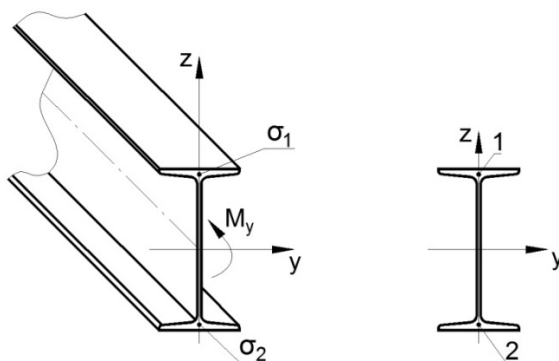


**Figure 4. Cross-section of the beam with considered points**

Then by using the value of moment in the middle of beam span  $M_{sp}$  we can determine the moment on beam support  $M_{sup}$ :

$$M_{sup} = M_{sp} - \frac{ql^2}{8} \quad (4)$$

For each value of stiffness the ratio of support moment  $M_{sup}$  to the theoretical moment on the support with absolutely rigid fixation  $M_{sup, theo}$ :

$$k = \frac{M_{sup}}{M_{sup, theo}} \quad (5)$$

In Figure 5 the graph of the dependence of coefficient  $k$  on the stiffness of joint C. The data represented on the graph are also represented in Table 1.

Туснина О.А., Данилов А.И. Жесткость рамных узлов сопряжения ригеля с колонной коробчатого сечения // Инженерно-строительный журнал. 2016. № 4(64). С. 40–51.

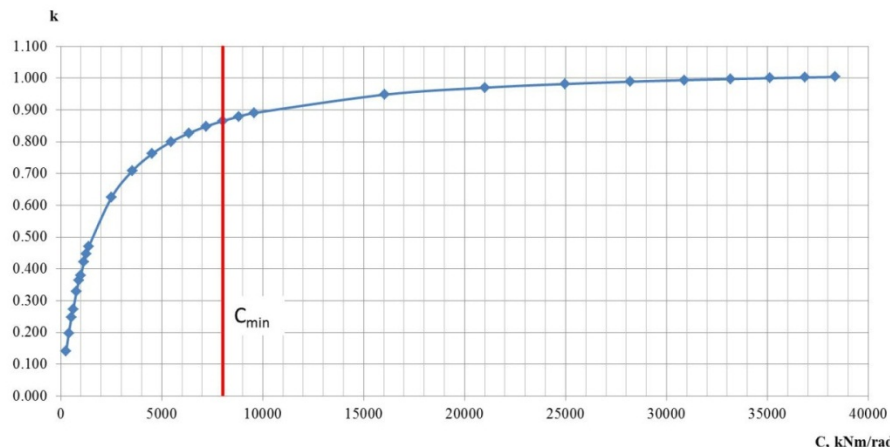


Figure 5. The graph of dependence of coefficient  $k$  on the stiffness of joint  $C$

Table 1. The values of coefficient  $k$  of different stiffness  $C$

$C, \text{kNm/rad}$	$k$	$C, \text{kNm/rad}$	$k$
264.90	0.141	6345.32	0.827
397.51	0.198	7196.56	0.848
527.78	0.248	8015.61	0.865
612.06	0.272	8804.42	0.879
781.66	0.330	9568.38	0.890
906.72	0.364	16035.40	0.948
989.34	0.379	20998.93	0.970
1150.06	0.422	24959.76	0.982
1270.63	0.448	28201.79	0.989
1388.65	0.471	30897.60	0.994
2511.90	0.625	33173.30	0.997
3551.21	0.709	35131.57	1.000
4529.17	0.762	36845.07	1.000
5457.17	0.799	38365.86	1.000

Coefficient  $k$  tends to 1 when the stiffness of connection increases. The joint is suggested for consideration as rigid if the difference between theoretical moment and actual moment is not bigger than 10...12 % (coefficient  $k \geq 0.88$ ).

On the graphs the minimum value of stiffness  $C_{min} = 8000 \text{ kNm/rad}$  is shown by a vertical red line. With this stiffness the value of  $k = 0.88$ .

The stiffness of the connection depends on its constructive solution. To estimate the stiffness of the joint of the beam with the columns of hollow sections numerical analysis of joints referring to different constructive solutions was made.

The joint of the beam (I22, GOST 8239–89) with the column (bent-welded tube 120x6, GOST 30245–2003) connection was considered.

The span of the beam was 6 m. The uniformly distributed load along the beam was 10 kN/m.

Three types of joints were considered:

- 1 – rigid joint with direct adjacently overlays on belts bolt to the column wall (Figure 6);
- 2 – rigid joint with the transfer to the column shearing force through angels attached to it (Figure 7);
- 3 – hinge joint on pad (Figure 8)

A finite element model of the considered sites was compiled using MSC.NASTRAN software package.

Half of the beam (3 m) was modeled with the corresponding constraints on the cross section on the symmetry axis. The load was applied in the nodes of the beam wall.

The influence of column deformations on the stiffness of the joint is not considered and simulated in the analysis model of the 0.8 m long column, with fixed ends of all movements.

The patches were connected with the column through rigid elements with the union movement relevant nodes overlapping the beam /column nodes (Figure 9).

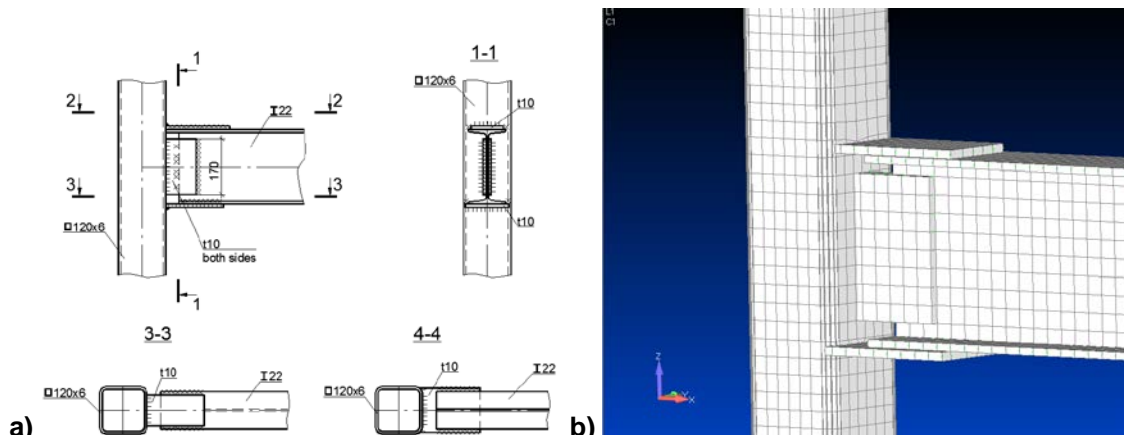


Figure 6. Rigid joint (1 type): a – constructive solution; b – finite-element model

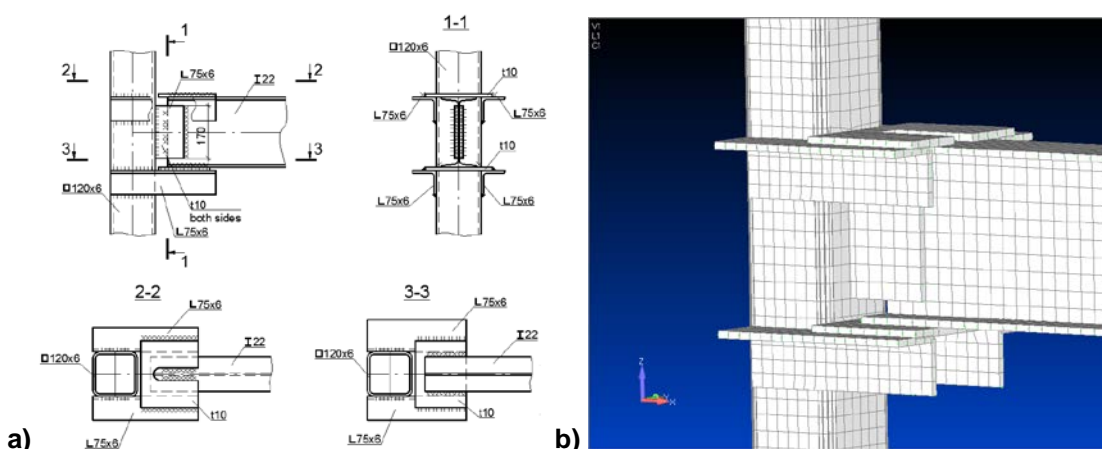


Figure 7. Rigid joint (2 type): a – constructive solution; b – finite-element model

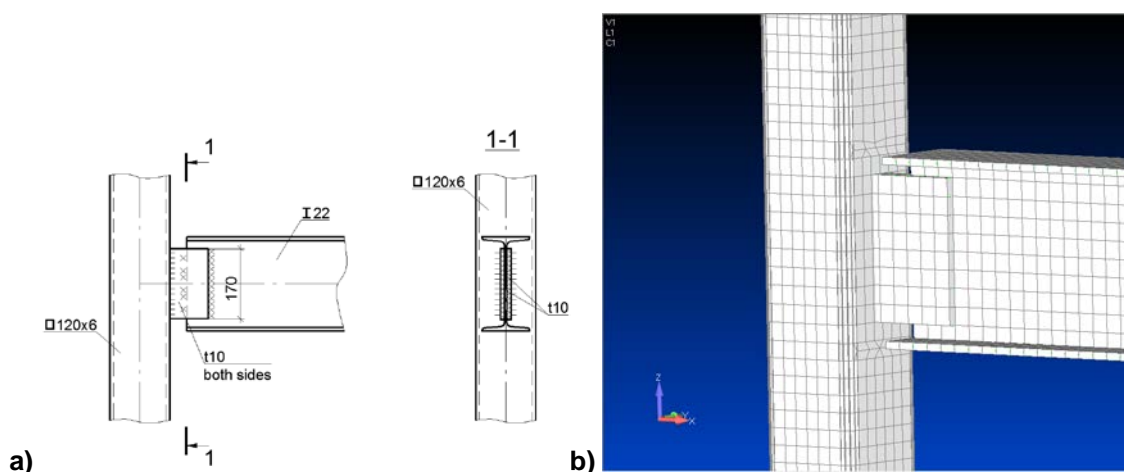
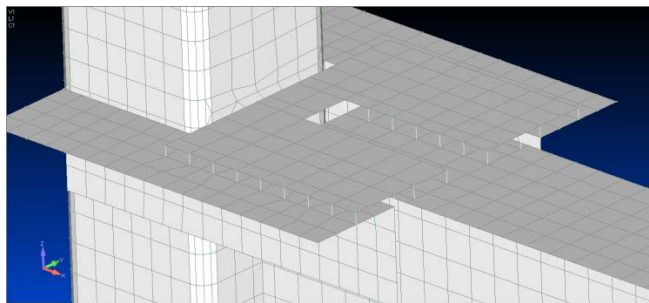


Figure 8. Hinged joint: a – constructive solution; b – finite-element model



**Figure 9. Connection of the nodes on the patch with a beam and angels**

## Results

The resulting numerical calculation of the stiffness values of the compound C, the angle of rotation of the support section crossbar  $\varphi_{sup}$ , bending moments on the support and in the span  $M_{sup}$  and  $M_{sp}$  respectively, and the coefficient  $k$  are given in Table 2.

Table 2 also shows the theoretical solutions for the beam absolutely rigidly fixed on the rotation supporting sections and the beam supported in a simple way.

**Table 2. The values of the coefficient  $k$  with different values of stiffness C**

Type of analysis	Joint	Stiffness of joint C, kNm/rad	Rotational angle of support cross-section $\varphi_{sup}$ , rad	Support moment $M_{sup}$ , kNm	$k = \frac{M_{sup}}{M_{sup, theo}}$	Span moment $M_{sp}$ , kNm
Numerical analysis	Hinged	419.3	0.0146	6.12	0.204	38.88
	Rigid 1 type	4116.5	0.00544	22.39	0.746	22.61
	Rigid 2 type	9602.89	0.00279	26.79	0.893	18.21
Theory	Hinged	-	0.0171	-	0	45.00
	Rigid	-	0	30.00	1.000	15.00

The angle of rotation of the support section with the patches on the hinge joint linings on the wall (Figure 8) is about 85 % of the theoretical one with absolutely free rotation.

In this constructive decision the joint has certain stiffness and provides a reference point, amounting to about 0.2 by the complete theoretical pinching. The decrease in the time span compared to the theoretical one with simple support girder is about 13.6 %.

Thus, the joint, which is traditionally perceived as a hinge, can be considered as compliant, in a similar way as it was done in [33] in relation to the connection node of the I-beam with a column on rails and angles.

The stiffness of the type 1 rigid joint (Figure 6) is small (less than 8000 kNm/rad) and not sufficiently hard to ensure assembly work (acting on the support point is 22.39 kNm compared to the theoretical 30 kNm, and the ratio  $k$  is less than 0.88 equaling to about 0.75), so the use of such units in the rack is not recommended.

The stiffness of the type 2 rigid joint (Figure 7) above proves that such nodes may be regarded as rigid. However, the magnitude of rigidity is close to the minimum, amounting to about 9600 kNm/rad, and the coefficient  $k = 0.893$ .

To assess the influence on the stiffness of the geometric parameters of the node connection elements the node was identified based on the stiffness of the following parameters:

- for the assembly of direct overlap adjacent to the column wall (joint of type 1) – the thickness of the casing wall, the thickness of lining the shelves and the height of the wall lining;
- for the assembly with transfer of forces through the angle (joint of type 2) – the thickness of the tower wall thickness over the height of the pads and the wall.

Tusnina O.A., Danilov A.I. The stiffness of rigid joints of beam with hollow section column. *Magazine of Civil Engineering*. 2016. No. 4. Pp. 40–51. doi: 10.5862/MCE.64.4

The results are shown graphically in Figures 10 and 11, and in a form of a table – Table 3, 4, 5.

The graphs and tables show that by increasing the thickness of the column by 5.5 mm to 8 mm, the rigidity of the type 1 joint increased by 56 %, the type 2 joint – by 18 %.

Increasing the stiffness of the type 1 joint by 56% however does not allow for sufficient assembly stiffness and an 8 mm thick unit cannot be considered as hard enough even if a column is used.

When the lining thickness increases from 6 mm to 14 mm the stiffness of the type 1 unit goes up by 17 %, while if the thickness of the angle increases from 5 mm to 9 mm the stiffness of the type 2 node enlarges by 20 %.

They are also plotted given the coefficient  $k$  from the parameters (Figure 12).

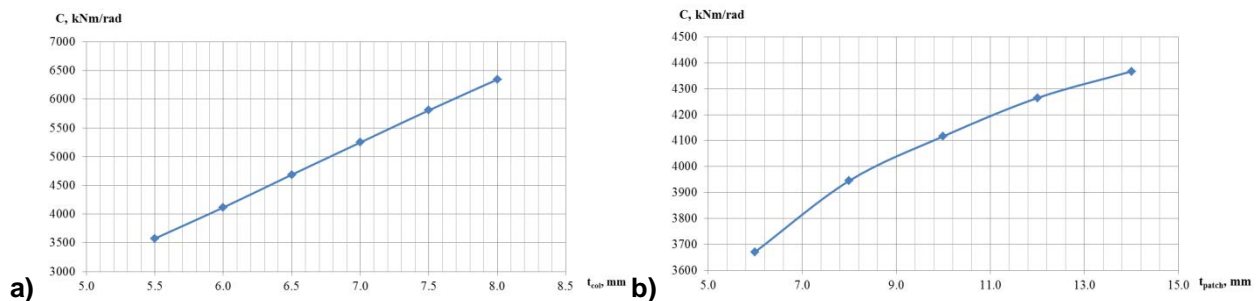


Figure 10. Graphs of stiffness dependence(1 type) on  
a – thickness of column wall; b – thickness of patch on flanges

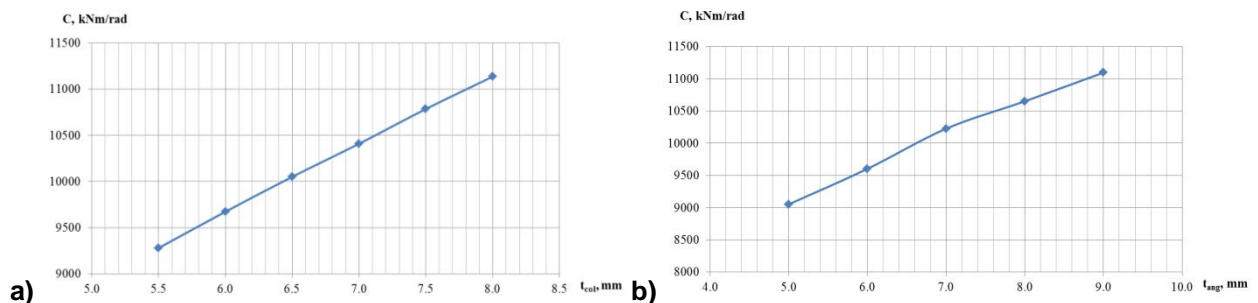


Figure 11. Graphs of stiffness dependence (2 type) on  
a – thickness of column wall; b – thickness of angels

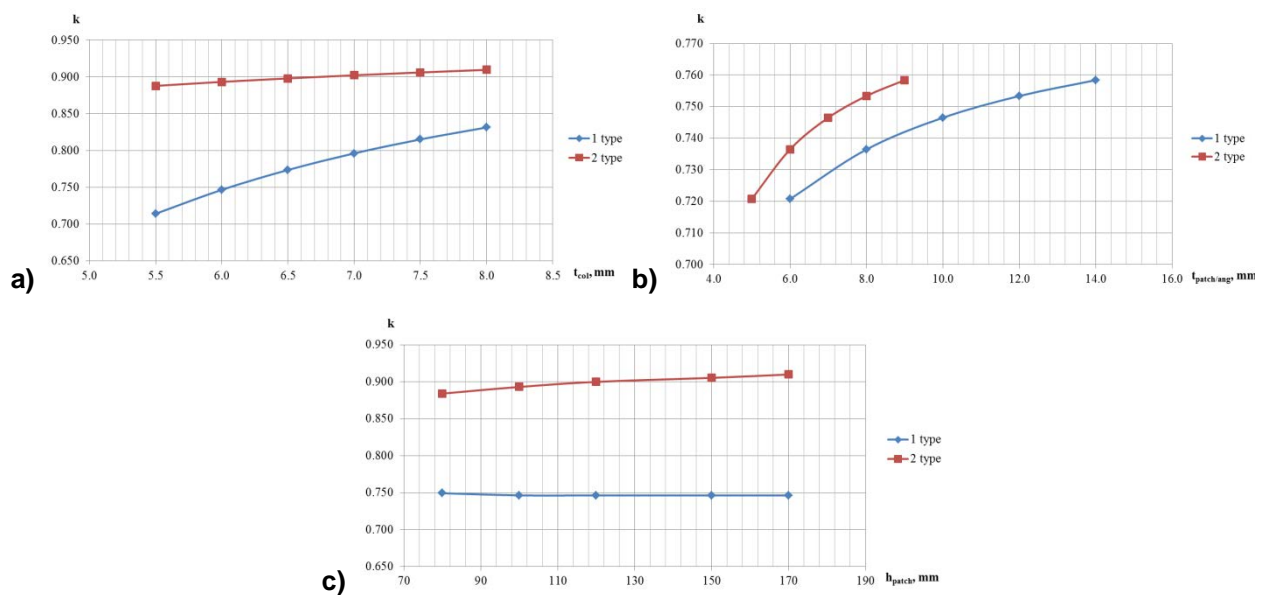


Figure 12. Graphs of coefficient  $k$  (1 type) dependence on: a – thickness of column wall;  
b – thickness of patches (1 type)/thickness of angles (2 type);  
c - height of the patch on beam wall

**Table 3. The value of coefficient  $k$  with the different stiffness of joint C**

Joint	Thickness of column $t_{col}$ , mm	$C$ , kNm/rad	$\varphi_{sup}$ , rad	$M_{sup}$ , kNm	$k$
1 type	5.5	3575.4	0.00599	21.41	0.714
	6	4116.5	0.00544	22.39	0.746
	6.5	4687.4	0.00495	23.20	0.773
	7	5248.1	0.00455	23.87	0.796
	7.5	5807.3	0.00421	24.44	0.815
	8	6344.6	0.00393	24.93	0.831
2 type	5.5	9278.6	0.00287	26.62	0.888
	6	9672.2	0.00277	26.79	0.893
	6.5	10050.1	0.00268	26.93	0.898
	7	10408.1	0.00260	27.06	0.902
	7.5	10784.4	0.00252	27.17	0.906
	8	11134.9	0.00245	27.28	0.909

**Table 4. The value of coefficient  $k$  with different stiffness of joint C**

Joint	Thickness of patch/angle $t_{patch/ang}$ , mm	$C$ , kNm/rad	$\varphi_{sup}$ , rad	$M_{sup}$ , kNm	$k$
1 type	6	3670.8	0.00589	21.62	0.721
	8	3945.1	0.00560	22.09	0.736
	10	4116.5	0.00544	22.39	0.746
	12	4264.2	0.00530	22.60	0.753
	14	4366.8	0.00521	22.75	0.758
2 type	5	9052.0	0.00293	26.52	0.884
	6	9602.9	0.00279	26.79	0.893
	7	10226.1	0.00264	26.99	0.900
	8	10651.3	0.00255	27.16	0.905
	9	11096.2	0.00246	27.29	0.910

**Table 5. The value of coefficient  $k$  with different stiffness of joint C**

Joint	Height of the patch on the wall $h_{patch}$ , mm	$C$ , kNm/rad	$\varphi_{sup}$ , rad	$M_{sup}$ , kNm	$k$
1 type	80	3937.3	0.00571	22.48	0.749
	100	3999.3	0.00560	22.39	0.747
	120	4049.3	0.00553	22.39	0.746
	150	4101.5	0.00546	22.39	0.746
	170	4116.5	0.00544	22.39	0.746
2 type	80	9646.7	0.00277	26.72	0.891
	100	9583.3	0.00279	26.73	0.891
	120	9588.8	0.00279	26.75	0.892
	150	9667.0	0.00277	26.77	0.893
	170	9602.9	0.00279	26.79	0.893

As it can be seen from Figure 12 and Tables 3–5 the  $k$  factor increases mostly if the column thickness changed from 5.5 to 8 mm in the type 1 node – 15 %, in type 2 node the change is insignificant and is about 2.4 %.

If the thickness of the lining on the shelves grows from 6 to 14 mm (joint of type 1) the increase in  $k$  is 5 %, while the thickness of parts increases from 5 to 9 mm (type 2 joint – almost 3 %).

Tusnina O.A., Danilov A.I. The stiffness of rigid joints of beam with hollow section column. *Magazine of Civil Engineering*. 2016. No. 4. Pp. 40–51. doi: 10.5862/MCE.64.4

Change in the height of pads on the walls does not affect the coefficient  $k$ , bringing it to a value of about 0.4 %.

Thus, it can be concluded that change of these parameters, and that of connecting elements attached to the joint do not increase significantly the rigidity of the assembly.

In order to implement the constructive solution it is required to obtain a hard knot.

## Conclusions

1. Joints of beam connection to the column conventionally used as a hinge, in some cases can be considered as elastically yielding since they provide reduction in the time span by 13.6 %, due to the occurrence of time on the anvil.

2. The joints of the beam with column connection on a patch, directly adjacent to the wall of the column cannot be considered as rigid (the proportion of the current support at the moment is less than the theoretical 0.83) and cannot be recommended for the use in the frame.

3. Joints with angles for transmission of forces in the belts crossbar on the column can be considered as rigid. However, it should be considered that the rigidity of such a compound is close to the minimum allowed for rigid nodes and the reference point is about 0.9 from its theoretical value in an absolutely rigid connection.

4. The need to develop a simple model for implementation of design solutions, providing a fairly rigid bolt connection with the column box section, or the development of guidelines for calculation and design of framework given the compliance of units depending on the constructive solution.

## References

- Kurazhova V.G., Nazmeyeva T.V. Vidy uzlovых соединений в легких стальных тонкостенных конструкциях [Types of connections in light steel thin-walled constructions]. *Magazine of Civil Engineering*. 2011. No. 3. Pp. 47–52. (rus)
- Sovetnikov D.O., Videnkov N.V., Trubina D.A. Light gauge steel framing in construction of multi-storey buildings. *Construction of Unique Buildings and Structures*. 2015. No. 3(30). Pp. 152–165. (rus)
- Ananina M.V. Vliyaniye korrozii na legkiye stalnye tonkostennyye konstruktsii [Influence of corrosion on the light steel gauge framing]. *Construction of Unique Buildings and Structures*. 2014. No. 7(22). Pp. 55–70. (rus)
- Trubina D.A., Kononova L.A., Kaurov A.A., Pichugin Y.D., Abdulaev D.A. Local buckling of steel cold-formed profiles under transverse bending. *Construction of unique Buildings and Structures*. 2014. No. 4 (19). Pp. 109–127. (rus)
- Trubina D., Abdulaev D., Pichugin E., Garifullin M. The loss of local stability of thin-walled steel profiles. *Applied Mechanics and Materials*. 2014. Vols. 633–634. Pp. 1052–1057.
- Trubina D., Abdulaev D., Pichugin E., Rybakov V., Garifullin M., Sokolova O. Comprasion Of The Bearing Capacity Of Lst-Profile Depending On The Thickness Of Its Elements. *Applied Mechanics and Materials*. 2015. Vols. 725–766. Pp. 752–757.
- Trubina D., Abdulaev D., Pichugin E., Rybokov V. Geometric nonlinearity of the thin-walled profile under transverse bending. *Applied Mechanics and Materials*, 2014. Vols. 633–634. Pp. 1133–1139,
- Rybakov V., Molchanova N., Laptev V., Suslova A., Sivokhin A. The effect of conjunction flexibility on the local stability of steel thin-walled slab beams. *MATEC Web of Conferences*. 2016. T. 53. 01017.
- Trubina D., Abdulaev D., Pichugin E., Rybakov V. Effect of constructional measures on the total and local loss stability of the thin-walled profile under transverse bending. *Applied Mechanics and Materials*. 2014. Vols. 633–634. Pp. 982–990.
- Tusnina V.M. Perspektivy stroitel'stva dostupnogo i komfortnogo zhilya na osnove stal'nykh karkasov

Туснина О.А., Данилов А.И. Жесткость рамных узлов сопряжения ригеля с колонной коробчатого сечения // Инженерно-строительный журнал. 2016. № 4(64). С. 40–51.

## Литература

- Куражова В.Г., Назмеева Т.В. Виды узловых соединений в легких стальных тонкостенных конструкциях // Инженерно-строительный журнал. 2011. №3. С. 47–52
- Советников Д.О., Виденков Н.В., Трубина Д.А. Легкие стальные тонкостенные конструкции в многоэтажном строительстве // Строительство уникальных зданий и сооружений. 2015. № 3 (30). С. 152–165.
- Ананина М.В. Влияние коррозии на легкие стальные тонкостенные конструкции // Инженерно-строительный журнал. 2014. № 7(22). С. 55–70.
- Трубина Д.А., Кононова Л.А., Кауров А.А., Пичугин Е.Д., Абдулаев Д.А. Местная потеря устойчивости стальных холодногнутых профилей в условиях поперечного изгиба // Строительство уникальных зданий и сооружений. 2014. №4 (19).
- Trubina D., Abdulaev D., Pichugin E., Garifullin M. The loss of local stability of thin-walled steel profiles // Applied Mechanics and Materials. 2014. Vols. 633–634. Pp. 1052–1057.
- Trubina D., Abdulaev D., Pichugin E., Rybakov V., Garifullin M., Sokolova O. Comprasion Of The Bearing Capacity Of Lst-Profile Depending On The Thickness Of Its Elements // Applied Mechanics and Materials. 2015. Vols. 725–766. Pp. 752–757.
- Trubina D., Abdulaev D., Pichugin E., Rybokov V. Geometric nonlinearity of the thin-walled profile under transverse bending // Applied Mechanics and Materials. 2014. Vols. 633–634. Pp. 1133–1139.
- Rybakov V., Molchanova N., Laptev V., Suslova A., Sivokhin A. The effect of conjunction flexibility on the local stability of steel thin-walled slab beams // MATEC Web of Conferences. 2016. Vols. 53. 01017.
- Trubina D., Abdulaev D., Pichugin E., Rybakov V. Effect of constructional measures on the total and local loss stability of the thin-walled profile under transverse bending // Applied Mechanics and Materials. 2014. Vols. 633–634. Pp. 982–990.
- Туснина В.М. Перспективы строительства доступного и комфортного жилья на основе стальных каркасов // Промышленное и гражданское строительство. 2015. № 6. С. 43–46.
- Кузнецов В.В. Справочник проектировщика.

- [Prospects of steel-framed low-rise residential construction as the solution of affordable and comfortable housing problem in Russia]. *Industrial and Civil Engineering*. 2015. No. 6. Pp. 43–46. (rus)
11. Kuznetsov V.V. *Spravochnik proektirovshchika. Metallicheskie konstruktsii*. Tom 2. [The designer guide. Steel structures]. Moscow: ASV, 1998. 512 p. (rus)
  12. Hart F., Henn W., Sontag X. *Atlas stal'nykh konstruktsiy mnogoetazhnykh zdanij* [Atlas of steel structures]. Moscow: Stroyizdat, 1977. 351 p. (rus)
  13. *Joints in Steel Construction: Simple Connection Publication* P 212. 2002. 490 p.
  14. Troitskiy P.N., Levitanskiy I.V. Issledovanie deystvitel'noy raboty svarnogo ramnogo uzla krepleniya i rekomendatsii po ego raschetu [Research of the frame joint behavior and recommendations on its analysis]. *Materialy po metallicheskim konstruktsiyam*. Vypusk 19. TsNII Proektstal'konstruktziya. Moskva, 1977. Pp. 120–132. (rus)
  15. Ostrikov G.M., Maksimov Yu.S. *Stal'nye seysmostoykie karkasy mnogoetazhnykh zdanij* [Steel seismic resistance structures of multistory buildings]. Alma-Ata: «Kazakhstan». 1985. 117 p. (rus)
  16. Azhermachev G.A., Perminov D.A. Effektivnye uzly sopryazheniya rigeley s kolonnami v ramnykh seysmostoykikh karkasakh mnogoetazhnykh zdanij [Effective beam-column joints at the frames of seismic resistance multistory buildings]. *Stroitel'stvo i tekhnogennaya bezopasnost'*. 2010. No. 32 Pp. 27–33. (rus)
  17. Azhermachev G.A., Perminov D.A. *Uzly stal'nykh karkasov povyshennoy seysmostoykosti* [The frame joints of increased seismic resistance]. *Stroitel'stvo i tekhnogennaya bezopasnost'*. 2007. No. 19-20. Pp. 13–16. (rus)
  18. Perminov D.A. *Povyshenie nesushchey sposobnosti uzlov ramnykh karkasov s kolonnami korobchatogo secheniya: dis. ... kand. tekhn. nauk: 05.23.01* [Increasing of bearing capacity of frame joints with columns of hollow sections]. Perminov Dmitriy Anatol'yevich. Simferopol'. 2016. 180 p. (rus)
  19. Jaspart J.P., Weynand K. Extension of the component method to joints in tubular construction // Proceedings of the IX international symposium and euroconference on tubular structures. Dusseldorf. Germany. 2001. Pp. 517–525.
  20. Nagao T., Tanaka T., Nanaba H. Performance of beam-column connections in steel structures. 13th world conference on earthquake engineering. Vancouver, B.C., Canada. 2004. Paper No. 1235.
  21. Heinisuo M., Laasonen M., Ronni H. Integration of joint design of steel structures using product mode. *Proceedings of the International Conference on Computing in Civil and Building Engineering ICCBE*. Nottingham. UK. 2010. Pp. 323–328.
  22. Heinisuo M., Laine V., Lehtimaki E. Enlargement of the component method into 3D. *Proceedings of the Nordic Steel Construction Conference NSCC*. Malmo. Sweden. 2009. Pp. 430–437.
  23. Guochang Li, Hongping Yu, Chen Fang. Performance study on T-stub connected semi-rigid joint between rectangular tubular columns and H-shaped steel beams. *Frontiers of Structural and Civil Engineering*. 2013. Vol. 7. Iss. 3. Pp. 296–303.
  24. Egarmirin K.A., Sysoev G.Yu., Vatin N.I., Vrublevskaya M.V. Analiz raboty ramnykh uzlov odnoetazhnogo stal'nogo karkasa v usloviyah vysokoy seismiki s ispol'zovaniem PK "SCAD" [Analysis of stress in frame nodes of a single-storey steel framework in high seismic load conditions with the use of SCAD software]. *Construction of Unique Buildings and Structures*. 2015. No. 2(29). Pp. 34–44. (rus)
  25. Vatin N.I., Havula Ja., Martikainen L., Sinelnikov A., Tusnina O.A., Danilov A.I. The stiffness of rigid joints of beam with hollow section column. *Magazine of Civil Engineering*. 2016. No. 4. Pp. 40–51. doi: 10.5862/MCE.64.4
  - Metallicheskie konstrukcii. Tom 2. M.: ACB, 1998. 512 c.
  12. Харт Ф., Хенн В., Зонтаг Х. Атлас стальных конструкций многоэтажных зданий. М.: Стройиздат. 1977. 351 с.
  13. Joints in Steel Construction: Simple Connection Publication. P 212. 2002. 490 p.
  14. Троицкий П.Н., Левитанский И.В. Исследование действительной работы сварного рамного узла крепления и рекомендации по его расчету // Материалы по металлическим конструкциям. Выпуск 19. ЦНИИ Проектстальконструкция. Москва. 1977. С. 120–132.
  15. Остриков Г.М., Максимов Ю.С. Стальные сейсмостойкие каркасы многоэтажных зданий. Алматы: «Казахстан». 1985. С. 117.
  16. Ажермачев Г.А., Перминов Д.А. Эффективные узлы сопряжения ригелей с колоннами в рамных сейсмостойких каркасах многоэтажных зданий // Строительство и техногенная безопасность. 2010. № 32. С. 27–33.
  17. Ажермачев Г.А., Перминов Д.А. Узлы стальных каркасов повышенной сейсмостойкости // Строительство и техногенная безопасность. 2007. № 19–20. С. 13–16.
  18. Перминов Д.А. Повышение несущей способности узлов рамных каркасов с колоннами коробчатого сечения: дис. ... канд. техн. наук: 05.23.01 / Перминов Дмитрий Анатольевич. Симферополь, 2016. 180 с.
  19. Jaspart J.P., Weynand K. Extension of the component method to joints in tubular construction // Proceedings of the IX international symposium and euroconference on tubular structures. Dusseldorf, Germany. 3-5 april 2001. Pp. 517–525.
  20. Nagao T., Tanaka T., Nanaba H. Performance of beam-column connections in steel structures // 13th world conference on earthquake engineering. Vancouver, B.C., Canada. 2004. Paper No. 1235.
  21. Heinisuo M., Laasonen M., Ronni H. Integration of joint design of steel structures using product mode // Proceedings of the International Conference on Computing in Civil and Building Engineering ICCBE. Nottingham. UK. 30 June – 2 July 2010. Pp. 323–328.
  22. Heinisuo M., Laine V., Lehtimaki E. Enlargement of the component method into 3D // Proceedings of the Nordic Steel Construction Conference NSCC. Malmo, Sweden. September 2-4, 2009. Pp. 430–437.
  23. Guochang Li, Hongping Yu, Chen Fang. Performance study on T-stub connected semi-rigid joint between rectangular tubular columns and H-shaped steel beams // Frontiers of Structural and Civil Engineering, 2013. Vol. 7. Iss. 3. Pp. 296–303.
  24. Егармин К.А., Сысоев Г.Ю., Ватин Н.И., Врублевская М.В. Анализ работы рамных узлов одноэтажного стального каркаса в условиях высокой сейсмики с использованием ПК "SCAD" // Строительство уникальных зданий и сооружений. 2015. № 2(29). С. 34–44
  25. Vatin N., Havula Ja., Martikainen L., Sinelnikov A., Orlova A., Salamakhin S. Thin-walled cross-sections and their joints and fem-modelling // Advanced Materials Research. 2014. No. 945-949. Pp. 1211–1215.
  26. Bzdawka K., Heinisuo M. Fin plate joint using component method of EN 1993-1-8 // Rakenteiden Mekaniikka (Journal of Structural mechanics). Vol. 43. No. 1. 2010. Pp. 25–43.
  27. Sinoes da Silva L. Towards a consistent design approach for steel joints under generalized loading // Journal of constructional steel research. 2008. Vol. 64. Pp. 1059–1075.
  28. Simoes da Silva L., Girap Coelho A.M. An analytical evaluation of the response of steel joints under bending

- Orlova A., Salamakhin S. Thin-walled cross-sections and their joints and fem-modelling. *Advanced Materials Research*. 2014. No. 945–949. Pp. 1211–1215.
26. Bzdawka K., Heinisu M. Fin plate joint using component method of EN 1993-1-8. *Rakenteiden Mekaniikka (Journal of Structural mechanics)*. 2010. Vol. 43. No. 1. Pp. 25–43.
  27. Sinoes da Silva L. Towards a consistent design approach for steel joints under generalized loading. *Journal of constructional steel research*. 2008. Vol. 64. Pp. 1059–1075.
  28. Simoes da Silva L., Girap Coelho A.M. An analytical evaluation of the response of steel joints under bending and axial force. *Computers and Structures*. 2001. Vol. 79. Pp. 873–881.
  29. Ferdous W. Effect of beam-column joint stiffness on the design of beams. *23rd Australian Conference on the Mechanics of Structures and Materials*. 2014. Pp. 701–706.
  30. Richard R., Gillet P., Krieger J., Lewis B. The analysis and design of single plate framing connections // *Engineering Journal AISC*. 1980. Vol. 17. No.2.
  31. Urbonas K., Daniunas A. Behaviour of semi-rigid steel beam-to-beam joints under bending and axial forces // *Journal of Constructional Steel Research*. 2006. Vol. 62. Iss. 12. Pp. 1244–1249.
  32. Tusnina, O. An Influence of the Mesh Size on the Results of Finite Element Analysis of Z-purlins Supported by Sandwich Panels // *Applied Mechanics and Materials*. 2014. Vols. 475-476. Pp. 1483–1486.
  33. Tusnina V.M. *Nesushchaya sposobnost' i deformativnost' podatlivykh uzlov stal'nykh karkasov mnogoetazhnykh zdaniy: dis. ... kand. tekhn. nauk 05.23.01*. Tusnina Valentina Matveevna. Moskva. 1989. 166 p. (rus)
- and axial force // *Computers and Structures*. 2001. Vol. 79. Pp. 873–881.
29. Ferdous W. Effect of beam-column joint stiffness on the design of beams // *23rd Australian Conference on the Mechanics of Structures and Materials*. 2014. Pp. 701–706.
30. Richard R., Gillet P., Krieger J., Lewis B. The analysis and design of single plate framing connections // *Engineering Journal AISC*. 1980. Vol. 17. No.2.
31. Urbonas K., Daniunas A. Behaviour of semi-rigid steel beam-to-beam joints under bending and axial forces // *Journal of Constructional Steel Research*. 2006. Vol. 62. Iss. 12. Pp. 1244–1249.
32. Tusnina, O. An Influence of the Mesh Size on the Results of Finite Element Analysis of Z-purlins Supported by Sandwich Panels // *Applied Mechanics and Materials*. 2014. Vols. 475-476. Pp. 1483–1486.
33. Tusnina B.M. Несущая способность и деформативность податливых узлов стальных каркасов многоэтажных зданий: дис. ... канд. техн. наук 05.23.01 / Туснина Валентина Матвеевна. Москва. 1989. 166 с.

Olga Tusnina,  
+7(910)4761677; lazoltus@mail.ru

Alexander Danilov,  
+79151834136; alenk070911@yandex.ru

Ольга Александровна Туснина,  
+7(910)4761677; эл. почта: lazoltus@mail.ru

Александр Иванович Данилов,  
+79151834136; эл. почта:  
alenk070911@yandex.ru

© Tusnina O.A., Danilov A.I., 2016

doi: 10.5862/MCE.64.5

## Analysis of the buckling of spatial truss with cross lattice

### Анализ прогиба фермы пространственного покрытия с крестообразной решеткой

**M.N. Kirsanov,**

National Research University "Moscow Power Engineering Institute", Moscow, Russia

**Д-р физ.-мат. наук, профессор**

**М.Н. Кирсанов,**

Национальный исследовательский университет "Московский энергетический институт", Москва, Россия

**Key words:** deformation; method of induction; spatial truss; coating; cross lattice

**Ключевые слова:** деформации; метод индукции; пространственная ферма; покрытие; крестообразная решетка

**Abstract.** The construction of a beam type spatial truss is proposed. The truss consists of three plane trusses with a cross lattice. The supports of the structure are modeled at the four corner points. The simple analytical dependence of the structure deflection on its size, load and a number of panels has been found for the case of an even number of panels. In the case of an odd number of panels the system is kinematically changeable, which is evident from the zero determinant of the system of equilibrium equations. The system of Maple computer algebra and the method of induction, previously proposed and developed by the author when solving the problems of planar and spatial trusses has been used. A nonmonotonic dependence of the deflection on the number of panels and the expected increase in stiffness at the increased truss height and unexpected decrease in stiffness at an increased base width have been found. The forces in some members of the truss change the sign depending on the parity of the number of panels in half of a span. Asymptotes of the solution are detected. The features of the solution allow optimizing the size of the structure.

**Аннотация.** Предлагается конструкция пространственной фермы балочного типа, состоящей из трех плоских ферм с крестообразной решеткой. Моделируется опирание конструкции на четыре угловые точки. Для случая четного числа панелей найдена простая аналитическая зависимость прогиба конструкции от ее размеров, нагрузки и числа панелей. При нечетном числе система кинематически изменяется, что яствует из равенства нулю определителя системы уравнений равновесия. Использована система компьютерной математики Maple и метод индукции, ранее предложенный и развитый автором в ряде задач о стержневых плоских и пространственных фермах. Обнаружен немонотонный характер зависимости прогиба от числа панелей, ожидаемое увеличение жесткости при увеличении высоты фермы и неочевидное ее снижение при увеличении ширины основания. Усилия в некоторых стержнях фермы меняют знак в зависимости от четности числа панелей в половине пролета. Найдены асимптотические свойства решения. Выявленные особенности решения позволяют оптимизировать размеры конструкции.

#### Introduction

In real projects the designs are rarely used as statically determinate systems, as in a statically determinate model of a truss there are rods and a pivot, swivel rods, that probably exist only in theoretical concepts. The model of the rod connections in the truss is sufficiently accurate but significantly simplified. However, the calculation of statically determinate planar and spatial structures has not lost its relevance yet. Firstly, the method of forces can be used for disclosure redundancies, and secondly, it can be successfully used as a test for many approximate methods, including finite element method. In addition, analytical solutions allow us to identify some characteristic features of the system, for example, the cases of the kinematic degeneracy, as it will be shown, in particular, in the present work. The problem of finding a new statically determinate beam structures is studied in [1, 2], some specific schemes of spatial trusses and approaches to their calculation (mainly numerical) are considered in [3-6]. Up-to-date problems of optimization of spatial trusses are discussed in [7-10]. The monograph [11] is devoted to theoretical and experimental study of regular spatial rod systems and the methods of their optimization. Spatial lattice

structures, composed of a flat truss are studied in [12]. The examples of analytical and numerically-analytical solutions of the problems of elasticity feature in the Maple computer algebra system [13] are given in [14, 15], and the flat ones are given in [16-20].

In the present work, the aim is to obtain a mathematical model of one statically determinate truss and identify its features. To achieve this purpose an algorithm for finding the forces in the bars of the truss in a symbolic form will be built, and a General formula for the deflection of the structure under the action of various loads will be derived. One of the main difficulties in solving this problem is to generalize the formulas to arbitrary number of panels using the method of induction.

### The design scheme

The coating consists of three plane trusses with a cross lattice, joined at their long sides (Fig. 1, 2). The side panels have an identical look. We take an even number of panels:  $n = 2k$ . At the midspan the design contains articulated rod circuit (highlighted in the figure), composed of three rods. The truss rests on the three pillars: spherical hinge, cylindrical, and one vertical rod support. The truss consists of  $n_s = 9(n + 1)$  elements, including six support rods and  $n_u = 3(n + 1)$  nodes. Given that in the method of cutting nodes there can be three equilibrium equations in projections for each node, the system of equilibrium equations is close and the construction is statically determinate.

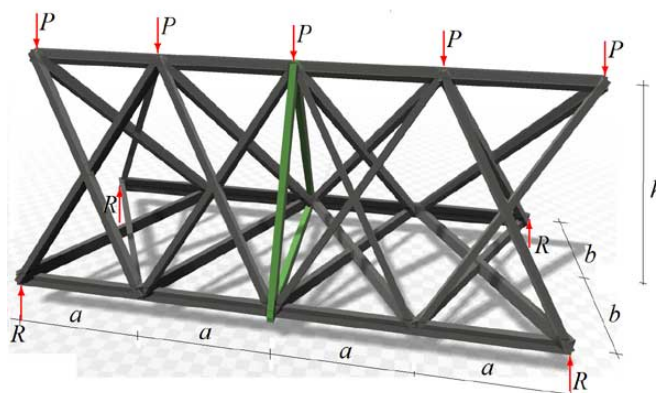


Figure 1. Truss,  $n = 4$

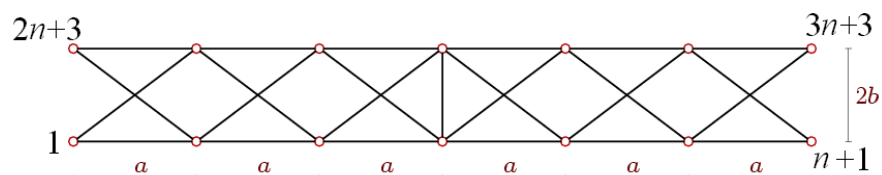


Figure 2. Lower truss belt and the number of supported nodes,  $n = 6$

To set the geometry of the truss, let us introduce the coordinate system with the longitudinal axis  $x$ , transverse  $y$  and vertical  $z$ . We put the original structure in a spherical hinge. To find the guides of the cosines by cutting out nodes we will need their coordinates:

$$\bar{r}_i = [x_i, y_i, z_i] = [(i-1)a, 0, 0],$$

$$\bar{r}_{i+n+1} = [x_i, b, h], \quad \bar{r}_{i+2n+2} = [x_i, 2b, 0], \quad i = 1, \dots, n+1.$$

Bearing, the spherical hinge, is modeled by three rods attached to node 1. The coordinates of the ends of the bars fixed on the base, are found as:

$$\bar{r}_{m+1} = [x_1, y_1, z_1 - 1], \quad \bar{r}_{m+2} = [x_1, y_1 - 1, z_1], \quad \bar{r}_{m+3} = [x_1 - 1, y_1, z_1], \quad m = 3n + 3.$$

A cylindrical joint is modeled by two rigid rods fixed in the node number  $2n + 3$  (Figure 2):

$$\bar{r}_{m+4} = [x_{2n+3}, y_{2n+3}, z_{2n+3} - 1], \quad \bar{r}_{m+5} = [x_{2n+3} - 1, y_{2n+3}, z_{2n+3}].$$

The vertical support rod attached to the node  $3n + 3$ :

$$\bar{r}_{m+6} = [x_{3n+3}, y_{3n+3}, z_{3n+3} - 1].$$

The order of connection of the rods and nodes is set by the conventional vectors  $\bar{q}_i$ ,  $i = 1, \dots, n_s$  with an arbitrary choice of direction. The chosen direction of the rod-vectors does not affect the force and signs of forces in the rods. The grating vectors ( $i = 1, \dots, n$ ) have the following form:

$$\begin{aligned}\bar{q}_i &= [i, i + n + 2], & \bar{q}_{i+n} &= [i + 1, i + n + 1], \\ \bar{q}_{i+2n} &= [i, i + 2n + 3], & \bar{q}_{i+3n} &= [i + 1, i + 2n + 2], \\ \bar{q}_{i+4n} &= [i + 1 + n, i + 2n + 3], & \bar{q}_{i+5n} &= [i + n + 2, i + 2n + 2].\end{aligned}$$

The longitudinal bars of the lower and upper belt are calculated as:

$$\bar{q}_{i+6n} = [i, i + 1], \quad \bar{q}_{i+7n} = [i + n + 1, i + n + 2], \quad \bar{q}_{i+8n} = [i + 2(n + 1), i + 2n + 3].$$

Components of vectors of secondary circuit are calculated as:

$$\bar{q}_{9n+1} = [k + 1, n + k + 2], \quad \bar{q}_{9n+2} = [2n + k + 3, n + k + 2], \quad \bar{q}_{9n+3} = [2n + k + 3, k + 1].$$

Support bars are encoded in the vectors:

$$\begin{aligned}\bar{q}_{9n+3+j} &= [1, m + j], \quad j = 1, 2, 3, \\ \bar{q}_{9n+6+j} &= [2n + 3, m + 3 + j], \quad j = 1, 2, \\ \bar{q}_{9n+9} &= [m, m + 6].\end{aligned}$$

### Method and Solution

Algorithm of composing the system of equations by the method of cutting out nodes is based on the calculation of the guides of the cosines of the force calculated at the given coordinate, and making the entries in the matrix  $G$ . Equilibrium equations are reduced to the system, which we write in matrix form

$$G\bar{S} = \bar{T}^{(j)}, \quad (1)$$

where  $\bar{S}$  – the vector of forces in rods,  $j = P, 1$ ;  $\bar{T}^{(P)}$  – vector of loads,  $\bar{T}^{(1)}$  – the vector of loading of the system corresponding to a single force.

The components of the vector of loads with numbers  $3i - 2$  correspond to the directions of the forces along the axis  $x$ , those with numbers  $3i - 1$  – along the axis  $y$ , and with the numbers  $3i$  – along the axis  $z$ , with  $i = 1, \dots, n_u$ . For the equations of equilibrium we will require the projection of the rod-vectors on the coordinate axes and their lengths:

$$l_{x,i} = x_{q_{i,1}} - x_{q_{i,2}}, \quad l_{y,i} = y_{q_{i,1}} - y_{q_{i,2}}, \quad l_{z,i} = z_{q_{i,1}} - z_{q_{i,2}}, \quad l_i = \sqrt{l_{x,i}^2 + l_{y,i}^2 + l_{z,i}^2}$$

The matrix guides of the cosines of  $G$  have the following components:

$$\begin{aligned}G_{3q_{i,1}-2,i} &= l_{x,i} / l_i, \quad G_{3q_{i,1}-1,i} = l_{y,i} / l_i, \quad G_{3q_{i,1},i} = l_{z,i} / l_i, \\ G_{3q_{i,2}-2,i} &= -l_{x,i} / l_i, \quad G_{3q_{i,2}-1,i} = -l_{y,i} / l_i, \quad G_{3q_{i,2},i} = -l_{z,i} / l_i.\end{aligned}$$

The load vector, uniformly distributed on the upper zone, has a form:  $T_{3i}^{(P)} = -1$ ,  $i = n + 2, \dots, 2(n + 1)$ . By setting a value of the vertical force on the fourth corner of the truss numbered  $n + 1$ , which does not have the support, it is possible to simulate more natural and symmetrical loading of the truss, thus avoiding the problem of statically indeterminate truss. In fact, the value

$T_{3(n+1)}^{(P)} = (n+1)/4$  is the solution to this problem under the assumption of equal stiffness supports. The remaining components of the vector  $\bar{T}^{(P)}$  are equal to zero. To determine forces from a single load applied to the node  $n_1 = 3k + 2$ , we have the following non-zero component:  $T_{3n_1}^{(1)} = 1$  and a component  $T_{3(n+1)}^{(1)} = -1/4$  which simulates a vertical base in the corner  $n+1$  joint of the lower belt.

The solution of the system of linear equations (1) is found in the symbolic form using Maple algebra:  $\bar{S} = G^{-1}\bar{T}$ , where  $G^{-1} = 1/G$  is the inverse matrix. The results of the program are analytical expressions for the forces in the rods of the truss. For the calculation of deflection we use Maxwell – Mohr's formula:

$$\Delta = \sum_{j=1}^{n_s} \frac{S_j s_j l_j}{EF},$$

where  $E$  is the modulus of elasticity of the rods,  $F$  – the cross-sectional area of the rods (same for the whole structure),  $l_j$  and  $S_j$  – the length of the  $j$ -th rod and the force in it from the action of a given load,  $s_j$  – a single vertical force applied at Midspan in the upper zone. The summation is over all the rods of the truss, except for the reference, which is assumed rigid. Let us now introduce the designation  $\tilde{\Delta} = \Delta EF / P$ . An induction method to get the relative deflection of the top node in the truss is used:

$$\tilde{\Delta} = \frac{A_k a^3 + B_k b^3 + C_k c^3 + D_k d^3 + Q_k q^3}{16h^2}, \quad (2)$$

where

$$\begin{aligned} c &= \sqrt{a^2 + b^2 + h^2}, \quad d = \sqrt{a^2 + 4b^2}, \quad q = \sqrt{b^2 + h^2}, \\ A_k &= 5k^4 + (1 + 6(-1)^k)k^2 + (4 + 3(-1)^2)k + 1 - (-1)^k, \\ B_k &= 8(2k+1), \quad C_k = 6k^2 + 4k + 1 - (-1)^k, \\ D_k &= k(2k+1), \quad Q_k = 4(1 + (-1)^k)(k+1). \end{aligned}$$

The coefficient  $A_k$  is obtained in Maple algebra by the synthesis of the following sequence: 3, 122, 365, 1420, 3007, 6774, 11769, 20984,..., 329584. To get the pattern, it was necessary to calculate a sequence of 16 trusses. To find the general term of the sequence the function `rgf_findrecur` from the package `genfunc` was used which is followed by a recurrence equation:

$$A_k = 2A_{k-1} + 2A_{k-2} - 6A_{k-3} + 6A_{k-5} - 2A_{k-6} - 2A_{k-7} + A_{k-8} \quad (3)$$

Note that this function only works with an even sequence number. The solution of equation (3) was found by `rsolve` operator. The verification decision will be made on trusses with an arbitrary number of panels with the help of the numerical solution carried out with the same program, but in a numerical mode.

Similarly, when uploading a truss by one concentrated force at the Central node we also get the solution for the deflection of the form (2), but with simpler coefficients:

$$A_k = k(4k^2 + 1 + 4(-1)^k), \quad B = 8, \quad C = 4k, \quad D = k, \quad Q = 4(1 + (-1)^k)$$

In addition, with such a load the length of the sequence number of the truss that detects a pattern, is slightly shorter and equals to 12. It is well known that the time of analytical transformations is noticeably larger than in the numerical calculation, and the number of panels increases approximately in geometric progression with a factor of 1.5 (that is tested empirically). In some cases this decline in the length of the sequence is crucial. Thus, if we calculate the four truss with a sequentially increased number of panels in half the span from 1 to 4 in the analytical form, the time of transformation on the average computer is 8.8 C, for ten trusses this time is equal to 178 C, and for sixteen trusses it takes 1024 or 17 min. This numerical example shows that the inductive method to obtain exact analytical solutions for trusses with a large number of panels can not be replaced by direct calculation of the

structure by means of symbolic mathematics. Up-to-date computers, with the enhanced processor, just change the time scale of the account, but do not solve the problem of the growth time of transformation with an increasing number of cores.

### Analysis

Let us consider the dependence of the deflection of the truss on the number of panels  $k$  for a fixed length of half the span  $L = 2ka$  and a given total load  $P_{sum} = (2k+1)P$ . The deflection is attributed to the value of the total load  $\tilde{\Delta} = \Delta EF / P_{sum}$ . The corresponding curves (Fig. 3, dimensions in metres) show the expected results: with the increase of height  $h$  increases the rigidity of the structure. The dependence of the deflection of the width of the truss  $b$  (Fig. 4) is less obvious. With the increase of the size decreases the stiffness. Much more interesting is the fact that the deflection depends on the number of panels. In this structure, it is non-monotonic, due to "flashing" in terms like  $(-1)^k$  of the coefficients of the solution. In addition, if you do not pay attention to the sharp drop of the curve at the beginning of the graph corresponding to unnaturally long panels ( $a = 20\text{m}$  with a truss height  $h = 5\text{m}$  or  $h = 6\text{m}$ ), we can see almost linear increase of deflection, which indicates the presence of an inclined asymptote. By the methods of Maple system (operator limit) it is easy to obtain the slope of the asymptotes:  $\gamma = (3q^3 + 8b^3) / (16h^2)$  and the asymptote  $\tilde{\Delta} = \Delta_0 + \gamma k$  where  $\Delta_0 = (\rho q^3 + 5L^3 + 16b^3) / (32h^2)$ . The coefficient  $\rho$  depends on the parity of the number of panels:  $\rho = 1$  for even  $k$  and  $\rho = 9$  for the odd one.

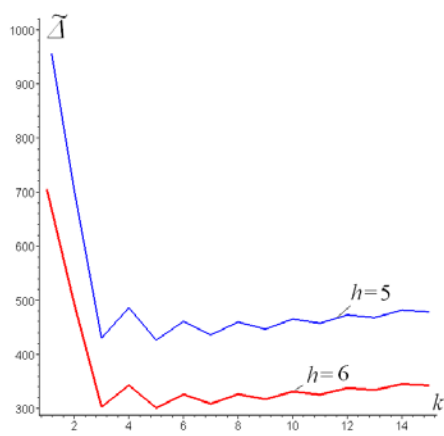


Figure 3.  $L = 40\text{ m}$ ,  $b = 5\text{ m}$ .

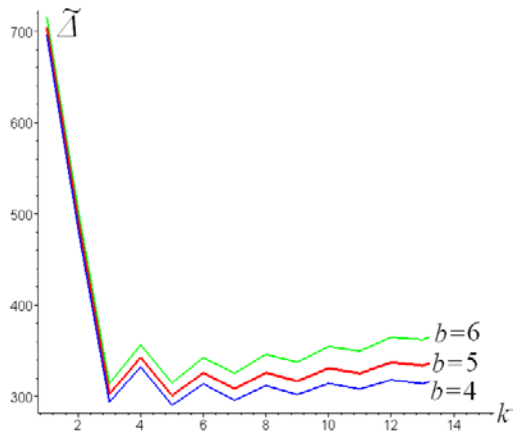


Figure 4.  $L = 40\text{ m}$ ,  $h = 6\text{ m}$ .

The solution (2) under any load is easily generalized to the case where the rigidity of the rods of the zones and grids is different. We denote the stiffness of the longitudinal bars bottom and top belt length  $a$  by 1, lattice rods of the lower belt length by  $d - 2$ , side bars – by 3, the rods of the average contour length by  $b$  and  $q - 4$ . To express the stiffness of the rods we use the reduced stiffness:  $EF_j = EF_0 / \mu_j$ ,  $j = 1, \dots, 4$ . In this case, from (2) it follows:

$$\tilde{\Delta} = \frac{A_k \mu_1 a^3 + B_k \mu_4 b^3 + C_k \mu_3 c^3 + D_k \mu_2 d^3 + Q_k \mu_4 q^3}{16h^2}$$

Another interesting and unusual design feature is the sign change of the forces at the secondary terminals of the circuit when the parity of the number of panels is changed. This follows from the analytical solution. So, the force at the bottom rod of the middle loop is the following:  $S_{m+3}^{(P)} = (-1)^k (2k+1)b / (2h)$ , with the forces in the side bars of the loop:  $S_{m+1}^{(P)} = S_{m+2}^{(P)} = -(-1)^k (k+1)q / (2h)$ . This fact should be taken into account in the calculation of cores for strength and stability.

In conclusion, let us note one more feature of this design. For the asymmetric version of the truss  $n = 2k - 1$ , when a triangular circuit cannot be placed in the plane of symmetry, it turns out that the

determinant of the matrix of the system of equilibrium equations is equal to zero. It can be missing in numerical analysis, which leads to erroneous solution. A similar effect was previously detected in spatial axisymmetric structures [21] and a lattice flat truss [22].

## Results and Discussion

One of the objectives of the present work is to describe the schemes of a statically determinate truss and identify its characteristics. Earlier [18, 21] the spatial patterns of trusses with cross-shaped grating panels were not calculated in the analytical form. The compact and precise formulas for determining the vertical deflection of the truss under the concentrated and uniformly distributed forces across the load balancing nodes are given. It is noted that in the case of one concentrated force, the sequence of solutions made by the method of induction, from which we can deduce the general formula for an arbitrary number of panels, is somewhat shorter than for a distributed load. Unlike in the solutions [3–12] the formulae are obtained due to the different stiffness in the rods of the truss. The effect of the parity of the number of panels in half the span on the signs of forces in the middle path is observed and the degeneracy of the system with an odd number of panels in the span truss is found.

## Conclusion

1. A mathematical model of spatial statically determinate truss schemes is obtained.
2. Formulas for the deflection of the structure for any number of panels are given.
3. A critical feature of the studied schemes, degenerated with an odd number of panels is detected.
4. The asymptotic solutions that are not available by numerical calculations [3–12] are found.
5. The given algorithm can be applied to develop calculation formulas for statically indeterminate structures of the regular type and for the analysis of inelastic systems.

## References

1. Hutchinson R. G., Fleck N.A. Microarchitected cellular solids – the hunt for statically determinate periodic trusses. *ZAMM Z. Angew. Math. Mech.* 2005. Vol. 85, No. 9. Pp. 607–617.
2. Hutchinson R.G., Fleck N.A. The structural performance of the periodic truss. *Journal of the Mechanics and Physics of Solids.* 2006. Vol. 54. No. 4. Pp. 756–782.
3. Ramaswamy G. S., Eekhout M., Suresh G. R. *Analysis, Design and Construction of Steel Space Frames.* Thomas Telford. 2002. 242 p.
4. Narayanan, S. *Space Structures: Principles and Practice.* Multi-Science Publishing Company. Brentwood, Essex, U.K. 2006. 844 p.
5. Chilton, J. *Space Grid Structures.* Architectural Press. Woburn, Massachusetts, U.S.A. 2000. 180 p.
6. Gasbarria P., Montia R., Sabatinib M. Very large space structures: Non-linear control and robustness to structural uncertainties. *ActaAstronautica.* 2014. Vol. 93. Pp. 252–265
7. Camp C. V., Farshchin M. Design of space trusses using modified teaching–learning based optimization. *Engineering Structures.* 2014. Vol. 62–63. Pp. 87–97.
8. Kaveh A., Sheikholeslami R., Talatahari S., Keshvari-Ikhichi M. Chaotic swarming of particles: A new method for size optimization of truss structures. *Advances in Engineering Software.* 2014. Vol. 67. Pp. 136–147.
9. Alpatov V.Yu., Kholopov I.S. Optimizatsiya geometricheskoy formy prostranstvenno-sterzhnevikh konstruktsiy [Optimization of the geometrical form of space frame structures]. *Metallichеские конструкции.* 2009. Vol. 15. No. 1. Pp. 47–57. (rus)
10. Lebee A., Sab K. Homogenization of a space frame as a thick plate: Application of the Bending-Gradient theory to a beam lattice. *Computers & Structures.* 2013. Vol. 127. October. Pp. 88–101.
11. Klyachin A.Z. *Metallichеские решетчатые пространственные конструкции регулярной структуры* [Metal lattice spatial structures with regular patterns]. Yekaterinburg: Diamant. 1994. 276 p. (rus)

Кирсанов М.Н. Анализ прогиба фермы пространственного покрытия с крестообразной решеткой // Инженерно-строительный журнал. 2016. № 4(64). С. 52–58.

## Литература

1. Hutchinson R. G., Fleck N.A. Microarchitected cellular solids – the hunt for statically determinate periodic trusses// *ZAMM Z. Angew. Math. Mech.* 2005. Vol. 85. № 9. Pp. 607–617.
2. Hutchinson R.G., Fleck N.A. The structural performance of the periodic truss // *Journal of the Mechanics and Physics of Solids.* 2006. Vol. 54. № 4. Pp. 756–782.
3. Ramaswamy G. S., Eekhout M., Suresh G. R. *Analysis, Design and Construction of Steel Space Frames.* Thomas Telford. 2002. 242 p.
4. Narayanan, S. *Space Structures: Principles and Practice.* Brentwood: Multi-Science Publishing Company. 2006. 844 p.
5. Chilton, J. *Space Grid Structures.* Woburn: Architectural Press. 2000. 180 p.
6. Gasbarria P., Montia R., Sabatinib M. Very large space structures: Non-linear control and robustness to structural uncertainties // *ActaAstronautica.* 2014. Vol. 93. Pp. 252–265.
7. Camp C. V., Farshchin M. Design of space trusses using modified teaching–learning based optimization // *Engineering Structures.* 2014. Vol. 62–63. Pp. 87–97.
8. Kaveh A., Sheikholeslami R., Talatahari S., Keshvari-Ikhichi M. Chaotic swarming of particles: A new method for size optimization of truss structures // *Advances in Engineering Software.* 2014. Vol. 67. Pp. 136–147.
9. Алпатов В. Ю., Холопов И. С. Оптимизация геометрической формы пространственно-стержневых конструкций // *Металлические конструкции.* 2009. Т. 15. № 1. С. 47–57.
10. Lebee A., Sab K. Homogenization of a space frame as a thick plate: Application of the Bending-Gradient theory to a beam lattice // *Computers & Structures.* 2013. Vol. 127. Pp. 88–101.
11. Клячин А.З. Металлические решетчатые пространственные конструкции регулярной структуры. Екатеринбург: Диамант. 1994. 276 с.
12. Марутян А. С., Григорьян М. Б., Глухов С. А. Пространственные решетчатые несущие конструкции

12. Marutyan A. S., Grigoryan M. B., Glukhov S. A. Prostranstvennyye reshetchatyye nesushchiye konstruktsii (moduli tipa "Pyatigorsk"-2) [ Spatial lattice supporting structures (modules of type "Pyatigorsk"-2)]. *Structural Mechanics and Analysis of Constructions*. 2014. No.1. Pp. 64–71.(rus)
  13. Goloskokov D.P. *Prakticheskiy kurs matematicheskoy fiziki v sisteme Maple* [Practical course in mathematical physicsin the Maple]. Saint-Petersburg: Izd-vo ParkKom. 2010. 644 p. (rus)
  14. Galileev S.M., Matrosov A.V. Method of initial functions: stable algorithms in the analysis of thick laminated composite structures. *Composite Structures*. 1997. Vol. 39. No. 3–4. Pp. 255–262.
  15. Goloskokov D. P. Modelirovaniye napryazhenno-deformirovannogo sostoyaniya uprugikh tel s pomoshchyu polinomov [Modeling of the stress-strain stateof elastic bodiesusingpolynomials]. *Vestnik gosudarstvennogo universiteta morskogo i technologicheskogo flota imeni admiraala S.O. Makarova*. 2013. No 1. Pp. 8–14. (rus)
  16. Reutov D.O. Induktivnyy analiz progiba fermy reguljarnoy struktury v sisteme Maple [Inductive analysis of the deflection of the regular trussstructure in the system Maple]. *Materialy mezdunarodnoy nauchno-prakticheskoy konferentsii ITON-2014 i trudy IV mezdunarodnogo seminara i mezdunarodnoi shkoly "Matematicheskoye i kompyuternoye modelirovaniye fundamentalnykh obyektov i yavleniy v sistemakh kompyuternoy matematiki"*. Kazan: Izd-vo OOO "Foliant", 2014. Pp. 256–261. (rus)
  17. Zaborskaya N.V. O horizontalnom smeshchenii opory ploskoy balochnoy fermy [On the horizontal displacement of the support flat girder]. *Perspektivy razvitiya nauki i obrazovaniya: sbornik nauchnykh trudov po materialam Mezdunarodnoy nauchno-prakticheskoy konferentsii 28.2.2015. Part 9*. Tambov: OOO «Konsaltingovaya kompaniyaYukom». 2015. Pp. 58–60. (rus)
  18. Larichev S. A. Induktivnyy analiz vliyaniya stroitel'nogo podyema na zhestkost prostranstvennoy balochnoy fermy [Inductive analysis of the impact of the construction hoist on the spatial stiffness of a girder]. *Trends in Applied Mechanics and Mechatronics*. 2015. Moscow: Infra-M. Vol. 1. Pp. 4–8. (rus)
  19. Tinkov D.V. Analiz vliyaniya usloviy zakrepleniya na progib ploskoy balochnoy fermy s niskhodyashchimi raskosami [Analysis of the influence of the fixing conditions for the deflection of a flat beam truss with down braces]. *Trends in Applied Mechanics and Mechatronics*. 2015. Moscow: Infra-M. Vol. 1. Pp. 52–56. (rus)
  20. Tinkov D.V. Sravnitel'nyy analiz analiticheskikh resheniy zadachi o progibe fermennykh konstruktsiy [Comparative analysis of analytical solutions to the problem of truss structure deflection]. *Magazine of Civil Engineering*. 2015. No. 5. Pp. 66–73.(rus)
  21. Kirsanov M.N. Raschet prostranstvennoy sterzhnevoy sistemy, dopuskayushchey mgnovenennuyu izmenyayemost [Calculation of spatial bar system that permits variability of instantly]. *Structural Mechanics and Analysis of Constructions*. 2012. No. 3. Pp. 48–51. (rus)
  22. Kirsanov M.N. Analiz progiba reshetchatoy balochnoy fermy raspornogo tipa [Analysis of the deflection of a strut-type lattice girder truss]. *Magazine of Civil Engineering*. 2015. No. 5. Pp. 58–65.(rus)
- (модули типа «Пятигорск»-2) // Строительная механика и расчет сооружений. 2014. № 1. С. 64–71.
13. Голосков Д.П. Практический курс математической физики в системе Maple. СПб.: Изд-во ПаркКом. 2010. 644 с.
  14. Galileev S.M., Matrosov A.V. Method of initial functions: stable algorithms in the analysis of thick laminated composite structures // Composite Structures. 1997. Vol. 39. № 3–4. Pp. 255–262.
  15. Голосков Д. П. Моделирование напряженно-деформированного состояния упругих тел с помощью полиномов // Вестник государственного университета морского и речного флота имени адмирала С.О. Макарова. 2013. № 1. С. 8–14.
  16. Реутов Д.О. Индуктивный анализ прогиба фермы регулярной структуры в системе Maple // Международная научно-практическая конференция ИТОН-2014. IV-й международный семинар и международная школа "Математическое и компьютерное моделирование фундаментальных объектов и явлений в системах компьютерной математики" // Материалы конференции и труды семинара. Казань: Изд-во ООО "Фолиант", 2014. С. 256–261.
  17. Заборская Н. В. О горизонтальном смещении опоры плоской балочной фермы // Перспективы развития науки и образования: сб. науч. тр. по мат-лам Междунар. науч.-практ. конф. 28 февраля 2015 г.: Часть 9. Тамбов: 2015. С. 58–60.
  18. Ларичев С. А. Индуктивный анализ влияния строительного подъема на жесткость пространственной балочной фермы// Trends in Applied Mechanics and Mechatronics. 2015. М: Инфра-М. Т. 1. С. 4–8.
  19. Тиньков Д. В. Анализ влияния условий закрепления на прогиб плоской балочной фермы с нисходящими раскосами// Trends in Applied Mechanics and Mechatronics. 2015. М: Инфра-М. Т. 1. С. 52–56.
  20. Тиньков Д.В. Сравнительный анализ аналитических решений задачи о прогибе ферменных конструкций // Инженерно-строительный журнал. 2015. №5(57). С. 66–73.
  21. Кирсанов М.Н. Расчет пространственной стержневой системы, допускающей мгновенную изменяемость // Строительная механика и расчет сооружений. 2012. № 3. С. 48–51.
  22. Кирсанов М.Н. Анализ прогиба решетчатой балочной фермы распорного типа // Инженерно-строительный журнал. 2015. №5(57). С. 58–65. doi: 10.5862/MCE.57.5

Mikhail Kirsanov,  
+7(495)3627314; mpei2004@yandex.ru

Михаил Николаевич Кирсанов,  
+7(495)3627314; эл. почта:  
mpei2004@yandex.ru

© Kirsanov M.N. 2016

doi: 10.5862/MCE.64.6

## Analysis of local stability of the rectangular tubes filled with concrete

# Анализ местной устойчивости трубобетонных конструкций прямоугольного сечения

**R. A. Kanischchev,***Technical University of Kosice, Kosice,  
Slovak Republic***Аспирант Р.А. Канищев,***Технический университет г. Кошице,  
г. Кошице, Словакия*

**Key words:** composite structures; local buckling;  
friction; finite element method; Eurocode

**Ключевые слова:** композитные конструкции;  
местная устойчивость; трение; метод  
конечных элементов; Еврокод

**Abstract.** The use of rectangular steel tubes filled with concrete allows combining the advantages of concrete (reinforced concrete) and steel structures with reciprocal compensation of their disadvantages. Building code Eurocode 4 is used for the design of such structures in the European Union, but the main disadvantage of this standard is its limitations for use of the class 4 rectangular steel cross-sections (classification according to standard EN 1993-1-1) filled with concrete. Therefore, the study of local stability of such structures and the impact of friction between the components of the composite section on it is relevant. The analysis of the influence of friction between the steel shell and the concrete core on the local buckling of composite structures was carried out using the ABAQUS computational-graphics software. The models of behavior of axial compressed rectangular cross-section samples with different coefficients of friction between the shell and the core were created for this. The load on the samples was applied in two variants: a) simultaneously through the steel section and the concrete core; b) only through the steel section. The variants with different fixing conditions of loaded edges of the steel section were also considered. Based on this research, the basic laws of development of local buckling deformation of the structures under study were analyzed. The influence of the conditions of fixing the loaded edges of the steel section to local buckling deformation of the composite structure was determined. The dependence of the friction effect between the components of steel-concrete section on the local stability of rectangular tube was shown.

**Аннотация.** Применение стальных прямоугольных труб, заполненных бетоном, позволяет использовать и сочетать преимущества бетонных (железобетонных) и стальных конструкций с взаимной компенсацией их недостатков. Для проектирования таких конструкций на территории Европейского Союза уже существует строительная норма Еврокод 4. Но основным недостатком данной нормы является ограничение в использовании стальных прямоугольных сечений 4-го класса (классификация согласно EN 1993-1-1), заполненных бетоном. Следовательно, на сегодняшний день являются актуальными исследования потери местной устойчивости данных конструкций и влияния на неё трения между составными частями композитного сечения. Анализ влияния трения между стальной оболочкой и бетонным ядром на местную устойчивость композитных конструкций проводился в расчетно-графическом комплексе ABAQUS. Для этого были созданы модели поведения центрально-скатых образцов прямоугольного сечения с разными значениями коэффициентов трения между оболочкой и ядром. Нагрузка на образцы прикладывалась в двух вариантах: а) одновременно на стальную оболочку и бетонное ядро; б) только на стальную оболочку. Также были рассмотрены варианты с различными условиями закрепления нагруженных граней стальной части сечения. На основании проведенного исследования были проанализированы основные закономерности проявления деформаций при потере местной устойчивости исследуемых конструкций. Установлено влияние условий закрепления нагруженных граней стальной части сечения на деформации локального выпучивания композитной конструкции. Показана зависимость влияния трения между составными частями сталебетонного сечения на местную устойчивость прямоугольной трубы.

## *Introduction*

A characteristic feature of modern building is a divergence from the legacy of constructive solutions of buildings, engineering structures, and the search for new technology of building objects. In these cases, the need for engineers is to design structural elements, which combine the advantages of concrete and steel materials with a mutual compensation of their disadvantages. These structural elements are steel-concrete structures.

Steel-concrete (composite) structures are constructions, in which the steel and concrete parts of the cross-section have their own bending stiffness, and contact areas are interconnected by means of friction forces. The main difference between composite and reinforced concrete structures is that flexural rigidity of steel reinforcement of reinforced concrete structures can be neglected before complete hardening of concrete.

Composite columns are a very important part of composite structures, and are widely used in the erection of high-rise buildings and bridge constructions, in places with high compressive loads with relatively small bending moments [1]. One type of composite columns are rectangular concrete-filled steel tubes (CFSTs). As noted in [2–10], these structures have their advantages in comparison with an empty steel pipe, but one main preference is a significant resistance to loss of local and global stability, which greatly reduces the cross-section of the element.

## *Review of literature*

World standards described in [11–14] exist for the design of the above mentioned structures. However, these standards have limitations in practice, such as mechanical properties of materials or the slenderness of steel elements of composite cross-sections etc. Authors, such as Mouli [15], Uy [16–18], Krishan [19], in their scientific works, devoted to enhancing validity of these standards, investigated the ultimate strength, stability and ductility characteristics of rectangular CFSTs subject to axial compression using high performance steels and lightweight concrete aggregates. Experimental tests, conducted by Lee [20] and Storozhenko [21] on high-strength concrete-infilled steel tube columns subject to eccentric loads, showed the influence of width-to-thickness ratio, buckling length-sectional width ratio and eccentricity ratio on the behavior of these structures. Patel *et al.* [22] proposed a multiscale numerical model for simulating the interaction of local and global buckling behavior of eccentrically loaded high strength rectangular CFSTs with large depth-to-thickness ratios. Yang and Han [23] presented the research aimed at the experimental investigation of the behavior of rectangular CFSTs loaded axially on a partially stressed cross-sectional area. The research conducted by Nethercot [24] and Bradford [25] was devoted to the problem of the loss of the local stability effect on the strength of thin-walled tubes filled with concrete.

Currently, the European Union uses EN 1994-1-1 (Eurocode 4) to design rectangular CFSTs [26]. The basic disadvantage of the standard is its limitations regarding the slenderness of the web of the rectangular cross-section. The design of more efficient composite structures is conducting research on class 4 hollow steel cross-sections, according to EN 1993-1-1 (Eurocode 3) [27], filled with concrete, which already lie beyond the validity of Eurocode 4. Since it is impossible to use connecting elements between the steel shell and the concrete core in such structures, the interaction or bond between the two materials is achieved by natural connection. Consequently, the problem of the impact of changes in friction between the two materials on the local buckling of the composite structure is a relevant topic.

## *Formulation of the problem*

The object of this research is a welded cold-formed hollow profile of rectangular cross-section RHS 200/100/3 (standard EN 10219 [28]), filled with concrete.

The objective of this work is to study the behavior of the compressed composite profile, which lies beyond the validity of Eurocode 4, and to analyze the changes of the natural connection characteristics between the steel shell and the concrete core on the local stability of the composite structure.

To achieve this objective, the following tasks were set:

- 1) Analytical review of scientific and technical material on local buckling of the steel-concrete element and the interaction between steel and concrete parts of the composite cross-section.
- 2) Modelling of the axially compressed composite element behavior using ABAQUS computer-graphics software.

3) Analysis of the impact in friction changes between the components of the composite section on the local stability of rectangular CFST.

### *Local stability of the axially compressed rectangular tubes*

According to the standard EN 1993–1–1, class 4 cross-section is the section in which the loss of local stability occurs up to the yield stress in one or several parts of the section. The sections of this class are calculated according to the technique, specified in standard EN 1993–1–5 (Eurocode 3 part 1–5) [29]. This technique is based on adding a full cross-section of the welded cold-formed hollow profile to the effective (reduced) one. The effective cross-section is a profile in which the eliminated from calculations parts of the webs of the rectangular cross-section are due to local buckling. The reduction of the section allows taking into account the effect of local buckling and loss of cross-sectional shapes on the load-bearing capacity of the compressed tube.

The basic principles of designing class 4 cross-sections were stipulated by Bryan [30], who offered a critical analysis of the elastic stress  $\sigma_{cr}$  for local buckling of long right-angled wall elements with simple (hinge) supports on all the edges acting under the influence of a uniform pressure load. The term "stress" includes various boundary conditions and distribution of forces over the element with the aid of the coefficient of critical stress  $k_\sigma$ :

$$\sigma_{cr} = k_\sigma \frac{\pi^2 E}{12(1-\nu^2)} \left( \frac{t}{b} \right)^2 \quad (1)$$

The minimum values of the coefficient of critical stress  $k_\sigma$  are stipulated in EN 1993-1-5. In the case of internally compressed cross-sections (rectangular tube wall), this coefficient varies from  $k_\sigma = 4$  for pure pressure to  $k_\sigma = 23.9$  for the combination of compression and bending. The coefficient can be used for hollow rectangular tubes. When the tube is filled with concrete, the standard does not provide the  $k_\sigma$  value.

In the research by prof. Timoshenko [31], devoted to the stability of right-angled walls with simple (hinge) supports, a differential equation was presented for a slender wall with length  $a$ , and width  $b$  (Fig. 1a), which is simply supported around its perimeter:

$$C \left( \frac{\partial^4 w}{\partial x^4} + 2 \frac{\partial^4 w}{\partial x^2 \partial y^2} + \frac{\partial^4 w}{\partial y^4} \right) + P \frac{\partial^2 w}{\partial x^2} = 0 \quad (2)$$

where  $w$  is the deflection of slender walls, m;

$P$  is the compression force, N.

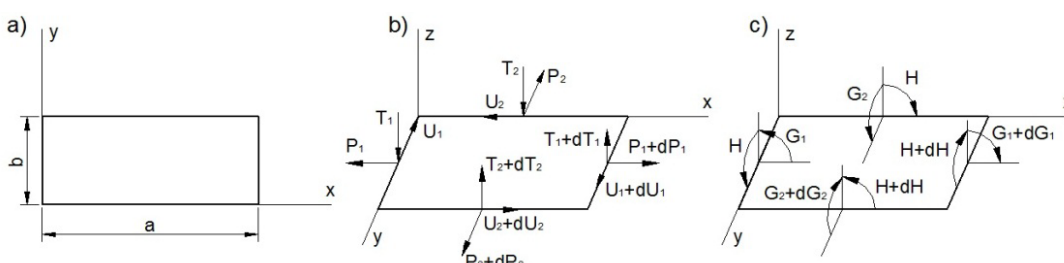


**Figure 1. Mathematical model of a slender wall:**  
**a) location of walls in the coordinate axes; b) components force in a unit element of the wall;**  
**c) components of the bending moment in a unit element of the wall.**

The cylindrical wall stiffness  $C$ :

$$C = \frac{Et^3}{12(1-\nu^2)} \quad (3)$$

where  $E$  is the modulus of elasticity of steel, MPa;

$t$  is the wall thickness, m;

$\nu$  is the Poisson ratio.

A particular solution to the differential equation (2) represents the balance of forces in one of the possible buckling forms of its walls:

$$w = A \sin \frac{m\pi x}{a} \sin \frac{n\pi y}{b} \quad (4)$$

The given solution satisfies the boundary conditions (Fig. 1b,c): for  $x = 0$  and  $x = a \rightarrow w = 0$  a  $G_1 = 0$ ; for  $y = 0$  and  $y = b \rightarrow w = 0$  a  $G_2 = 0$ . The following conditions are fulfilled for stress:  $P_1 = -P$ ,  $U_1 = U_2 = P_2 = 0$ .

The compressive force  $P$  can be determined by substituting the expression (4) for equation (2):

$$P = C\pi^2 \frac{\left(\frac{m^2}{a^2} + \frac{n^2}{b^2}\right)^2}{\frac{m^2}{a^2}} \quad (5)$$

where  $m$  and  $n$  are half-waves along the length and across the width of the wall.

Of all the possible buckling forms of the force balance in the cross-section of the wall, we need to find one where the value of the force  $P$  will be minimal. This will be achieved if  $n = 1$  and the value  $m$  according to [31] is expressed by equation (6). From the above relationship, it follows that the limit value for the length  $a$ , at which the wall reaches its first buckling form, comprises the  $m$  half-waves.

$$a = b\sqrt{m(m+1)} \quad (6)$$

If we consider that  $P = P_{cr}$  and  $P_{cr}/t = \sigma_{cr}$ , where  $\sigma_{cr}$  is the value of the critical compressive stress, i.e. formula (5) adjustments for  $n = 1$  and the cylinder wall stiffness are taken as:

$$\sigma_{cr} = \left( \frac{b}{a} + \frac{1}{m} \frac{a}{b} \right)^2 \frac{\pi^2 Et^2}{12(1-\nu^2)b^2} \quad (7)$$

According to EN 1993-1-5, expression (7) is the value of the elastic critical stress of the wall  $\sigma_{cr} = k_\sigma \sigma_E$ , and the first factor of this expression is the coefficient of the elastic critical stress  $k_\sigma$ .

### *Interaction of steel shell and concrete core when loading composite columns in high-rise buildings*

The load in frames with hinged columns (Fig. 2a) is introduced into the columns at the top, in frames with continuous columns (Fig. 2b) through column-beam joints at each floor level.

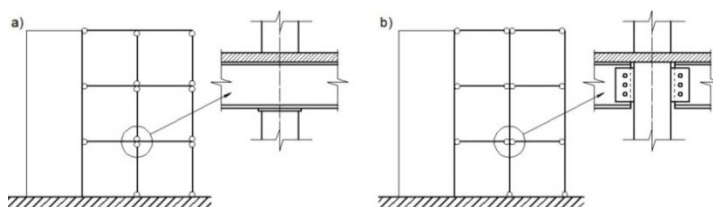


**Figure 2. Load introduction:**  
**a) hinged columns; b) continuous columns**

The load at the top of a hinged column may be introduced as follows:

- a) simultaneously through the steel section and the concrete core;
- b) only through the steel section;
- c) only through the concrete core.

The total interaction between steel and concrete elements of the composite cross-section is due to the natural bond of the two materials which includes: adhesion, interlock due to surface unevenness, and friction.

Adhesion or adhesive bond is considered to be elastic-brittle and it is activated mainly at the initial loading stage. The maximum shear strength detected according to [3] is 0.1 MPa. In steel-concrete Kanishchev R.A. Analysis of local stability of the rectangular tubes filled with concrete. *Magazine of Civil Engineering*. 2016. No. 4. Pp. 59–68. doi: 10.5862/MCE.64.6

composite columns this component of shear transfer may be neglected, since the shear resistance is excessive at the value of the slip smaller than 0.01 mm and concrete shrinkage diminishes the effect of such connection.

Interlock due to surface unevenness occurs as a result of concrete leakage and its hardening in troughs on the surface of a steel element. This method of interaction is effective only when steel and concrete elements are connected perpendicularly to the shear flow. The interlocking of the two materials due to their surface unevenness contributes to the initial stiffness of a column. Shear connection disappears when relative deformation/strain of the concrete in the contact area reaches 0.035 %. Similar to adhesion, concrete shrinkage has a negative impact on the effectiveness of this connection.

Shear transfer by friction is closely related to interlock due to surface unevenness and it depends on the normal force in the contact area and the relevant coefficient of friction  $\mu$ . Friction is a resistance force acting against separation of composite elements or their sliding against each other. This type of interaction between physical bodies consists of two components: normal and tangential ones. The normal component is hard contact acting perpendicularly to a steel section that allows individual movements of steel and concrete under some specific loading conditions. However, the tangential component acts against these movements and it depends on a number of factors such as surface structure, roughness of the material used, temperature, and humidity.

The overview of research works shows that the coefficient of friction  $\mu$  varies from 0 (when a steel surface is painted) to 0.7 (when a steel surface is unfinished/unpainted). Rabbat and Russell [32] have tested 15 specimens and concluded that the value of this coefficient was within the range between 0.57 and 0.70. Baltay and Gjelsvik [33] have specified the mean value of the friction coefficient as 0.47. Evirgen and Tuncan [34] have empirically detected in their experiments that the coefficient of friction was 0.55, while it weakly correlated to the compressive strength of concrete.

The design shear strength  $T_{Rd}$  is lower than the tensile strength of concrete and it depends on the type of section. It is dependent on the friction produced between steel and concrete elements; therefore, the values 0.29 ÷ 0.35 MPa calculated according to [34] and 0.4 MPa, given in standard EN 1994-1-1, are applicable only to an unfinished steel surface with no coat or paint, free from oil, grease, loose scale or rust. The design values of shear strength can be used only if there is no separation between the surface areas. The influence of "pressing" concrete to a steel element/creep on the design shear strength manifests itself more in circular concrete-filled hollow sections than rectangular ones.

### *FEM modelling of the concrete-filled rectangular tubes*

A test with 36 "short" specimens was modelled using the ABAQUS 6.13-4 software application to analyze the impact of friction between the steel shell and concrete core on the local stability of rectangular CFSTs. The behavior of rectangular tubes (steel part of composite cross-section) with a section of RHS 200x100x3 (according to EN 10219) was investigated. The test specimens were divided into 3 groups by length: a) 200 mm (4 specimens); b) 400 mm (4 specimens); c) 600 mm (4 specimens). The length of the specimens in each group is selected according to expression (6) based on occurring the estimated number of half-waves (from 1 to 3 half-waves) along the length of an element.

When modelling steel cross-sections, the material characteristics defined by EN 1993-1-1: steel class S235, elastic modulus  $E = 210\,000$  MPa, the Poisson's ratio in the elastic state  $\nu = 0.3$ , were used. The behavior of the material was modelled as an elastic-plastic with hardening, according to the norm EN 1993-1-5. The core of the composite section was modelled as concrete class C20/25 with elastic modulus  $E = 30\,000$  MPa and the Poisson's ratio in elastic state  $\nu = 0.2$ , according to the standard EN 1992-1-1 (Eurocode 2) [35].

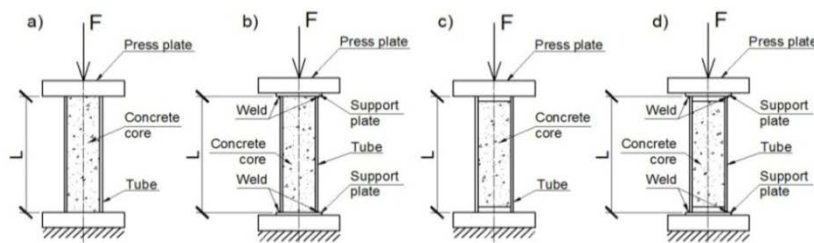


**Figure 3. Scheme of loading steel-concrete specimens:**  
**a) on the steel tube and the concrete core;**  
**b) on the steel tube and concrete core through the welded support plate;**  
**c) on the steel tube; d) on the steel tube through the welded support plate**

The library of ABAQUS elements [36] was used for the modelling: the steel section was made of «shell-type» S4R elements and the concrete core of “solid-type” C3D8 elements. The maximum mesh size of finite elements is 10 mm. The interaction of steel and concrete materials was modelled by means of two components: the «normal» one as compression of concrete on the steel section and the “tangential” one as shear resistance at the steel-concrete interface. To determine the impact of friction on the local stability of rectangular CFSTs, the coefficients of friction  $\mu$  were taken 0; 0.35 and 0.7.

The loading of elements was simulated with a type of hinged columns (see Fig. 2a): a) simultaneously on a steel tube and concrete core (Fig. 3a,b); b) only on the steel tube (Fig. 3c,d). The fixation of loaded edges of the steel tube walls was modelled in two versions: simply supported (Fig. 3a,c) and clamped (Fig. 3b,d). In reality it can be achieved by welding the support plates at the ends of the column. The loading of columns was modelled as short-term, rising steadily at a constant rate, introduced through the plate of a hydraulic press. The process of loading is stopped after a pronounced buckling deformation. The critical compressive stresses were recorded in the places of local buckling of the greater wall of the rectangular steel tube (Fig. 4 ÷ Fig. 6).

### *Discussion of the results*

As a result of modelling the behavior of the short composite columns under axial compression using ABAQUS computational-graphics software, it can be stated that deformation of the buckling of the steel tube (loss of local stability) for various boundary conditions of loaded edges of the steel section has a different character.

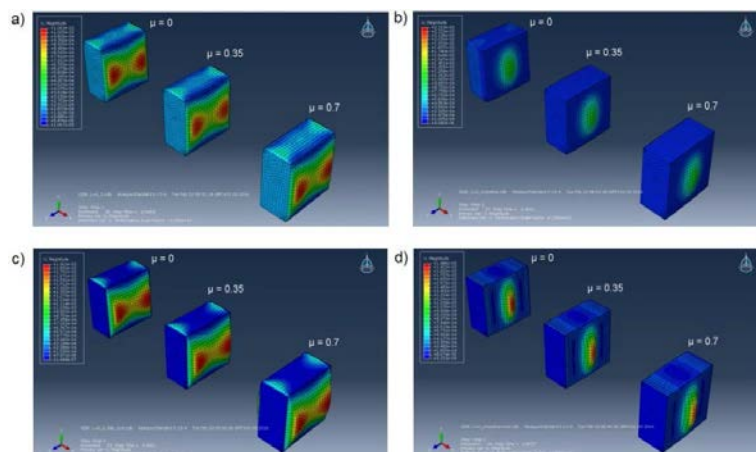


**Figure 4. Local buckling deformations of the specimens with length  $L = 200$  mm and loading:**

- a) simultaneously on the simply supported steel tube and concrete core;
- b) simultaneously on the clamped steel tube and concrete core;
- c) on the simply supported steel tube; d) on the clamped steel tube

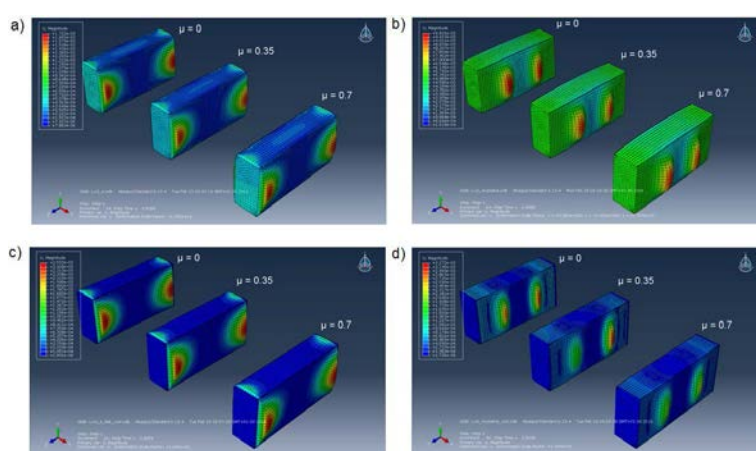


**Figure 5. Local buckling deformations of the specimens with length  $L = 400$  mm and loading:**

- a) simultaneously on the simply supported steel tube and concrete core;
- b) simultaneously on the clamped steel tube and concrete core;
- c) on the simply supported steel tube; d) on the clamped steel tube

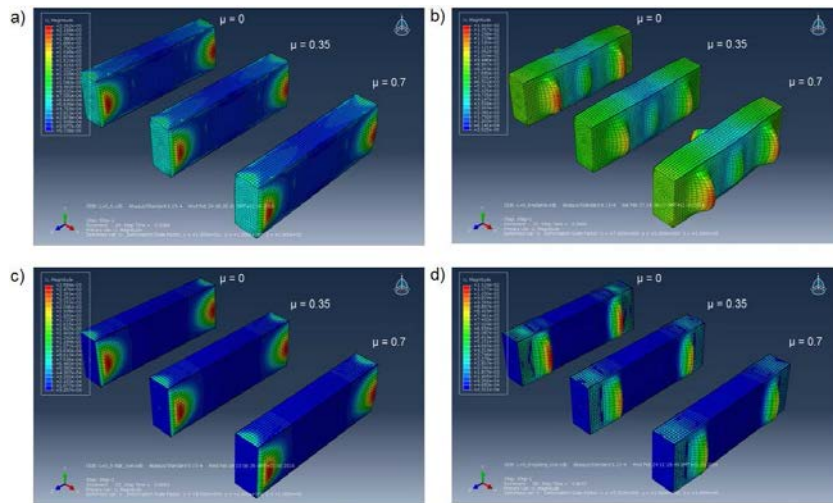


**Figure 6. Local buckling deformations of the specimens with length  $L = 600$  mm and loading:**  
**a) simultaneously on the simply supported steel tube and concrete core;**  
**b) simultaneously on the clamped steel tube and concrete core;**  
**c) on the simply supported steel tube; d) on the clamped steel tube**

In the case of compression of the specimen without a welded plate, the development of buckling deformation of the tubes is shown close to the ends of the test specimens (Fig. 4a,c ÷ 6a,c). In specimens with clamped end edges of the tube, these deformations tend to occur at the middle of the specimen length (Fig. 4b,d ÷ 6 b,d).

**Table 1. Results of modelling**

Coefficient of friction $\mu$	Compression of the composite cross-section		Compression of the composite cross-section through the welded support plate		Compression of steel part of the composite cross-section		Compression of steel part of the composite cross-section through the welded support plate	
	$\sigma$ , [MPa]	$k_\sigma$	$\sigma_{cr}$ , [MPa]	$k_\sigma$	$\sigma$ , [MPa]	$k_\sigma$	$\sigma_{cr}$ , [MPa]	$k_\sigma$
$L=200$ mm								
0	269.441	-	216.977	4,71	240.295	-	224.443	4,88
0.35	269.442	-	217.117	4,72	240.554	-	224.891	4,89
0.7	269.457	-	218.344	4,74	240.556	-	226.997	4,93
$L=400$ mm								
0	268.393	-	223.393	4,85	255.037	-	230.647	5,01
0.35	268.397	-	223.891	4,86	255.312	-	230.648	5,01
0.7	268.418	-	223.81	4,86	255.574	-	230.847	5,02
$L=600$ mm								
0	271.922	-	225.120	4,89	242.743	-	227.653	4,95
0.35	271.927	-	225.058	4,89	242.453	-	227.748	4,95
0.7	272.039	-	224.954	4,89	242.239	-	227.840	4,95

When compressing the specimens without end support plates during buckling deformation of the walls, the magnitude of compressive stress lies beyond the elastic stage of the work material, which is limited in this case, the yield strength is equal to 235 MPa (Tab. 1). For this reason, the coefficients of elastic critical stresses were not calculated. In the specimens with end support plates, the magnitude of critical compressive stress  $\sigma_{cr}$  lies in the elastic stage of steel material functioning and coefficients of the elastic critical stress exceeds the standard value  $k_\sigma = 4$ , specified in the standard EN 1993-1-5 for the walls of hollow tubes. This indicates that filling hollow cross-sections with concrete increases their local stability. As seen from Table 1, the values of this coefficient under compression only the steel part of the composite section is higher than in the case of compressing the whole of cross-section. In these specimens, the excess is negligible and has the maximum value of 3.5 %. The reason for different values of the critical compression stress is that the concrete core is deformed in the transverse direction in the

specimens, in which a compressive load is applied to both parts of the section. It promotes early development of the local buckling of the tube at a lower value of compressive stresses. But in terms of bearing capacity of the considered columns, the load imposed on the whole cross-sections is more advantageous.

From the viewpoint of the influence of friction between the components of the composite cross-section on the local stability of a rectangular tube, it must be emphasized that the maximum difference between the values of the compressive stress at  $\mu = 0$  and  $\mu = 0.7$  is 1.1 % (see Tab. 1) in all cases of fixation conditions of loaded edges of the walls, the lengths of the specimens, and methods of introducing the loading.

## Conclusion

General conclusions and results of the research are the following:

1. One of the basic types of composite sections in the form of a rectangular steel tube with a profile of RHS 200x100x3 (EN 10219), filled with concrete, which lies beyond the validity of European construction standard Eurocode 4, was investigated.

2. Based on modelling the specimens' behavior under axial compression using ABAQUS computational-graphics software, it was shown that the development of the local buckling of the steel part of the composite cross-section occurs at a higher value of the coefficient of the elastic critical stress in comparison with normative data EN 1993-1-5 for tubes not filled with concrete. The lack of welded support plates in the investigated composite columns leads to plastic deformation of the local buckling of the rectangular tube walls, which indicates the impossibility and classified as a steel cross-section class 4, according to standard EN 1993-1-1.

3. Analysis of the influence of friction between the components of the composite section on the local stability of the steel-concrete element showed that the change of the friction coefficient has a negligible effect on the critical stresses.

4. Based on the results of this work, it can be stated that in studying the local stability of axial compressed composite structures with a cross-section in the form of rectangular tubes filled with concrete, there is no necessity of «push out» test to establish the natural bond parameters, because they have a negligible influence on the result.

## References

1. Ovchinnikov I.I., Ovchinnikov I.G., Chesnokov G.V., Mihaldykin E.S. O probleme rascheta trubobetonnyh konstrukcij s obolochkoj iz raznyh materialov. Chast 1. Opyt primenienia trubobetona s metallicheskoy obolochkoj [About the problem of calculating the pipe-concrete structures with a shell made of different materials. Part 1. Experience of use the pipe-concrete with a metal shell]. *Online Magazine "Naukovedenie"*. 2015. Vol. 7 No. 4. [Electronic resource]. System requirements: AdobeAcrobatReader. URL: <http://naukovedenie.ru/PDF/95TVN415.pdf> (date of application: 14.12.2015). (rus)
2. Kanishchev R., Kvocak V. Spriahnuté ocel'obetónové tlačené prúty a stípy vyplnene betónom [Composite steel and concrete compression bars and columns filled with concrete]. *Vedecko-výskumná činnosť UIS 2013* [Research activities UIS 2013]. UVZ TU Herlany: TUKE, SvF, UIS, Kosice, 2014. Pp. 107–116. (sk)
3. Kvocak V., Varga G., Vargova R. Composite steel concrete filled tubes. *Procedia Engineering*. 2012. Vol. 40. Pp. 469–474.
4. Duricova A., Rovnak M. *Navrhovanie ocelovo – betónových konštrukcií* [Design of steel – concrete structures]. Bratislava: VEDA, 2008. 264 p. (sk)
5. Kozak J., Gramblicka S., Lapos J. *Spriahnuté a kombinované ocel'obetónové konštrukcie pozemných stavieb* [Composite and combined steel and concrete structures in civil engineering]. Bratislava: Jaga, 2000. 161 p. (sk)
6. Kikin A.I., Sanzharovskiy R.S., Trul V.A. *Konstrukcii iz stalnyh trub, zapolnennyh betonom* [Construction of steel tubes filled with concrete]. Moscow: Stroyizdat, 1974. 144 p. (rus)
7. Storozhenko L. I., Plachotnyj P. I., Černyj A.Y. *Raschet Kanishchev R.A. Analysis of local stability of the rectangular tubes filled with concrete. Magazine of Civil Engineering*. 2016. No. 4. Pp. 59–68. doi: 10.5862/MCE.64.6

## Литература

1. Овчинников И.И., Овчинников И.Г., Чесноков Г.В., Михалдыкин Е.С. О проблеме расчета трубобетонных конструкций с оболочкой из разных материалов. Часть 1. Опыт применения трубобетона с металлической оболочкой // Интернет-журнал «НАУКОВЕДЕНИЕ». 2015. Том 7, №4. [Электронный ресурс]. Систем. требования: AdobeAcrobatReader. URL: <http://naukovedenie.ru/PDF/95TVN415.pdf> (дата обращения: 14.12.2015).
2. Kanishchev R., Kvocák V. Spriahnuté ocel'obetónové tlačené prúty a stípy vyplnene betónom // Vedecko-výskumná činnosť UIS 2013. UVZ TU Herlany: TUKE, SvF, UIS, Košice, 2014. Pp. 107–116.
3. Kvocak V., Varga G., Vargova R. Composite steel concrete filled tubes // Procedia Engineering. 2012. Vol. 40. Pp. 469–474.
4. Ďuricová A., Rovnák M. Navrhovanie ocelovo – betónových konštrukcií. Bratislava: VEDA, 2008. 264 p.
5. Kozák J., Gramblicka Š., Lapos J. Spriahnuté a kombinované ocel'obetónové konštrukcie pozemných stavieb. Bratislava: Jaga, 2000. 161 p.
6. Кикин А.И., Санжаровский Р.С., Труль В.А. Конструкции из стальных труб, заполненных бетоном. М.: Стройиздат, 1974. 144 с.
7. Стороженко Л.И., Плахотный П.И., Черный А.Я. Расчет трубобетонных конструкций. К: Будивелник, 1991. 120 с.
8. Онищенко О.Г., Пічугін С.Ф., Онищенко В.О., Семко, О.В., Стороженко Л.І., Емельянова І.А., Ландар О.М. Високоекспективні технології та комплексні конструкції в будівництві. Полтава: Форміка, 2009. 404 с.
9. Garanzha I., Vatin N. Analytical methods for determination

- trubobetonnyh konstrukcij* [Calculation of steel tubes filled with concrete]. Kiev: Budivelnik, 1991. 120 p. (ua)
8. Onishchenko O.G., Pichugin S.F., Onishchenko V.O., Semko O.V., Storozhenko L.I., Emelianova I.A., Landar O.V. *Visokoeffektivni tehnologii ta kompleksni konstrukcii v budivnictvi* [High-technology and complex construction in buildings]. Poltava: Formika, 2009. 404 p. (ua)
  9. Garanzha I., Vatin N. Analytical methods for determination a load capacity of concrete-filled tubes under axial compression. *Applied Mechanics and Materials*. 2014. No. 633–634. Pp. 965–971.
  10. Duvanova I.A., Salmanov I.D. Trubobetonnye kolonny v stroitelstve visotnyh zdanij i sooruzhenij [Pipe-concrete columns in the construction of tall buildings and structures]. *Construction of Unique Buildings and Structures*. 2014. No. 6(21). Pp. 89–103.
  11. Kanishchev R., Kvocak V. Effects of Stability on the Resistance of Composite Concrete-Filled Rectangular Steel Pipes According to World Standards. *Elegance in Structures*. Zurich: IABSE, 2015. Pp. 1–8.
  12. Kang W.-H., Uy B., Tao Z., Hicks S. Design strength of concrete-filled steel columns. *Advanced Steel Construction*. 2015. No. 11(2). Pp. 165–184.
  13. Ovchinnikov I.I., Ovchinnikov I.G., Chесnоков G.V., Mihaldykin E.S. O probleme rascheta trubobetonnyh konstrukcij s obolochkoj iz raznyh materialov. Chast 2. Raschet trubobetonnyh konstrukcij s metallicheskoy obolochkoj [About the problem of calculating the pipe-concrete structures with a shell made of different materials. Part 2. Calculation of pipe-concrete structure with the metal shell]. *Online Magazine "Naukovedenie"*. 2015. Vol. 7 No. 4. [Electronic resource]. System requirements: Adobe Acrobat Reader. URL: <http://naukovedenie.ru/PDF/112TVN415.pdf> (date of application: 14.12.2015). (rus)
  14. Nesvetaev G.V., Revzan I.V. Ocenna prochnosti trubobetona [Evaluation of pipe-concrete strength]. *Technical sciences*. 2011. No. 12–13. Pp. 580–583. (rus)
  15. Mouli M., Khelafi H. Strength of short composite rectangular hollow section columns filled with lightweight aggregate concrete. *Engineering Structures*. 2007. Vol. 29. Pp. 1791–1797.
  16. Uy B. Stability and ductility of high performance steel sections with concrete infill. *Journal of Constructional Steel research*. 2008. Vol. 64. Pp. 748–754.
  17. Uy B. Local and post-local buckling of concrete filled steel welded box columns. *Journal of Construction Steel research*. 1998. No. 47. Pp. 47–72.
  18. Uy B., Bradford M. A. Local buckling of composite steel-concrete rectangular columns. *Fifth international conference on steel structures*. Jakarta: 1994. Pp. 313–322.
  19. Krishan A.N., Melnichuk A.S. Prochnost trubobetonnyh kolonn kvadratnogo secheniya pri osevom szhatii [The strength of pipe-concrete square columns under axial compression] *Vestnik magnitogorskogo gosudarstvennogo tekhnicheskogo universiteta im. G I. Nosova* [Bulletin of the Nosov magnitogorsk state technical university]. Magnitogorsk: MGTU, 2012. No. 3. Pp. 51–54. (rus)
  20. Lee S. Capacity and the moment-curvature relationship of high-strength concrete filled steel tube columns under eccentric loads. *Steel and Composite Structures*. 2007. Vol. 7. No. 2. Pp. 135–160.
  21. Storozhenko L.I., Ermolenko D.A., Demchenko O.V. Rabota pod nagruzkoj szhatyh trubobetonnyh elementov s usilennymi jadrami [The work under load of compressed pipe-concrete elements with strengthened nuclei]. *Resursoenergoefektivnye tekhnologii v stroitelnom komplekse regiona* [Efficiency of resource energy of technology in the construction industry of region]. Poltava: PNTU, 2014. No. 4. Pp. 288–292. (rus)
  22. Patel V. I., Liang Q. Q., Hadi M. Inelastic stability analysis of high strength rectangular concrete-filled steel tubular slender beam-columns // *Interaction and Multiscale Mechanics*. 2012. Vol. 5. № 2. Pp. 91–104.
  23. Yang Y., Han L. Experiments on rectangular concrete-filled steel tubes loaded axially on a partially stressed cross-sectional area // *Journal of Constructional Steel Research*. 2009. Vol. 65. Pp. 1617–1630.
  24. Nethercot D. A. *Composite construction*. New Yourk: Spon press, 2004. 242 p.
  25. Bradford M. A., Oelhers D.J. *Composite steel and concrete structural members. Fundamental behaviour*. London: Pergamon, 1995. 536 p.
  26. EN 1994–1–1: 2004. Eurocode 4. Design of composite steel and concrete structures. Part 1–1: General rules and rules for buildings. Brussels: CEN, 2004. 120 p.
  27. EN 1993–1–1: 2005. Eurocode 3. Design of steel structures. Part 1–1: General rules and rules for buildings.

Канищев Р.А. Анализ местной устойчивости трубобетонных конструкций прямоугольного сечения // Инженерно-строительный журнал. 2016. № 4(64). С. 59–68.

- slender beam-columns. *Interaction and Multiscale Mechanics*. 2012. Vol. 5. No. 2. Pp. 91–104.
23. Yang Y., Han L. Experiments on rectangular concrete-filled steel tubes loaded axially on a partially stressed cross-sectional area. *Journal of Constructional Steel Research*. 2009. Vol. 65. Pp. 1617–1630.
  24. Nethercot D. A. *Composite construction*. New Yourk: Spon press, 2004. 242 p.
  25. Bradford M. A., Oelhers D.J. *Composite steel and concrete structural members. Fundamental behaviour*. London: Pergamon, 1995. 536 p.
  26. EN 1994-1-1: 2004. *Eurocode 4. Design of composite steel and concrete structures. Part 1-1: General rules and rules for buildings*. Brussels: CEN, 2004. 120 p.
  27. EN 1993-1-1: 2005. *Eurocode 3. Design of steel structures. Part 1-1: General rules and rules for buildings*. Brussels: CEN, 2005. 92 p.
  28. EN 10219-2: 2006. *Cold formed welded structural hollow sections of non-alloy and fine grain steels. Part 2. Tolerances, dimensions and sectional properties*. Brussels: CEN, 2006. 40 p.
  29. EN 1993-1-5: 2006. *Eurocode 3. Design of steel structures. Part 1-5: General rules – Plated structural elements*. Brussels: CEN, 2006. 56 p.
  30. Bryan G.H. On the stability of a plane plate under trusts in its own plane, with applications to the “bukling” of the sides of a ship // Proceedings of the London Mathematical Society. 1891. Vol. 22. Pp. 54–67.
  31. Тимошенко С. П. Устойчивость стержней, пластин и оболочек. М.: Наука, 1971. 807 с.
  32. Rabbat B. G., Russell H. G. Friction coefficients of steel on concrete or grout // ASCE, Journal of Structural Engineering. 1985. Vol. 111. Pp. 505–515.
  33. Baltay P., Gjelsvik A. Coefficient of friction for steel on concrete at high normal stress // ASCE, Journal of Materials in Civil Engineering. 1990. Vol. 2. Pp. 46–49.
  34. Evirgen B., Tuncan A. Determination of frictional behaviour between concrete and steel tube interaction // EUROSTEEL 2014, September 10–12. Brussels: ECCS, 2014. Pp. 419–425.
  35. EN 1992-1-1: 2005. *Eurocode 2. Design of concrete structures. Part 1-1: General rules and rules for buildings*. Brussels: CEN, 2005. 200 p.
  36. Simulia. *Abaqus 6.13: Analysis Users Guide. Volume I*. Dassault Systems, 2013. 840 p.

Ruslan Kanishchev,  
+421(944)596743; ruslan.kanishchev@gmail.com

Руслан Александрович Канищев,  
+421(944)596743; эл. почта:  
ruslan.kanishchev@gmail.com

© Kanishchev R.A., 2016



**ПОЛИТЕХ**

Санкт-Петербургский  
политехнический университет  
Петра Великого

Инженерно-строительный институт

Центр дополнительных профессиональных программ

195251, г. Санкт-Петербург, Политехническая ул., 29,  
тел/факс: 552-94-60, [www.stroikursi.spbstu.ru](http://www.stroikursi.spbstu.ru),  
[stroikursi@mail.ru](mailto:stroikursi@mail.ru)

Приглашает специалистов проектных и строительных организаций,  
не имеющих базового профильного высшего образования  
на курсы профессиональной переподготовки (от 500 часов)  
по направлению «Строительство» по программам:

**П-01 «Промышленное и гражданское строительство»**

Программа включает учебные разделы:

- Основы строительного дела
- Инженерное оборудование зданий и сооружений
- Технология и контроль качества строительства
- Основы проектирования зданий и сооружений
- Автоматизация проектных работ с использованием AutoCAD
- Автоматизация сметного дела в строительстве
- Управление строительной организацией
- Управление инвестиционно-строительными проектами. Выполнение функций технического заказчика

**П-02 «Экономика и управление в строительстве»**

Программа включает учебные разделы:

- Основы строительного дела
- Инженерное оборудование зданий и сооружений
- Технология и контроль качества строительства
- Управление инвестиционно-строительными проектами. Выполнение функций технического заказчика и генерального подрядчика
- Управление строительной организацией
- Экономика и ценообразование в строительстве
- Управление строительной организацией
- Организация, управление и планирование в строительстве
- Автоматизация сметного дела в строительстве

**П-03 «Инженерные системы зданий и сооружений»**

Программа включает учебные разделы:

- Основы механики жидкости и газа
- Инженерное оборудование зданий и сооружений
- Проектирование, монтаж и эксплуатация систем вентиляции и кондиционирования
- Проектирование, монтаж и эксплуатация систем отопления и теплоснабжения
- Проектирование, монтаж и эксплуатация систем водоснабжения и водоотведения
- Автоматизация проектных работ с использованием AutoCAD
- Электроснабжение и электрооборудование объектов

**П-04 «Проектирование и конструирование зданий и сооружений»**

Программа включает учебные разделы:

- Основы сопротивления материалов и механики стержневых систем
- Проектирование и расчет оснований и фундаментов зданий и сооружений
- Проектирование и расчет железобетонных конструкций
- Проектирование и расчет металлических конструкций
- Проектирование зданий и сооружений с использованием AutoCAD
- Расчет строительных конструкций с использованием SCAD Office

**П-05 «Контроль качества строительства»**

Программа включает учебные разделы:

- Основы строительного дела
- Инженерное оборудование зданий и сооружений
- Технология и контроль качества строительства
- Проектирование и расчет железобетонных конструкций
- Проектирование и расчет металлических конструкций
- Обследование строительных конструкций зданий и сооружений
- Выполнение функций технического заказчика и генерального подрядчика

По окончании курса слушателю выдается диплом о профессиональной переподготовке установленного образца, дающий право на ведение профессиональной деятельности

